ADVANCED MATERIALS TECHNOLOGIES
www.advmattechnol.de

Revolutionizing Monolithic Catalysts: The Breakthroughs of Design Control through Computer-Aided-Manufacturing

Adriana Parra-Marfil, Agustín Francisco Pérez-Cadenas, Francisco Carrasco-Marín, Raúl Ocampo-Pérez, and Esther Bailón-García**

Additive manufacturing (AM) presents a promising opportunity for the innovative design and production of structured catalytic materials. Given the critical role of catalysts in industrial catalytic processes, AM has the potential to contribute to the development of improved catalysts by reducing activation energy and enhancing selectivity. Conventional synthesis methods limit the choice of structural materials and composition for producing monoliths. Additionally, the deposition of catalytic compounds is also restricted by commonly applied techniques that may require prior coverage or treatments to improve adherence or do not achieve a homogenous coat. Moreover, production is limited to monoliths with straight and parallel channels. However, this format drives to laminar regime flow thus restricting the radial mass and heat transfer. Conversely, AM allows the production of a wider variety of compositions and more complex structures that have proven to rise their effectiveness by increasing reagents-catalyst interaction, making catalytic processes more cost-effective. Therefore, in this review an outline of the recent progress of AM methods in the development of monolithic catalysts is presented focusing on the requirements, advantages, and disadvantages of each technique, hence providing a practical overview of their novel opportunities to overcome current limitations in catalyst synthesis.

1. Introduction

Recently, additive manufacturing (AM) has opened new opportunities in the catalysis field.[1,2] Since ≈85–90% of industrial processes contain at least one catalytic step,[3] the generation of catalysts that decrease the reactions activation energy and increase the selectivity of target products is of major necessity to benefit the processes efficacy. In this sense, the versatility to obtain complex structures designs, non-achievable through conventional methods but through additive manufacturing, represents an advantage in catalytic improvement. Consequently, AM is freshly being applied to produce reactors, monolithic catalysts, mixers, and ancillaries.[4-7]

On the other hand, the advancement in the production of structured catalysts made of a 3D support coated by catalytically active species and their use in catalytic processes, is considered as an excellent alternative to traditional packed and fluidized bed systems. This is due to the fact that using structured catalysts like monoliths not only reduces the processing costs by avoiding the filtration stage, but also involves a lower pressure-drop and better thermal and mechanical stability regarding powders or pellets, especially for high flow rates.[8–11] Besides, monoliths offer lower axial dispersion, reduction of the diffusion path length, and flow resistance, as well as easy cleaning of particulates accumulated on the channel walls, improving regeneration and recyclability of the catalyst.[9,11] The deposition of highly active catalytic phases with suitable thickness, homogeneity, and adhesion to the support, determines the stability of the coating as well as the catalytic activity. In this respect, wash-coating technique is reported as the most popular and adaptable way to deposit catalysts on structured supports, using slurries or sols prepared from catalysts previously synthesized.[9,10]

The monolithic structures geometry, as previously mentioned, has been restricted by the technology available for their fabrication and the techniques feasible to support the active phases. Honeycomb monoliths are usually produced by extrusion, corrugated sheets, compression, or injection molding; and the catalytically active phases are subsequently incorporated, usually by dip-coating.[10,12–15] Nevertheless, those fabrication procedures limit the design of monoliths to aligned regular channels. This configuration implies that although the flow of the feed gas is turbulent, it becomes laminar as it passes through the monolith due to viscous forces within the narrow channels. Hence, the enforced

A. Parra-Marfil, A. F. Pérez-Cadenas, F. Carrasco-Marín, E. Bailón-García
Materiales Polifuncionales Basados en Carbono (UGR-Carbon)
Facultad de Ciencias
Universidad de Granada
Campus Fuente Nueva s/n., Granada 18071, España
E-mail: adrianaparra@correo.ugr.es; estherbg@ugr.es

A. Parra-Marfil, R. Ocampo-Pérez
Centro de Investigación y Estudios de Posgrado
Facultad de Ciencias Químicas
Universidad Autónoma de San Luis Potosí
San Luis Potosí 78260, México

The ORCID identification number(s) for the author(s) of this article can be found under https://doi.org/10.1002/admt.202400064

DOI: 10.1002/admt.202400064

laminar flow results in its lack of uniformity and radial mass and heat transfer limitations, impeding an appropriate usage of the active phases.[16] Thus, the progress of monoliths manufacturing techniques that enhance: the complexity of the designs, active phases deposition, and the interaction between reactants and catalysts represent an advancement opportunity at the industrial level to diminish costs of commonly expensive catalytic materials and increase their efficiency. Thus far, various AM technologies have been applied to catalysis to simplify the monolithic catalyst preparation and active phase loading process. Moreover, 3D printing techniques have been used to analyze the performance of several materials (such as zeolites, metals, metal oxides, and polymers) in many processes. Along with the generally used dip-coating method (which can be applied to deposit the catalytic active phase on a printed object), this synthesis technique also allows to integrate the active phase in the monolithic structure while printing, as some studies have shown.[17–23] In this regard, the innovation of AM technology is demonstrating to be an excellent implement that helps to obtain specific, different, and complex structures, that are otherwise unattainable with conventional methods.[24–27] Moreover, the use of 3D printing techniques in combination with fluid and chemical simulation, could be taken into advantage to optimize heat and mass transfer[4] and hence catalytic processes.

The broad diversity of techniques and materials available make the AM technology an advantageous prospect for exploring and enhancing the catalysts production. Monolithic catalyst manufacture through AM can be done following two strategies, obtaining them directly by 3D printing, or through the generation of templates used in succeeding processing (filling, loading, or coating). Thus, the chemical composition, physicochemical properties, and monolithic structure of 3D printed catalyst materials can be customized for specific reactions or experiments. Therefore, this work presents a comparative assessment of the 3D printing techniques, materials, potential, and limitations to produce monolithic catalysts, according to different printing methods, in order to offer a useful review of the innovative possibilities in catalysts fabrication.

2. Additive Manufacturing Overview

The additive manufacturing (AM) is a technology developed by Charles Hull in 1986,[28] which consists in the successive addition of material, printing one layer at a time, to build up a final product. The additive manufacturing process starts by generating a 3D computer-aided-design (CAD) of the desired object. This model is sliced into a stack of flat layers of patterned areas, which are printed with diverse materials and, afterwards, solidified (or crosslinked) into a structure. There is a wide variety of raw materials that can be used depending on the additive manufacturing process, among them can be mentioned: polymers, ceramics, composites, powders, glass, building materials, biomaterials, metals, and carbonaceous materials (with binder matrix). This technology has reduced manufacturing limitations by allowing the development of a vast range of simple and complicated geometries, with design freedom and excellent dimensional accuracy even in small-scale. Furthermore, due to the advantages offered by AM, such as ease of access, high-speed productions, minimization of materials wastage, and, therefore, cost-effective products,[29] its applications are constantly expanding.

There are several ways to classify AM processes, for example, according to their baseline technology or the type of raw material employed. Nonetheless, most accepted classification is given by ASTM/ISO (**Figure 1**), and consists of seven process categories: vat photopolymerization, powder bed fusion, material extrusion, material jetting, binder jetting, sheet lamination, and direct energy deposition.[30]

According to ASTM definition, vat photopolymerization, powder bed fusion, and direct energy deposition processes, solidify the raw material either disposed in a vat container or provided from a material feeder, following each layer pattern. On the other hand, techniques grouped in the material extrusion, material jetting, and binder jetting categories, deposit the building material by means of a nozzle in a build platform to be cured afterwards, while in the sheet lamination technique the printing material links without curing. **Table 1** shows a comparison of the AM categories in terms of their advantages, disadvantages, and applicability. Hereunder, an outline of the main additive manufacturing methods that have been applied so far to produce monolithic catalysts is given, therefore, giving relevant and useful references in the field.

3. Vat Photopolymerization

Vat photopolymerization (VPP) was the first introduced additive manufacturing process, which employs a light source to cure liquid photosensitive materials contained in a vat. There are some general characteristics required in the light curing materials including good stability, low viscosity, suitable transmission, fast curing speed, and low curing shrinkage.[31] By means of a lens system, the scanning path is controlled to perform selective light-activated polymerization, from which the liquid photopolymer is solidified according to a pre-programmed pattern.[32,33] The main characteristics of vat photopolymerization printing are the high precision and rapid prototyping, moreover, the active phases can be dispersed in the raw material to be used in these techniques. There are several vat polymerization techniques differentiated by the light source and mechanism used for polymerization.[34] These techniques are: Stereolithography (SLA), Digital Light Processing (DLP), Continuous Liquid Interface Production (CLIP), and Volumetric Printing.

3.1. Stereolithography

In the stereolithography (SLA) process a beam of ultraviolet (UV) light emitted from a laser is used to react and cure photopolymer resins. The low viscosity photocurable material is deposited in a vat and a movable platform, onto which the final product is fabricated and hold, is placed inside. The UV beam scans the surface of the vat in the X-Y axes following a predefined layer cross-section selectively curing the resin. After completing a layer, the build platform moves in the Z axis a layer thickness, either in bottom-up approach (**Figure 2a**) or top-down approach (Figure 2b), filling it with more photopolymer resin. Then, the process is repeated several times creating successive layers until the entire object is finished. Finally, the structure is removed

Table 1. Comparison of the characteristics, advantages, and disadvantages of the different additive manufacturing techniques.

Printing Technique	Process	Layer Formation Method	Typical Materials	Strengths	Weaknesses	Resolution[μm]	Printing speed	References
Vat Photopolymerization	Stereolithography (SLA)	Laser/Digital light projector	Photopolymers such as acrylates, epoxies, filled resins (glass, ceramic, metal, etc.)	Do not need support material	Costly photopolymers	>10	High	[34–38]
	Digital Light Processing (DLP)		Preceramic polymers	High precision	Requirement of post-processing treatments	>10		
			Monomers	High quality	Poor thermal stability			
				Smooth surface				
				Complexity				
				Excellent mechanical properties				
	Continuous Light Interface Production (CLIP)			Layerless structure		75-162		
	Volumetric Printing					>80		
Powder Bed fusion	Laser Sintering (LS)	Laser/Electron beam	Thermoplastics	High level of complexity	Poor surface quality and accuracy caused by the fluidity of powder	>50	Moderate	[26,39]
	Laser Melting (LM)		Waxes			>20	Moderate	
	Electron Beam Melting (EBM)		Polymer, metal, and ceramic powders	Do not need support material		n.d.	High	
			Alloys	Wide range of materials	Requirement of post-processing treatments			
Directed Energy Deposition		Melting by focused heat source	Metal wire or powder	High single-point deposition rates	Low resolution	>250	Low	[26]
			Ceramics	Printing on irregular surfaces	Limited materials			
					Reduced ability to manufacture complex parts			
Material Extrusion	Direct Ink Writing (DIW)	Extrusion from a nozzle	Plastic	Simply fabrication process	Reduced porosity due to binders	30-250	Low	[26,31,40]
			Metal		Need of post treatment to remove additives			
			Ceramic Zeolites	Variety of materials				
			Carbon based materials					
	Fused Deposition Modelling (FDM)		Thermoplastic filaments (PLA, ABS, polyurethane, etc.)	Easy operation	Restriction of nozzle, diameter, and viscosity	50-200	Moderate	
				Inexpensive				
				Good structural properties	Layer-by-layer appearance			
					Poor surface quality			

(*Continued*)

Table 1. (Continued)

Printing Technique	Process	Layer Formation Method	Typical Materials	Strengths	Weaknesses	Resolution[µm]	Printing speed	References
Material Jetting	Ink Jetting Drop on Demand Aerosol Jetting	Ink-jet printing	Photopolymers Polymers Waxes Sol-gel Metals	Enable multiple materials in a single part High level of accuracy and complexity	Expensive materials and printer Limited material types Need of support material Long process	13-16 200-300	Low	[26,33,41]
Binder Jetting		Binder drops on command	Metal and ceramics powders Polymers	Low temperature process High productivity	Low definition Poor mechanical properties	>50	Moderate	[26,42,43]
Sheet Lamination	Laminated Object Manufacture (LOM) Ultrasonic Lamination (UAM) Friction Stir Additive Manufacturing (FSAM)	Binding of sheets through use of sticky substance, ultrasonic welding, or friction stir welding	Paper Plastic sheets Metal foils	High volumetric build rates Large size samples Low cost	Design limitations/Not adapted to detailed structures Depends on the thickness of the laminates Bonding efficiency impacted by laser cut Misalignment of layers	Variable	n.d.	[26,41]

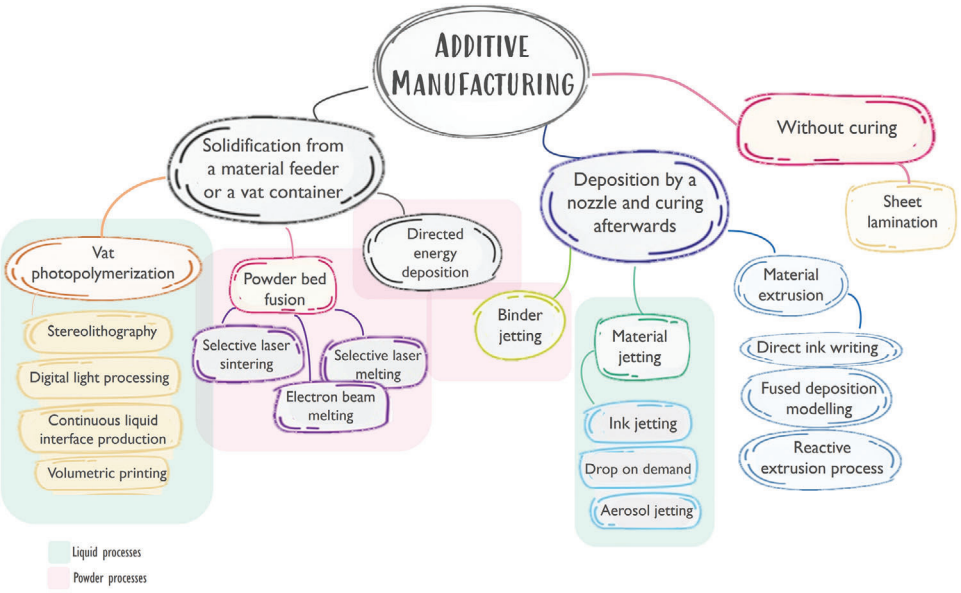

Figure 1. Additive manufacturing technologies classified according to type of process.

from the platform, cleaned, and put in a UV oven for further curing.[32,35,44] Compared to other techniques, the SLA process offers higher resolution and better surface quality since the resin curing does not depend on the particle size and nozzle characteristics such as in material extrusion-based technologies.

Nonetheless, research utilizing the SLA technique to prepare monolithic structures for directly applying them in catalysis is limited due to the characteristics of the raw materials that restrict their use to low temperature and pressure operational conditions (Table S1, Supporting Information). Among these studies, those realized by Chaparro et al.[45,46] who printed monoliths with non-conventional structure using the Visijet FTX Green resin, can be mentioned. After a stabilization treatment, the polymer resulted stable up to 270 and 300 °C in oxidizing and inert atmospheres respectively, which establishes the maximum working temperature. Therefore, the catalytic performance of the monoliths was tasted in the CO-PrOx reaction at atmospheric pressure with temperatures up to 250 °C. Similar maximum operating temperature was set by Franchi et al.,[47] who produced catalytic substrates for H_2 oxidation with a high temperature resin, Formlabs FLH-TAM01 High Temp V1, which has a heat distortion temperature (HDT) of 289 °C at 0.45 MPa.

Furthermore, the use of polymers also implies some trouble to disperse and anchor the active phase on its surface. Therefore, some pre- or post-treatments have been made to improve the deposition of the active phase, though, this implies additional stages in the obtention of catalytic monoliths. Different strategies have been tried to increase the loading of active phase including: i) thermal treatments; ii) attacking the polymer with different solvents such as ethanol or isopropyl alcohol before the impregnation; iii) attacking the polymer during the impregnation by using different solvents for the catalysts suspension; iv) doping the resin liquid before the printing process; and v) structures of advanced designs containing cavities.

For instance, the previously mentioned 3D printed structures produced by Franchi et al.[47] were loaded with the active compound (Pd/CeO_2) by spin coating at 2500 rpm followed by a treatment at 200 °C in air for 3 min to consolidate the washcoat. Due to the HDT, to stabilize and activate the catalytic coat a

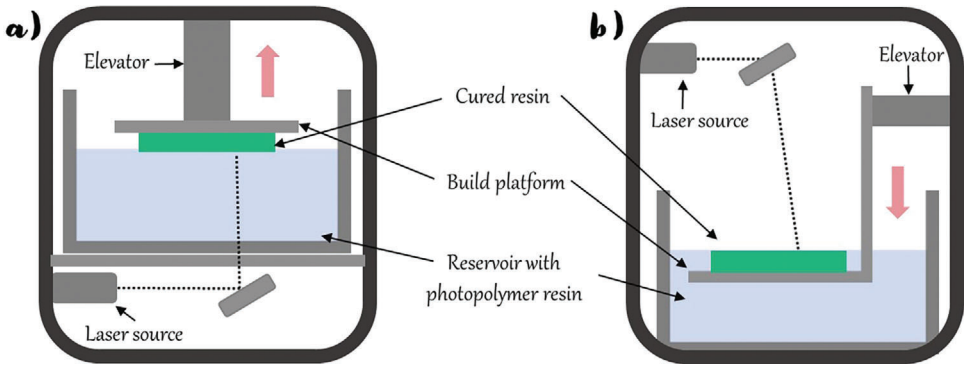

Figure 2. Schematic representation of SLA process: a) bottom-up approach; b) top-down approach.

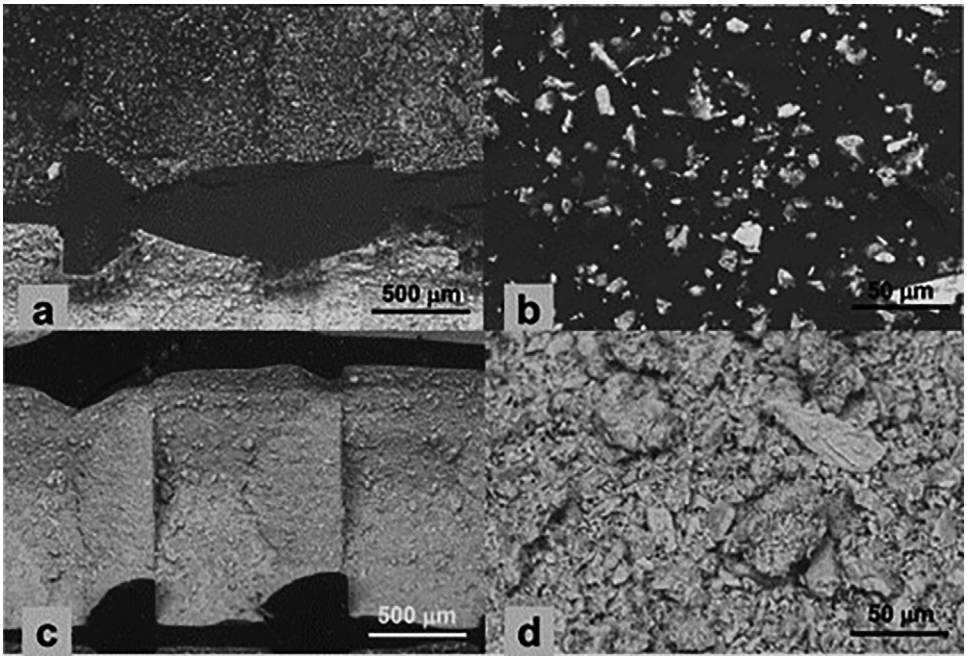

Figure 3. SEM images of the channels of a polymeric monolith loaded with CuO/CeO_2 active phase: a,b) after a thermal stabilization treatment in N_2; c,d) and after a subsequent thermal treatment in air to increase accessibility of CuO/CeO_2. Reproduced with permission.[45]

two-steps in-situ activation procedure was performed. First a heat treatment under N_2 atmosphere at 260 °C for 6 h, further cooled to room temperature, and then a second step of reduction also at 260 °C for 6 h in a flow of 2.5% H_2 in N_2. Repeated tests were performed on these supports, and results suggested that the deposition and activation procedures led to stable washcoat layers at the conditions employed. Besides, the treatment of the resin with ethanol or isopropyl alcohol was studied by Chaparro et al.[45] Results showed that chemical attack, either before or during the dip-coating process, interferes the active phase incorporation to the monoliths reducing the active phase anchored ≈70% regarding impregnation without chemical attack. According to SEM-EDX analysis, the active phase forms a layer on the surface and does not diffuse into the polymeric walls. On the other hand, thermal treatment favors the anchoring but embeds part of the catalytic phase as shown in **Figure 3**a,b, hence making necessary a cleaning treatment in air to burn part of the polymer and let the active phase accessible to reagents (Figure 3c,d). The authors also investigated the effect of doping the liquid resin with different amounts of carbon and SiO_2 in the active phase anchoring and thermal stability of the polymeric structures. The addition of the inorganic material did not lead to changes in the thermal stability. Furthermore, the presence of both inorganic materials generated anchoring points by changing the chemistry and rugosity of the resin, thus slightly increasing the attaching capacity, especially with SiO_2. However, they also proved that the use of non-conventional monoliths with grooves along the structure augmented the active phase attachment and retained similar amount of active phase regarding doped monoliths but requiring fewer steps. This represents a great alternative and advantage considering that when using traditional monoliths (e.g., cordierite materials) the addition of inorganic materials such as the SiO_2 or Al_2O_3, the use of binders or additives in repetitive dipping processes, and chemical or thermal treatments, are generally applied to improve active phase loading.[48–53]

To overcome the restrictions imposed by polymers when printing catalysts directly with commercial resin (**Figure 4**a), this AM technique can be used to create templates to fill with other materials (Figure 4b). Such is the case of the study realized by Davó et al.,[54] who produced ceramic monoliths with different geometries to analyze the effect of their configuration on the oxidation of CO. They employed the SLA technique with Visijet FTX green polymer to print two templates for monoliths with symmetrical and asymmetrical channels, maintaining the same total area in both cases. Templates were filled with cordierite paste, and then they were removed by combustion in static air at 500 °C for later sintering of the cordierite. The CuO/CeO_2 active phase for CO oxidation was loaded by dip-coating and no differences on the coating between the monoliths were observed. The asymmetrical design favored turbulent regime improving the reaction rate and the radial diffusion of molecules in comparison with the symmetrical one enhancing the catalytic performance.

An alternative to using monolith templates produced by this technique, is the modification of the resin employed for improving its characteristics for catalysis (Figure 4c). However, this may result challenging for the attainment of a photocurable resin with low viscosity which allows dipping and recoating for its layer-by-layer treatment, and able to solidify rapidly by light-initiated polymerization. One option is the use of a photosensitive resin mixture containing: prepolymers which are polymerized by a photoinitiator under light, reactive diluents to adjust the properties of the mixture, and additives.[31,55] Ceramic structures have been obtained by adding ceramic or glass particles to SLA resins, which after the printing process, followed thermal treatments

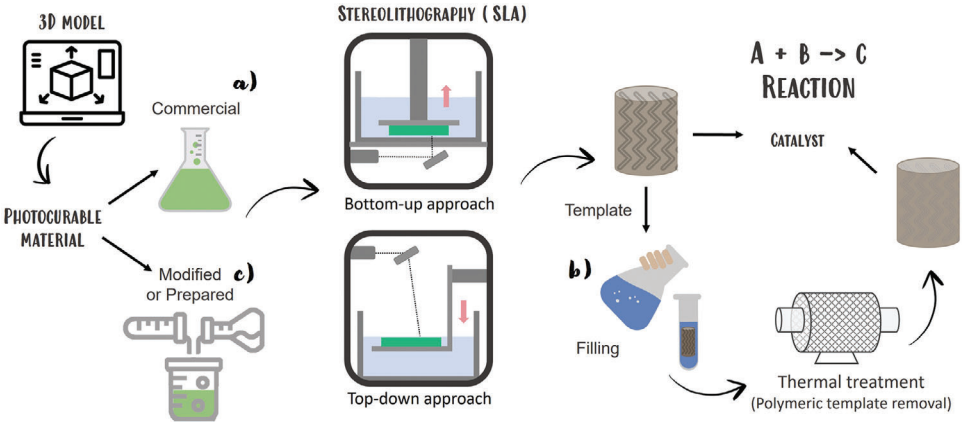

Figure 4. Methodologies followed to produce monolithic catalyst applying SLA technique: a) directly printing with commercial resin; b) using the 3D printed object as a template; and c) directly printing with a modified commercial resin or a prepared one.

to burn out the cross-linked polymer binder and sinter the ceramics.[56,57] In this context, Hensleigh et al.[58] developed a graphene oxide-based resin (XGO) to print complex designed graphene monoliths by micro-stereolithography. To obtain the XGO resin, GO was first crosslinked to form a hydrogel, which was further dispersed by sonication and added with acrylates and a photoinitiator, using N,N-dimethylformamide (DMF) as solvent. The acrylates and initiator serve to trap the XGO in the desired 3D shape, while the DMF was used to get high quality GO dispersions and eliminate amorphous carbon. Once printed, the structures were kept in solvent until dried by supercritical or freeze-drying for conserving the surface area. The 3D structures achieved ≈10 μm resolution with a GO successfully reduced, showing good characteristics for catalysis.

Two-Photon Lithography (TPL) is a promising way to produce 3D printed electrodes where a substrate is covered with a photoresist which is polymerized via laser lithography. Only certain voxels polymerize where the two lasers coincide, emitting photons at the same location; hence, the spatial resolution reaches ≈1 μm. However, after washing away the unpolymerized photoresist, the resulting structure lacks electroactivity, thus, an annealing treatment is required to transform into pyrolyzed glassy carbon through high-temperature heating to obtain and electroactive surface[59] Using this technique, C. Yang et al.[60] fabricated free-standing microelectrodes with a carbon electroactive surface to be used as implantable neural microsensors by two-photon nanolithography followed by pyrolysis. Spherical and conical electrodes where printed and electrochemical characterized. Spherical 3D-printed microelectrodes detected dopamine in a brain slice and in vivo, demonstrating they are robust enough for tissue implantation. While TPL presents itself as a highly adaptable and promising method for creating intricate 3D structures, it has not yet reached a stage of commercial scalability due to several limitations: (1) slow processing speed, (2) absence of commercial Two-Photon Polymerization Resins (TPPRs), (3) limited processing volume, (4) constrained dynamic range resulting from a higher writing threshold, and (5) a low two-photon absorption cross-section of TPPR.[61]

3.2. Digital Light Processing

The digital light processing technique (DLP) works on a similar principle as SLA but employing a digital micro-mirror device (DMD) instead of a moving laser, therefore avoiding the restriction of curing a single spot at a time. It is a bottom-up process that begins with the build platform placed one layer thickness above the vat floor (**Figure 5**). By means of the DMD set beneath the tank, a 2D image is projected into the build platform, curing the whole coat at once within a few seconds, it is even possible to simultaneously print more than one monolith, thus reducing the printing time while improving the precision.[44,62,63] The method continues by tilting the vat to separate the cured resin from the vat floor and then rising the platform one layer depth to print next layer, and so on until the object is finished. Besides, DLP allows controlling the light intensity distribution within the 2D image to attain heterogeneous cross-linking density along the layer.[32] Due to its advantages, DLP has been used for manufacturing polymers and ceramics monolithic structures,[64] and some of these works are mentioned below according to the strategy used, direct manufacturing or template production (see **Figure 6**).

For direct manufacturing of monoliths by DLP, most researchers have developed their own resin from zero or doped a commercial one. In this sense, among the works realized using DLP to directly produce monoliths that of Zhakeyev et al.[2] can be

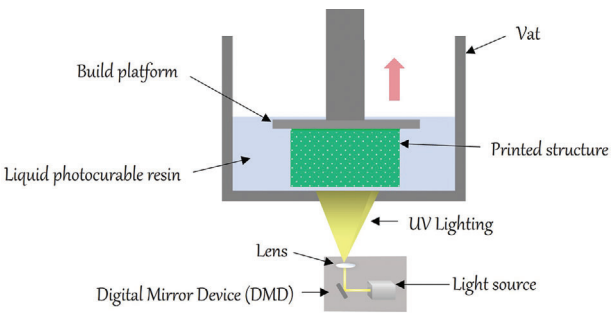

Figure 5. Illustrative diagram of the Digital Light Processing performance.

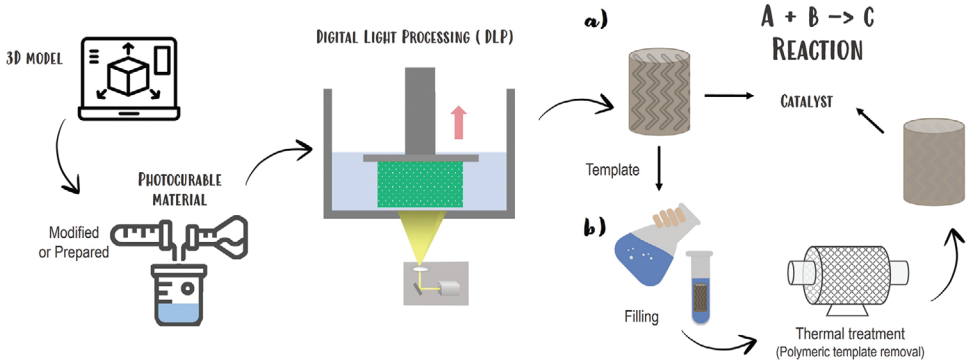

Figure 6. Approaches employed for manufacturing monolithic catalyst using DLP: a) straightly printing with commercial, commercial resin modified or a prepared one; and b) using the printed structure as a template.

mentioned. They integrated a 2,1,3-benzothiadiazole-based photosensitiser (St-BTZ) with a commercial resin to produce photocatalytic monoliths for furoic acid degradation. The DLP printer projected each pattern at 385 nm to cure the resin, which was later washed with isopropanol and post-cured under UV light for 1 h. The St-BTZ was selected due to its compatibility with acrylates, moreover, it also absorbs at 385 nm which helps to reduce over-irradiation and improve printing resolution. The optimal St-BTZ loading, 0.19 wt%, allowed the obtention of monoliths of different shapes without defects, and a uniform emission observed when they were irradiated with a UV lamp as presented in **Figure** 7.

Notwithstanding, the elaboration of light curing resins involves several factors to be considered, such as those previously mentioned in SLA section: rapid solidification with light-induced polymerization, and low viscosity to facilitate immersion and recoating. Furthermore, when adding the catalytic compounds sedimentation should be avoided and an appropriate solid loading must be ensured since it influences the physical properties of the resin. Too low solid content may lead to loose slurries, as well as cracking problems due to failed sintering. In contrast, too high solid content may result in viscous and heavy mixtures, long curing time, or deficient curing.[62] For example, Cu_2O microparticles (0.05 – 0.5 wt%) were dispersed by Xie et al.[22] in a previously prepared mixture of ionic surfactant Teric G9A6, isopropanol, and a commercially available photocurable resin. The resin mixture composition was established looking for a stable formulation without perceptible phase separation for up to 24 h at room temperature, which allows its use in DLP printing. This modified resin was employed to print heterogeneous Cu_2O catalytic monolith with meshed geometry, to use it in the degradation of ofloxacin by sulfate radical-based advanced oxidation processes. After printing, the monolith was calcined at 200 °C for 2 h under N_2 atmosphere showing structural integrity without shape changes or cracking. According to SEM images, the active phase was homogeneously distributed along the structure and the particle size remained unchanged. Besides, XRD and XPS analyses corroborated that the main component of the monoliths was Cu_2O. Gyak et al.[65] generated their own resin to produce catalysts for ammonia cracking. To obtain the resin they mixed pre-modified polyvinylsilazane (PVSZ), MEK-EC-2130Y solution containing silica nanoparticles, photoinitiators, and a UV absorber. The amount of silica nanoparticles was optimized to achieve a balance between the increase of ceramic yield and viscosity of the resin to get acceptable resolution of the printing. Projected patterns of UV light (405 nm) were used to cure each layer within 11 seconds of UV exposure. Once the catalyst was printed, it was washed with isopropyl alcohol, followed by a

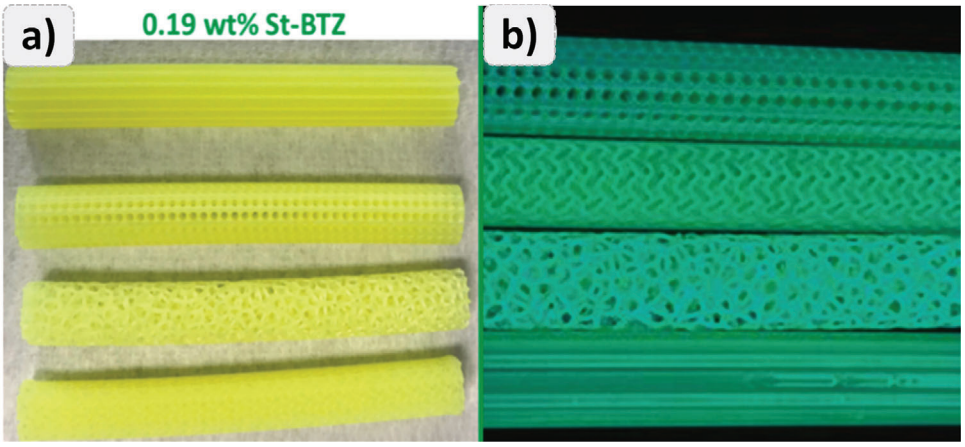

Figure 7. Directly DLP printed monoliths: a) cured photo-active monoliths with 0.19 wt% of St-BTZ; and b) image of the blue radiance observed owing to the St-BTZ monomers by lighting the monoliths with long-wave UV irradiation. Reproduced with permission.[2]

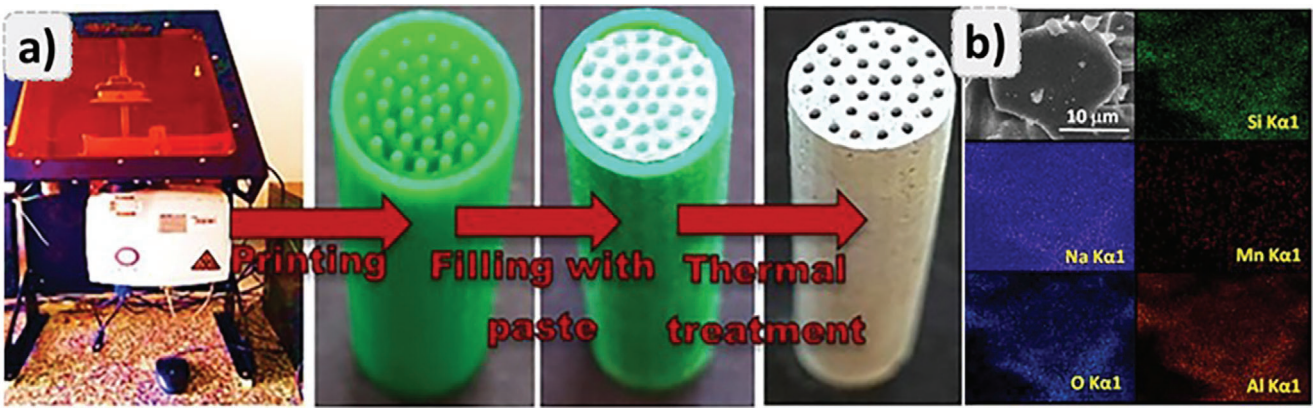

Figure 8. Ceramic monolithic catalyst obtained by means of DLP printed templates: a) scheme of production; b) EDS images showing the homogeneous elemental distribution within the monolith channel. Adapted with permission.[66]

post-curing with UV light, a heat treatment under argon atmosphere (up to 1000 °C), and finally, a washcoating with Ru. Catalysts exhibited high thermal stability (up to 1000 °C) and mechanical strength (78 GPa) after pyrolysis, and chemical stability after the reaction in corrosive conditions using a 2 mL min^{-1} flow. Likewise, Zhaojing et al.[62] prepared a resin to produce electrocatalysts for hydrogen evolution reaction. They formulated the resin with a mixture of acrylate monomers (TMPTA, TPGDA, and PUA), NiO powders (up to 56.4 wt%), TiC or Co or Fe_2O_3 powders (4.4–5.6 wt%), and additives such as stabilizer (YSZ), dispersant (BYK-111), and BYK-410 and KH-570 to reduce the viscosity and increase light curing efficiency. The slurry required also microwave ultrasound for 1 h and vacuum defoamation to get low viscosity, stability, and good dispersion properties. The authors found that a resin with ≈55 wt% solid loading presented the most proper characteristics for printing with a UV wavelength of 405 nm. They printed four samples at a time, and after printing, the structures were ultrasonically cleaned with ethanol to remove residues, followed by degreasing in a muffle to remove organics, a heating treatment in a tubular furnace, and finally reduced in H_2 5%/Ar atmosphere, observing a 15% volume shrinkage. The process led to surface with gluten-like cubic structure, and metals added in an amorphous state. This method generates a close connection between the catalyst and substrate, improving the electron transfer and stability during electrolysis without significant morphological or compositions changes.

On the other hand, the DLP-printed templates reported so far have been filled with ceramic precursors (basically α-Al_2O_3), thermally treated, and finally covered and/or loaded with active phases (as shown in Table S2, Supporting Information). By instance, Bogdan et al.[66] printed templates using DLP for obtaining conventional honeycomb monoliths with different cell densities (**Figure 8a**). The templates were filled with a mixture of α-Al_2O_3, Mn_2O_3, water, and sodium silicate solution, then they were dried and calcined at 850 °C for 8 h in air flow. The catalysts were nonporous materials and SEM-EDS analysis (shown in Figure 8b) corroborated homogenous distribution of Mn, Si, and Na on alumina particles. Mn_2O_3 partially transformed into Mn_3O_4 during thermal treatment as was confirmed in XRD patterns. Some of the authors[67] followed the same procedure using a double impregnation (**Figure 9a**), first with an aqueous solution of Na_2WO_4, and then with $Mn(NO_3)_2$ realizing a drying and calcination process after each impregnation. The elemental mapping showed a better distribution of W compared to that of Mn.

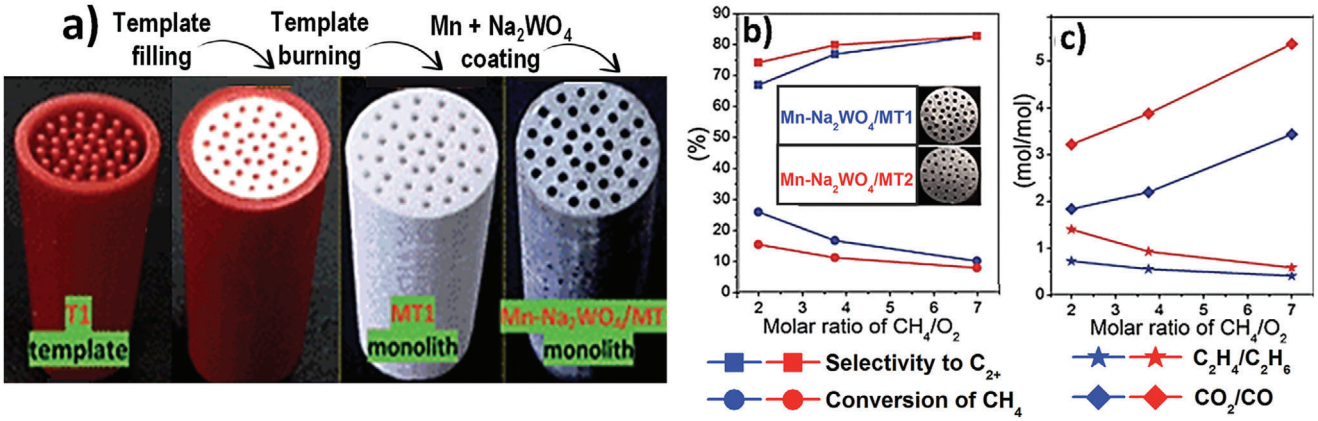

Figure 9. Double impregnated ceramic monolithic catalyst manufactured using DLP printed templates: a) scheme of production; b) conversion and selectivity obtained in the oxidative coupling of methane (OCM) process catalyzed with both monoliths (GHSV = 4400 cm^3 g_{cat}^{-1} h^{-1}). Adapted with permission.[67]

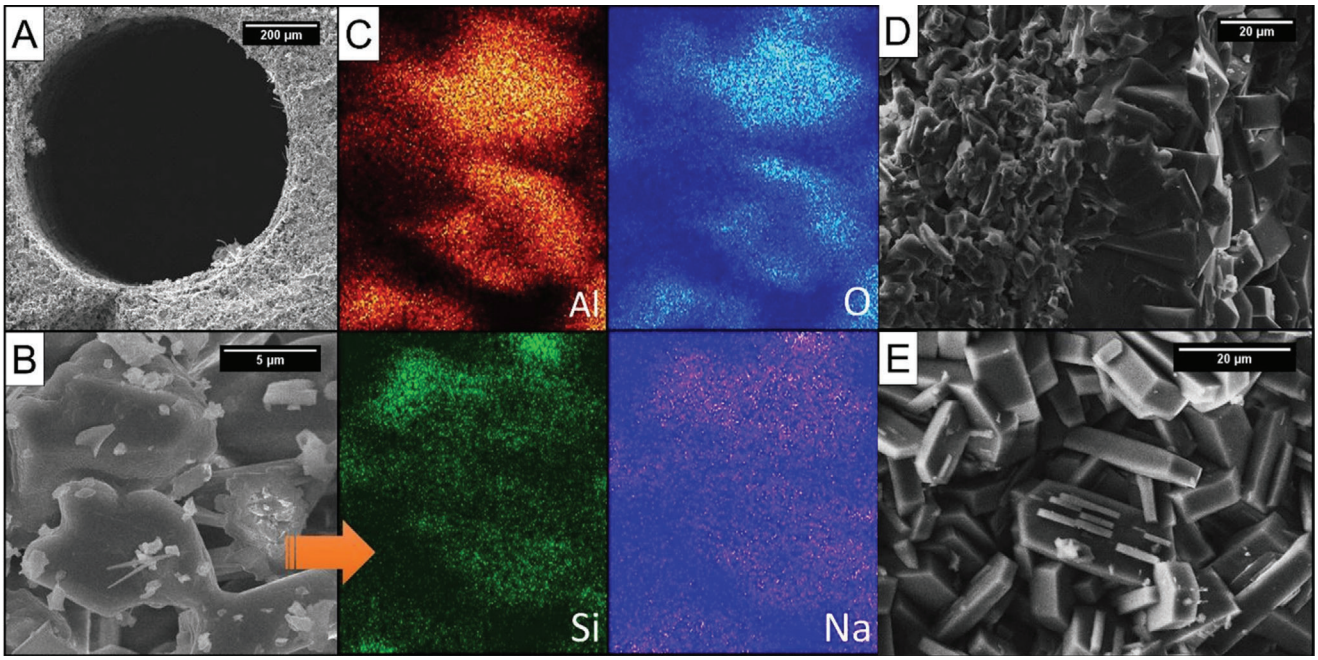

Figure 10. Alumina-based catalyst coated with cobalt-modified MFI zeolite for toluene combustion: a-c) SEM micrographs and elemental mapping of the ceramic monolith; and d-e) cross-section and top view of the MFI zeolite layer covering the monolith. Reproduced with permission.[69]

The catalysts exhibited CH_4 conversion that varies between 20 and 30%, and the channel size resulted to have an impact on the performance of the catalyst, mainly in the products distribution for which the smaller channels led to greater selectivity especially CO_2/CO (see Figure 9b).

Hędrzak et al.[68] used B9R-4-Yellow resin to obtain a mold for conventional honeycomb monolith synthesis. The template was filled with a paste of α-Al_2O_3 and sodium silicate, subsequently dried and calcined at 850 °C for 4 hours. After the template was removed by calcination, a layer of zeolite type MFI was deposited on monoliths by one-pot hydrothermal process, to increase the porosity of the materials (up to 73 $m^2\ g^{-1}$), followed by an ion-exchange with ammonium nitrate solutions at room temperature. SEM images showed that zeolite crystals grew randomly on the surface without any preferred orientation, and the presence of alumina in the zeolitic layer observed by EDS suggests that some alumina from the monolith could be dissolved due to hydrothermal conditions taking part of the zeolite synthesis. Alumina also controlled the acidity, since acid sites were reduced with the increase in Si/Al. Catalytic performance of those monoliths was tested in the gas phase isomerization of α-pinene, obtaining the highest conversion in the monolith with the highest amount of Al (95%). However, conversion and selectivity over all materials decreased gradually with the time on stream, which is attributed to the deposition of conjugated by-products.

Similar procedure was followed by Rokicińska et al.,[69] who prepared a ceramic monolith covered with MFI zeolite modified with cobalt to use it in the combustion of toluene. A conventional honeycomb monolith template, made of B9R-4-Yellow resin, was filled with α-Al_2O_3 powder and sodium silicate. After removing the template by calcination, the structure was covered with MFI zeolite by means of a hydrothermal treatment to provide a higher surface area (≈64 vs 0.1 $m^2\ g^{-1}$) and ion exchange capacity. Later, some monoliths were also ion-exchanged in an ammonium nitrate solution and, finally, both monoliths were modified with a Co-containing active phase by ion-exchange or impregnation. SEM analysis corroborated that alumina particles and sodium silicate were linked, and that all elements were homogenously dispersed (**Figure 10**a–c). The grown MFI zeolite crystals did not exhibit any specific orientation forming a coat of 40–50 µm thickness as presented in Figure 10d,e. The ion-exchange method resulted in a lower Co load but a higher dispersion since Co species occupy mainly extra-framework sites in the zeolite. The monoliths showed excellent catalytic performance (≈68% conversion and ≈99% selectivity to CO_2) and stability (up to 2000 min) in the combustion of toluene.

Volumetric 3D printing and continuous liquid interface production (CLIP) are other vat photopolymerization techniques. Although they offer advantages such as higher resolution and speed printing, they have not yet been employed in the production of monolithic catalysts since SLA and DLP are much simpler and easier to use giving good enough prints.

On the other hand, compared to commonly used methods for preparing polymer monoliths (for instance, polymerization and induced phase separation processes[70,71]), vat photopolymerization techniques present different advantages. While traditional methods may control the porosity characteristics of the materials prepared, the structural configuration and design cannot be controlled.[72–74] Conversely, SLA and DLP methods are characterized by versatility and high resolution, leading to a wide possibility of shapes and configurations. The use of polymers, in general, is associated with a restricted maximum operation temperature. Therefore, polymer monoliths prepared so far have been employed principally in separations processes,[71,75,76] and barely in low temperature reactions[77–79] and photocatalytic processes.[80,81] Consequently, when using VPP, some

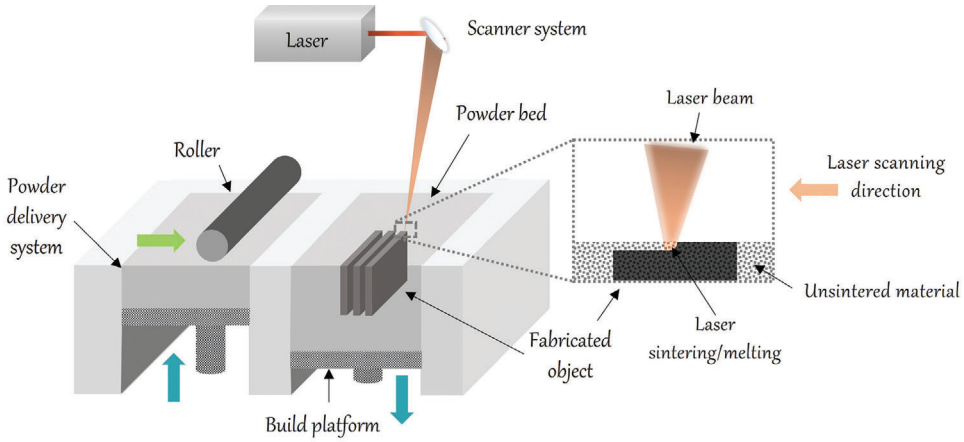

Figure 11. General scheme of Powder Bed Fusion printing processes.

alternatives have been proposed for increasing structure stability, including thermal treatments of printed objects, doping commercial resins or formulation of new ones, and the production of templates filled with different materials (mostly ceramics). Thermal treatments have shown to lightly increase the stability and allow to work up to 250 °C, while dopants addition and template fillers enable superior temperatures (up to 850 °C depending on material composition), far surpassing conventional materials. Per contra, the preparation and use of own resins may result challenging since it implies: i) requirement of different techniques to ensure well mixing and dispersion of solid compounds, ii) necessity of adjusting the consistency of the samples also avoiding sedimentation,[62] and iii) application of post treatments that may include washing and debinding to remove residues and organic compounds, post curing, and heat treatments to stabilize the materials. At the same time, the active phase loading has been approached with different methodologies: thermically or chemically attacking the structure surface either before, during, or after washcoating, adding the catalytic compound within the resin prior to AM, and using advanced designs that produce more anchoring cavities. First two approaches increase the loading but let it embed within the structure and no accessible for the reagents. Thus, the use of complex designs seems to be the best option for arising the catalyst deposition. Moreover, the use of templates seems to be more useful to achieve high resolution of complex structures of a specific non photocurable material.

4. Powder Bed Fusion

Powder bed fusion (PBF) processes continue with the principle of the additive manufacturing techniques, layer-by-layer production based on a 3D CAD. In powder bed fusion the raw material (such as metals, polymers, and ceramics) is in the form of powder, and a heat source (laser or electron beam) is used to consolidate the material. A rolling pin disposes a powder bed onto the build platform with a certain thickness (see **Figure 11**). Then, the heat source is applied to the cross section of the powder bed according to the CAD. The build platform moves down as the layer is finished, and the roller spreads more powder from a supply chamber to prepare next layer.[82,83] This process must be done inside a chamber with inert atmosphere to avoid the oxidative degradation of the material.[84] Laser sintering (LS), Laser Melting (LM), and Electron Beam Melting (EBM) are some of the widely used PBF processes.[85]

4.1. Laser Sintering and Laser Melting

Selective Laser Sintering and Laser Melting are PBF processes based on sintering technique that uses high power carbon dioxide laser as a tool to fabricate patterns. The laser beam selectively scans the powder which tends to sinter or melt when the energy source is applied.[86] Sintering occurs when particles fuse only on the surface, generating pieces with inherent porosity, while in melting a liquid state is reached where all the particles fuse completely, resulting in pieces with almost zero porosity. Among its advantages can be mentioned that no support structures are required and the unsintered material can be reused, reducing wastage.[87] Besides their high precision, both techniques allow the use of catalytically active metal materials during printing, making possible the attainment of catalysts with harsh reaction conditions. However, they present some drawbacks: i) internal stress caused by temperature gradients,[88] ii) roughness of the surfaces obtained because of the unsintered/unmolten particles added on the structure depending on the process parameters used,[89] iii) necessity of a post treatment or coating to enable the attachment of active phases, and iv) requirement of an inert atmosphere to protect metals from oxidation.[89–91] To date, few works are reported for the LS or LM printing of monolithic supports for catalysis. Notwithstanding, due to the generally metallic nature of raw materials used in PBF processes, the structures obtained may be used directly as catalyst using this metal base as the active phase. Moreover, it also provides them with great heat transfer, thus, being advantageous for reactions that are fast and very exothermic or endothermic.[92] This was demonstrated by Fratalocchi et al.,[93] who improved Fischer-Tropsch process by enhancing heat transfer with periodic cellular monoliths 3D-printed in AlSi7Mg0.6 by LM. Conversions of ≈80% were achieved due to the management of Fischer-Tropsch exothermicity. This characteristic of PBF methods signifies a valuable advantage over conventional synthesis, which typically involves coating commercial monoliths with metals such as Fe,

Figure 12. Comparison of fuel selectivity obtained from Fischer-Tropsch synthesis using monoliths with three different channel configurations. Adapted with permission.[99]

Ni, Pd, etc.[94–98] In this sense, Qinhong et al.[99] printed metallic monoliths through LS to directly serve as catalyst for the conversion of C1 molecules into high value-added fuels. Fe, Co, and Ni alloys were used to obtain the monoliths with different channels configurations. In order to enable them as catalyst, they were activated by calcination (at 873–1073 K for 24–60 h) and reduced in H_2 (40 mL min^{-1} at 673–1073 K for 6–10 h), and in the case of the Co-catalyst an acid treatment was done prior to the reduction to boost the catalytic centers activation. As result, Fe and Co catalysts exhibited good performance in Fischer-Tropsch synthesis and CO_2 hydrogenation, while Ni-catalyst proficiently produces syngas by CO_2 reforming of CH_4. The characterization analyses revealed that element distribution and surface chemical states were maintained after de LS process, therefore, we can assert the technique does not affect the chemical surface properties. Moreover, thermal conductivity and temperature tolerance (1000 K) were superior to other reported materials. To analyze the advantage of design freedom, Co-catalysts of several inner geometric configurations were applied in the Fischer-Tropsch synthesis. Results revealed that, although monoliths presented similar CO conversion, their structure increased and influence the liquid fuel products selectivity, as exhibited in **Figure 12**.

In the same manner, Komendová et al.[100] realized a treatment to enable the application of a 3D printed object. They carried out an oxidation process, at 600 °C in air during 6 h, of a monolithic structure LM-printed from Ti-6Al-4 V alloy, to form a reactive layer of titanium oxide. Likewise, powder of stainless steel was selectively laser sintered under nitrogen atmosphere by Agueniou et al.[90] to fabricate metallic honeycomb monoliths with excellent heat transfer properties. This technique allowed to obtain a wall thickness of ≈270 µm and a cell density of 230 cpsi. The monolith underwent a calcination process in N_2, and an aqueous slurry of Ce/Zr nickel and alumina was added with polyvinyl alcohol as binder to enhance the washcoating of the structure. A last calcination step was performed to finally achieve a load of 0.39 mg cm^{-2} of active phase. The metal structure got a good roughness that allowed an acceptable adherence without any extra surface treatment as also observed by other authors[89] (**Figure 13a,b**). XRF and SEM-EDX results showed signals of Ni-Ce-Zr in the same locations suggesting an adequate interaction between those elements. Also, the catalytic activity of the bare and coated monoliths was evaluated in the methane dry reforming. Monoliths did not show relevant deactivation after long time, and activation time was not necessary because of their great heat transfer. Due to its intrinsic nickel content, the bare monolith exhibited conversions ≈40% and 20% for CO_2 and CH_4 at 900 °C respectively, increasing to 95% and 75% in the case of the coated one. This fact highlights the opportunity of choosing an appropriate raw material that includes the active phase, thus obviating the need of its later deposition.

In contrast, other authors have pointed out the necessity of carrying out different surface pretreatments to enhance the active phase fixing (Table S3, Supporting Information). For instance, Lind et al.[92] 3D-printed a AlSi10Mg support for Pt and used it as catalyst in NO oxidation. They employed laser sintering to obtain a cubic iso-reticular channeled monolith, which was further electrolytically anodized to high surface alumina for allowing the final Pt deposition. Direct anodization advantage is the chemical attachment of the oxide layer to the metal body, nonetheless, the process resulted challenging owing to the content of silicon (10%) of the alloy used, and the complexity of the design. The conditions leading to an acceptable alumina layer (3–4 µm)

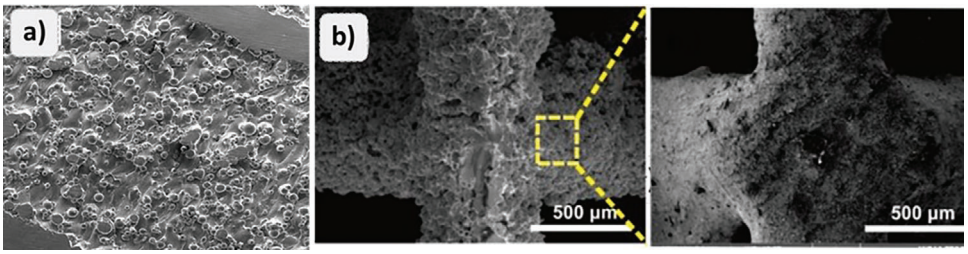

Figure 13. SEM images showing the roughness of metallic monoliths printed by PBF techniques. a) stainless-steel piece obtained by LS; b) SEM images of a LM printed copper monolith unpolished and polished. Reproduced with permission.[89,90]

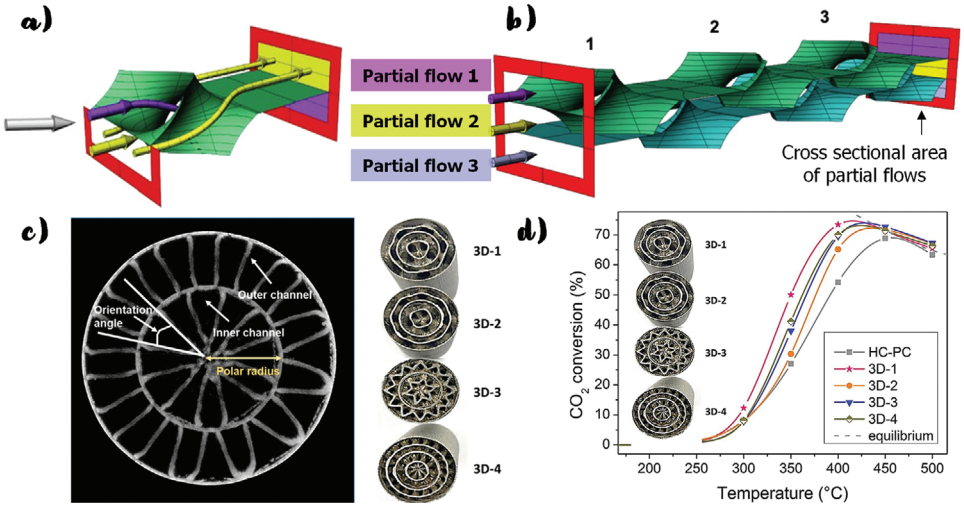

Figure 14. 3D printed catalysts for CO_2 methanation based on pseudo-gyroid geometries: a) illustration of a fluid guiding unit (FGU); b) arrangement of FGUs connected in series and parallel giving a different flow pattern; c) printed structures varying the number and size of the constituting channels; and d) Comparison of the CO_2 conversion at 120 L g,h)$^{-1}$ and a H_2/CO_2 ratio of 4 achieved with 3D printed and honeycomb-parallel channel (HC-PC) monoliths. Adapted with permission.[102]

with minimum SiO_2 formation (30%) were sulfuric acid (15%), potential (15 V), time (15 min), and equilibrium current density (1.5–3.5 A dm^{-2}). Deposition of platinum was realized by wet impregnation, further dried, calcined (at 300 °C for 6 h in He atmosphere) and reduced with H_2 (300 °C for 3 h). SEM images revealed that Pt was homogeneously distributed through the surface and the porous layer. During the reaction, the outlet temperature only increased ≈1 K thanks to the high heat transfer coefficient of the catalyst. Moreover, the catalyst exhibited ≈50% NO conversion. Lapp et al.,[101] developed a monolith with non-intersecting straight radial and axial channels to use as solar receiver/reactor for the dry reforming of methane. For which, they realized LM process using a high temperature alloy Inconel 618 as the raw material. This technique allowed them to fabricate a dense material, however, an acid etching procedure was needed to provide roughness to the surface for the catalyst to adhere. In addition, the 3D printed structure demonstrated good thermal properties and stability allowing its use up to 1200 °C. Alternatively, the catalytic phase deposition may be improved by including additives that augment adhesion of the washcoating slurry. This is the case of the procedure followed by Gonzalez et al.,[102] who prepared monolithic catalysts for the methanation of CO_2. They configured the channels as an arrangement of fluid guiding elements that subdivide the flow and exchange their positions along the channel (**Figure 14a**), returning to its initial position after going through three fluid guiding units (shown in Figure 14b). Different monoliths were produced by changing the number and size of the fluid guiding units as function of the polar radius and orientation angle of gyroid (Figure 14c). To obtain the monoliths, authors used a LM printer with stainless steel powder and realized an annealing post treatment (900 °C in air for 12 h). Slurries of 15% Ni and 0.5% Ru $MgAl_2O_4$-supported were prepared along with deionized water, colloidal alumina, and PVA to adequate their properties for the washcoating. Finally, the catalysts were calcined at 500 °C during 4 h, and the load achieved with this method was around 0.220 g. Further, the improved design showed to benefit the turbulence, mixing, and heat transfer along the monolith, therefore increasing the conversion up to 75% regarding a conventional honeycomb with parallel channels monolith (see Figure 14d).

Contrary to commonly used washcoating method, Cheng et al.[91] proposed a strategy to synthesize 3D graphene (3DG) by LM printing a porous copper structure in which graphene was further in-situ grown through chemical vapor deposition (CVD). The raw material was micron-sized copper powder, mainly of spherical shape which increases the fluidity and packing density compared to polyhedral ones. For the PBF, a Nd:YAG fiber laser of wavelength of 1060 nm was employed, allowing to produce 20 µm thick walls, under nitrogen atmosphere. Moreover, the authors looked for the most effective parameters of laser power and scanning speed to produce a continuous and stable melting to avoid cracks, and deficient or excessive sintering (presented in **Figure 15a–d**), observing good results for 350–450 mm s^{-1} and 180–200 W.

For the CVD growth of graphene, monoliths were heated to 1000 °C under Ar and H_2 for five minutes, then a 30 cm^3 min^{-1} CH_4 flow was introduced into de reactor at ambient pressure over 20 min, and finally the CH_4 flow was stopped, and the system was rapidly cooled to room temperature. XRD patterns of the printed monoliths kept similar to those of the raw material, with a light shift of the diffraction peaks to higher angles because an enhanced residual stress. Also, SEM images (**Figure 16**) showed good bonding of copper powder, EDS and Raman results confirmed the successful growth of graphene with even distribution, and the monoliths exhibited electromagnetic interference and thermal conductivity.

The authors followed similar methodology to produce copper monoliths coated with a grown in-situ diamond film.[89] Before the CVD, some samples were polished by abrasive flow with loading of 90 kg for 12 min to analyze the effect of surface roughness on the coating film. Diamond growth was performed under

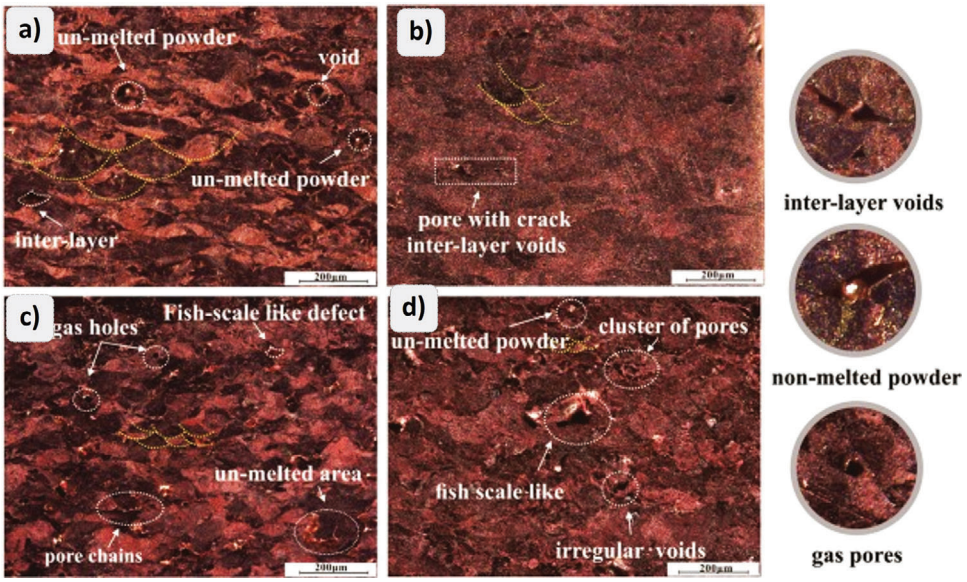

Figure 15. Morphology of copper samples fabricated by LM with various input energy, from excessive to low energy: a) 3000 J mm^{-3}; b) 857 J mm^{-3}; c)285 J mm^{-3}; and d) 128 J mm^{-3}. Reproduced with permission.[91]

CH_4 and H_2 at 2000 °C for five hours. Results showed that the surface roughness benefits the diamond nucleation. Raman and SEM analysis confirmed high density of diamond on unpolished samples. Moreover, excellent thermal conductivity was achieved in all materials, and a maximum compressive strength of 78 MPa was obtained.

4.2. Electron Beam Melting

Another PBF technique is the Electron Beam Melting (EBM) process which follows the same steps that LS and LM, with the difference that it employs an electron beam at sufficient speed to work as a large area heat source to melt the powder material

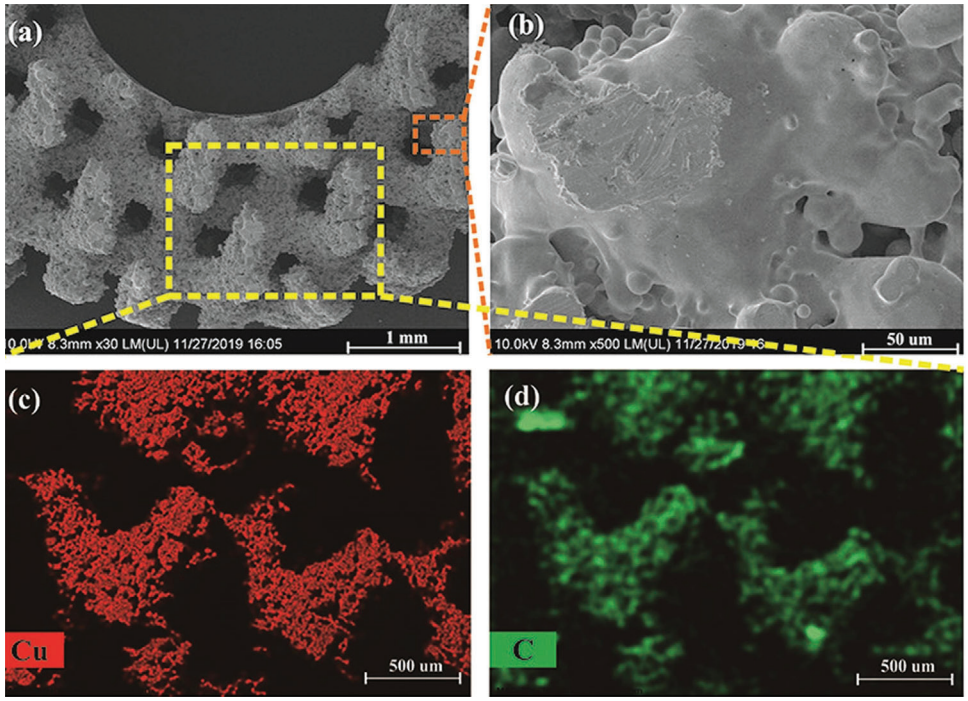

Figure 16. a,b) SEM micrographs of the 3DG/Cu structure; and c,d) EDS analysis of Cu and C, correspondingly. Reproduced with permission.[91]

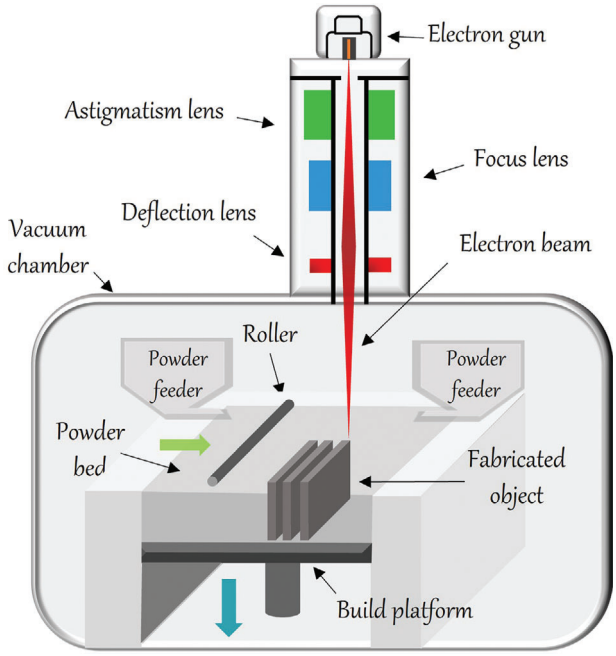

Figure 17. Illustration of Electron Beam Melting (EBM) system.

(**Figure 17**). It is considered more energy efficient since the electron beam has higher plug efficacy regarding the laser beam system.[103]

Nevertheless, EBM has some disadvantages such as the need to operate in a vacuum to prevent air-electron interaction, the powder should be electrically conductive leading to fewer material options in comparison to LS and LM, and the coarse powder need to be pre-sintered.[82,104] These factors lead to rougher surfaces and generally larger minimum feature size compared to laser processing. Besides, it is important to mention that the necessity of removing the non-melted powder may limit the monolithic geometric design and cell density, making it disadvantageous regarding other AM techniques.[105]

EBM technique has scarcely been used to prepare monolithic catalysts, probably, due to its higher requirements. Among the works published in literature (Table S3, Supporting Information), mainly focused on hydrogenation reactions, that realized by Peters et al.[105] may be cited. The authors prepared a Pt on alumina-coated catalyst through EBM for the dehydrogenation of perhydro-N-ethylcarbazole. The electron beam melting process was applied to a gas atomized Ti-6Al-4 V alloy powder under He atmosphere and 2×10^{-3} mbar. Once printed, the excess metal powder adhered to the exterior surface of the structure was removed by "sand" blasting with the same metal powder. For coating, a solution prepared with commercial boehmite powder, dispersal, nitric acid, and a commercial active phase containing Pt was used to immerse the monolith, which was further calcined in air at 500 °C for 6 h reaching a 3.5 g loading. Tests showed a hydrogen release capacity of 1.75 kW with up to 1.12 g_{H2} min^{-1} g_{Pt}^{-1}, as well as a good reproducibility and stability at least for 48 h.

In the same manner that in LS and LM techniques, structures obtained through EBM should undergo pretreatments to prepare their surfaces for the active phase deposition. Such is the case of studies realized by Nguyen et al.[106,107] who have produced different catalysts for continuous flow hydrogenation processes. First, structures were printed by electron beam melting of pre-sintered 316 L stainless steel at 850 °C, and later loaded with Ni or Pd by cold spraying or electroplating, correspondingly. In this case, before the electrodeposition, materials were cleaned and activated to assure even adhered layers of metallic palladium (done by standard galvanostatic procedures). In the other side, nickel powder was sprayed onto the 3D printed monoliths through a plasma Giken PCS-1000 cold spray system, providing a high and uniform surface coverage on the accessible surfaces of the structures. Catalysts exhibited an optimum operating temperature around 120 °C (12 – 20 bar) at which excellent catalytic activity for the reduction of vinyl acetate to ethyl acetate was displayed. In general, produced catalysts resulted efficient and versatile since they also showed good performance in other reaction such as the reduction of alkenes, alkynes, carbonyls, nitriles, and imines.

Kundra et al.[6] 3D printed catalyst from nickel alloys and treated them either with chemical etching or leaching processes to activate their surfaces and use them in hydrogenation of alkanes, aldehydes, and nitro-groups. Inconel and Monel were used as the raw materials (pre sintered at 1050 and 600 °C, respectively) and, after the electron beam melting, they were subjected to etching with Marble's reagent (**Figure 18a–c**) and leaching in ammonium sulphate (Figure 18d–f), respectively, to rise the porosity and partially oxidate Ni and other metals within the alloy. After a further treatment to reduce the oxides obtained, those monoliths were suitable for hydrogenation reactions. As expected, the longer the chemical etching the higher the surface change, which kept the metal ratios the same but increased the oxygen amount due to the oxides formed. On the contrary, the Monel-catalyst resulted with a surface layer richer in nickel (Ni/Cu ratio between 4 and 8) after the leaching process that selectively removed copper, thus in a higher catalytic activity and selectivity toward unsubstituted double bonds.

Using a similar methodology to that followed by Cheng et al.[91] in LM, Knorr et al.[108] combined EBM of Ti-6Al-4 V with chemical vapor deposition and carbide-derived carbon approach to obtain a metallic catalyst covered with microporous carbon, which was further impregnated with platinum, for the hydrogenation of ethene. Nevertheless, prior to SiC deposition an oxidation process (550 °C in air for up to 2 h) was needed to favor the coating. Chemical vapor deposition of SiC was carried out at 950 °C with methyltrihlorosilane as precursor, leading to a surface area of 32 m^2 g^{-1}. Later, the structures with the carbide layer were chlorinated to obtain carbide-derive carbon layer (800 °C for 10 – 30 min), and finally, wet impregnated with a hexachloroplatinum solution to get the 1.83 wt% Pt loaded in the Pt/EBM catalyst. High thermal and electrical conductivity were observed inherent to material nature, as well as high surface area of the carbon coating. Comparing the catalytic activity of the synthesized material with that of a commercial one, the Pt/EBM catalyst presented ≈50% more conversion attributed to the different diffusion length, and to the dispersion and accessibility of platinum.

As shown in the cited studies, PBF techniques allow the direct attainment of metallic structures, which due to their nature exhibit great thermal characteristics and stability, and it is possible to conform them in more complex shapes than those

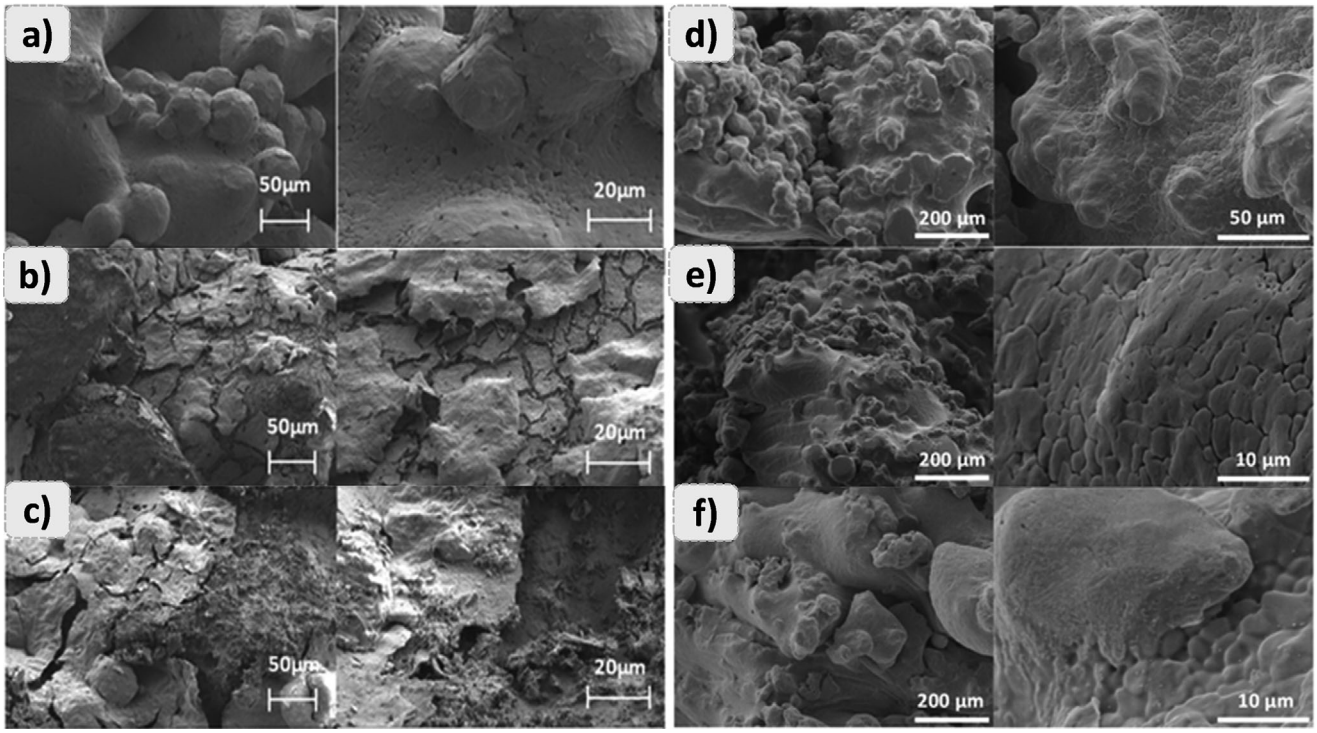

Figure 18. SEM micrographs of nickel alloys catalysts chemically treated: a) untreated Inconel sample; Inconel samples etched with Marble's reagent for b) 2 h, and c) 48 h; d) untreated Monel sample; Monel sample treated with e) 0.2 M ammonium persulfate, and f) 1 M ammonium sulfate. Adapted with permission.[6]

limited by conventional production methods. The principal raw materials used so far are stainless steel and Al, Ni, or Ti alloys. In some cases, it is also feasible to activate the metals after printing and applied them directly in catalytic processes. However, when the loading of an active phase is required, the incorporation procedure is often arduous implying in most of the cases more than one step, therefore, a cost-benefit analysis may be useful to establish its convenience. On the other side, traditional production of metal-based monoliths may include corrugating metal foils, extrusion, or pressing under high pressure which limit the configuration and shape of channels, often with a reduced porosity;[109,110] Likewise, other strategies such as sol-gel process, foaming, and coating over pre-synthesized templates may offer the opportunity to adjust porosity but lack control over the structural configuration.[111–115] Conversely, PBF methods have shown their versatility to generate a wide range of designs that enhance their catalytic activity and selectivity.[91,99,102]

5. Material Extrusion

One of the most popular additive manufacturing processes are the material extrusion techniques, which present advantages like low material wastage, simple operation, and cost-effectiveness.[116,117] These extrusion-based technologies are suitable for employing viscoplastic materials such as ceramic pastes, hydrogels, and thermoplastics, as well as composites as raw material.[118] The printing filaments or semiliquid materials are fed through a nozzle (when using filaments, the nozzle most be pre-heated in order to melt them), and then selectively dispensed onto a support, layer upon layer. These materials are commonly used owing to their low melting temperature and melt viscosity that allow its uniform extrusion.[119] Once the extruded material cools it solidifies again resulting in the final print.

5.1. Direct Ink Writing

Direct ink writing (DIW), also known as direct write fabrication, robocasting, or robot-assisted shape deposition, consists of extruding a paste—known as "ink"—through a fine nozzle that moves in the X-Y direction in a controlled manner to generate patterns for each slice of a CAD model (see **Figure 19**). As the object is built in a layer-by-layer manner, the extruded paste impinges on the previously deposited part and fuses with it due to surface tension. This is a versatile technique that allows to work with a broad range of materials, such as ceramics, polymers, metals, alloys, and composites. Nevertheless, there are some aspects that must be taken into consideration, such as the conditions and characteristics of the ink and the conditions of the printing and drying procedures. Principally, rheological properties of the ink are critical as it needs good fluidity to obtain a smooth and constant extrusion and avoid ink clogging, for which, it must lower its viscosity under the pressure applied during extrusion. Though, it must also recover its viscosity after the deposition to have enough consistence to conserve the shape, prevent structural deformation and the printed structure collapse.[31,120]

The rheological control of the slurry can be achieved by choosing the appropriate binder-material ratio, additives, but

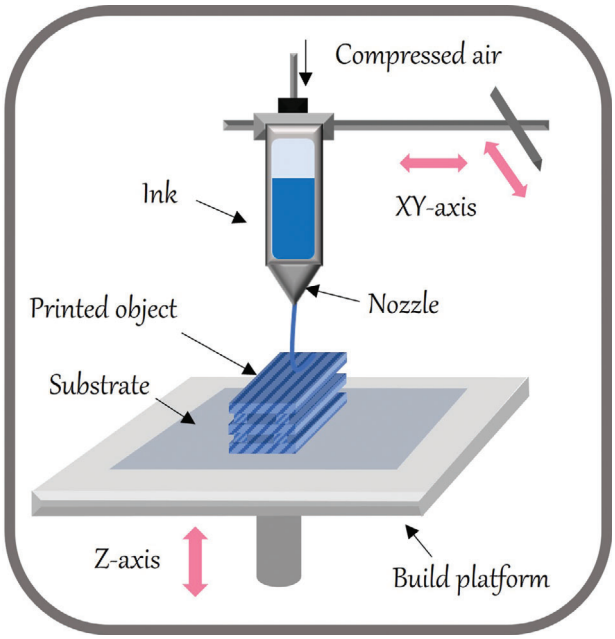

Figure 19. Schematic illustration of Direct Ink Writing process.

also using external stimulus (such as pH, temperature, and magnetic fields).[121] In this sense, additives not only function to obtain the appropriate rheological properties of the slurry but can also provide useful characteristics to the final printed object. Contrary, the binder has been associated to a porosity blockage, therefore, when binders are added in the printing paste there is commonly a calcination step to remove them.[18,20,122–124] The 3D structures are obtained by the disposal of the printing paste through a nozzle by air pressure or mechanical devices, in a layer-by-layer mode, while moving according to a CAD by a robotic arm. The restrictions for the minimum possible print size, and thus cell density, depend not only on the nozzle diameter but on the rheology and ink particle size to avoid nozzle obstruction—this must be at least an order of magnitude smaller than the nozzle diameter to avoid its blockage—.[120,125,126] Once the printing has finished, the structure must be carefully dried to avoid shrinkages, breakages, or deformations. The drying technique, along with the printing speed, diameter of the nozzle, and viscosity of the ink, are the principal parameters that have an impact on the final properties and surface finish.[121,127] It is important to consider that after the drying process, there is usually a shrinkage that change the desired dimension of the 3D object.

To date, this technique is the most extensively used AM technology to directly print monolithic catalysts due to the wide range of possible raw materials, some of them are listed in Table S4 (Supporting Information). Among the large list of materials, ceramics have been largely used for the DIW. Such is the case of the work realized by Hossain et al.,[128] who prepared an amorphous silica monolith by depositing an ink paste made of template-impregnated silica particles, ether solvent, and dispersant. To increase dispersity and homogeneity, the mixture was milled at 2000 rpm, and further centrifuged also at 2000 rpm to drive out the trapped air bubbles. Silica particles adsorbed a considerable amount of water owing to its hygroscopicity; therefore, the optimal solid loading was ≈27 wt%. Printed monoliths were calcined (500 °C for 2 h) and partially sintered (600 °C for 2 h), leading to the formation of micro and mesopores and a S_{BET} up to 981 $m^2 g^{-1}$ due to elimination of solvent and template, as well as a volume shrinkage of 22.6%. The materials compressive strength was ≈0.48 MPa.

Other broadly used materials are the zeolites, which have been applied not only as coating,[129] but, unlike conventional methods, they have also been employed to conform the structure alone or doped with metal oxides. For instance, Li et al.[130] 3D printed HZSM-5 monoliths. The authors also studied the incorporation of SAPO-34 to control their porosity and the density of acid sites and tested them as catalysts for the conversion of methanol to dimethyl ether. The conventionally shaped 3D-HZSM-5 monoliths were obtained by directly writing an ink prepared with HZSM-5 powder, bentonite clay powder, methylcellulose, and water on a Teflon substrate, which were further dried and calcined. The SAPO-34 was grown via secondary growth method by immersing the HZSM-5 monoliths in a water suspension of SAPO-34 and then treating them hydrothermally. The characterization results showed the agglomeration of HZSM-5 caused for the use of binder and the calcination step. The conformation into the monolithic structure promoted a diminution in total surface area regarding powder form due to the addition of less porous binder and pore clogging with the SAPO-34 crystals grown on the HZSM-5. Moreover, whereas the use of binder during the production of the HZSM-5 monolith also affected the accessibility to acid sites, the SAPO-34 growth raised ≈40% the strong acid sites. As result of the reduction of acid sites and the pore clogging, a lower methanol conversion over the monoliths was observed, however, the monolithic configuration helps to increase the selectivity toward dimethyl ether. Authors also employed similar method to incorporate SAPO-34 crystals but changing the zeolite monolith composition and used it as catalyst for n-hexane cracking reaction.[131] To synthesize the conventional honeycomb like zeolite monoliths, HZSM-5 and HY zeolites were used together with the above-mentioned additives to prepare inks for DIW. Then, monoliths went through the same secondary growth procedure. Since the pores of HY are bigger and more accessible to the SAPO-34 solution than those of the ZSM-5, a higher growth of SAPO-34 crystals and decrease of porosity for pore blockage were observed. The XRD analysis showed both, the peaks corresponding to the zeolites ZSM-5 and HY, and the peaks attributed to the CHA framework of SAPO-34. In both cases, the coated monoliths exhibited greater amounts of strong acid sites. Although the monolithic configuration increased the selectivity to light olefins because of a better diffusion of intermediate products, the acidity enrichment boosts the aromatization to benzene, toluene, and xylene (BTX) and diminishes light olefins. Additionally, Li et al.[20,124] synthesized bare and metal-doped zeolite monoliths for methanol transformation. The authors prepared pastes with ZSM-5 powder, deionized water, bentonite binder, methylcellulose as plasticizer, and, in the case of the doped monoliths, metals (Ce, Cr, Cu, Ga, La, Mg, Y, or Zn) in its nitrate form. Conventional honeycomb monoliths were printed on an alumina substrate, dried, and finally calcined to remove the plasticizer, enhance the mechanical strength, and immobilize the metal atoms. The structure and crystallinity of the zeolite were kept, nevertheless, its surface area was reduced, mainly due to the addition of binder.

It was observed some mesopore formation in bare ZSM-5 monolith which was attributed to the decomposition of methylcellulose during calcination, therefore existing a wide size distribution and shapes. However, mesopores clogging with the metal dopants was also detected. By element mapping, homogeneous distribution of metal oxide nanoparticles was confirmed. A better performance of the 3D printed monolith catalyst in methanol conversion regarding its ZSM-5 powder counterpart was correlated to its structure, in which the coke species were fewer generated. Moreover, the Cr, Mg, and Y doping led to higher improvement of methanol conversion, being the catalyst doped with 10 wt% Mg the best catalyst (methanol conversion ≈95%, selectivity to ethylene and propylene of 24% and 33%, correspondingly).

Metal oxide/ZSM-5 or H-ZSM-5 catalysts have been elaborated by several authors following a similar strategy. Lawson et al.[132–135] synthesized this type of catalysts through DIW as an alternative to incipient impregnation for the dehydrogenation of propane, n-hexane cracking, and methanol conversion. ZSM-5 and H-ZSM-5 were selected as catalyst supports owing to their high surface area, pore volume, and acid site density; whilst Ga_2O_3, V_2O_5, ZrO_2, and Cr_2O_3 were chosen as dopants because of their oxidation states and redox properties. For this purpose, the authors prepared several ink pastes including the zeolite ZSM-5/H-ZSM-5 (up to 85 wt%), different amounts and combinations of metal oxides (3.8–30 wt%), bentonite clay as binder, methylcellulose like plasticizer, and distilled water as solvent. After printing, the structures were left to dry at 25 °C and calcined either at 550 or 750 °C for 6 h. XRF spectra demonstrated the control of the loading amounts and good dispersion of the metal oxides. Likewise, XRD spectra exhibited that the crystalline structure of zeolite was not affected by the procedure followed, however, concentrations of V_2O_5 over 2 wt% may cause dealumination of zeolite. The N_2 physisorption results showed the greater loss in textural properties for vanadium and mixed oxides, which has been attributed to a ZSM-5 dealumination during calcination by high concentrations of V_2O_5. Catalysts probed to have excellent activity in the different reactions: the mixed metal oxides monolith produced ≈40% propane conversion, ≈50% CO_2 conversion, and 91% propylene selectivity; Cr-doped catalyst led to 85% n-hexane conversion with high selectivity to olefins and no BTX production; and Ga_2O_3 doped catalyst produced great methanol conversion with dimethyl ether selectivity while the other oxides were more selective to aromatic carbon. Same methodology was followed using $CaCO_3$ combined with V_2O_5, NiO, TiO_2, or Ga_2O_3, to obtain ≈10 wt% metal-CaO doped H-ZSM-5[136]. As previously seen with vanadium, results also suggested a possible interaction between titania and the zeolite, but it exhibited a better dispersion of the metal oxide phase. Though, the crystalline structure of H-ZSM-5 was retained to some degree in all samples, as well as the metal dopants. Those materials, particularly the V-CaO/ZSM-5 presented excellent performance in combined CO_2 capture/oxidative dehydrogenation of ethane (ODHE) conversion (65.2% CO_2 conversion, 36.5% C_2H_6 conversion, with 98% C_2H_4 selectivity). In the same manner, Farsad et al.[137] prepared 3D printed mixed metal oxides-HZSM-5 monolithic catalysts for the oxidative dehydrogenation of propane (ODHP). To do this, they also mixed HZSM-5, bentonite, methylcellulose, water, and different amounts of the metal oxides Ga_2O_3, V_2O_5, and ZrO_2 for obtaining extrudable pastes which were employed in the printing of cylindrical monoliths with woodpile shaped layers. In the case of the paste containing V and Zr oxides the viscosity was low during printing thus the monolith had some imperfections. According to XRD analysis, interactions between Si-OH group and oxides during calcination led to structural changes in the zeolite. Propane conversion was in the same range for all monoliths (30-40%), showing good performance for ODHP reaction (90% selectivity to propylene) thanks to the null affectation of the catalytic activity of the ZSM-5 and a great active sites distribution. The authors noticed the importance of selecting the metal oxides mixture since, for example, the use of the three oxides led to the worst performance as their interactions affected their redox capabilities.

On the other hand, the DIW method has also been applied to some metallic materials. For example, stainless steel (316 L) was used as raw material for producing monolithic catalyst for methanol conversion. The monoliths with different shape configurations produced by Lefevere et al.[129] were evaluated in the methanol to olefins reaction, and they showed a better performance in comparison to packed bed, achieving ≈20% higher conversion. Tubio C.R. et al.[138] proposed a strategy to fabricate a palladium-alumina (Pd^0/Al_2O_3) cermet monolithic catalyst for microwave assisted organic synthesis (MAOS) employing DIW to control composition, surface area (33.2 cm^2 cm^{-3}), shape, and dimensions. The Pd° catalyst resulted permanently active, did not show leaching, was stable, and reusable up to 200 reaction cycles. The ink used was prepared by mixing $PdCl_2$ with Al_2O_3 (for thermal and mechanical stability) in deionized water, then adding hydroxypropyl methylcellulose (HPMC) and polyethylenimine (PEI) to adjust the characteristics of the paste for printing. Later, the samples were sintered at 1500 °C to attain a cermet material in which Pd^0 metallic species were obtained inside and in the surface of the ceramic matrix. SEM, EDS, XRD, TPR, and CO-chemisorption confirmed Pd metal already reduced was well distributed and integrated in the alumina matrix. Monoliths proved to be efficient in organic synthesis because of the synergistic effects of the metal-oxide interfaces. Besides, nanoporous gold catalysts for selective oxidation of methanol to methyl formate were prepared by Zhu et al.[120] following printing, annealing and dealloying processes. Ag-Au composite inks were prepared by mixing Ag and Au clays with organic solvent, and polymeric binder (atomic ratio Ag/Au = 70:30) in a planetary centrifugal mixer for 1 min. To form homogeneous Ag-Au alloys, the printed structures were annealed at 850 °C in air for 12 h. Solvent evaporation creates microporosity (1–10 μm), whereas the dealloying process creates nanoscale porosity (10–100 nm), therefore, the porosity can be adjusted by changing the solvent and polymer binder content. SEM confirmed the uniform nanoporous structure, and EDS showed a ≈2 atomic% of residual Ag. The high frequency leading to good capacitance (10 times larger than powder catalyst), low pressure drop achieved for all tested flows (less than 6.8 kPa), and great catalytic activity (up to 90% methyl formate selectivity) corroborated that the configuration of the printed nanoporous metals improved the mass transport and reaction rate for liquid and gases.

Metal organic frameworks (MOFs) can be listed as usable structural materials of directly ink written monoliths. In this sense, a zirconium-based MOFs monolithic catalyst was elaborated by Young et al.,[123] who dispersed UiO-66 (52 wt%) into

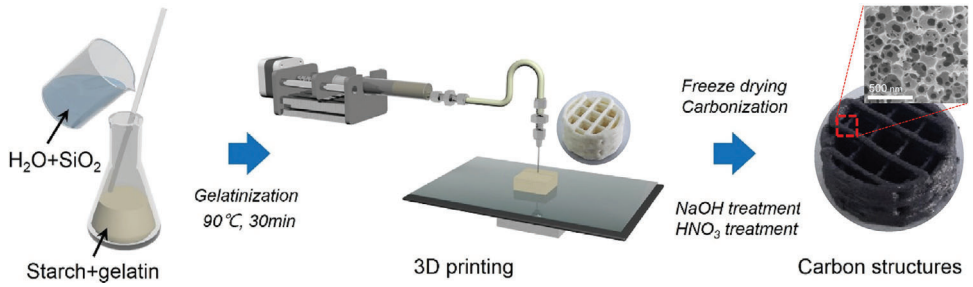

Figure 20. Synthesis procedure of porous carbon catalyst prepared as a replica of SiO_2 template (diameter of 200 nm). Adapted with permission.[139]

a mixture of polymer binders (44 wt%, TMPPTA and EBECRYL 8413), and a photoinitiator blend (4 wt%). Monoliths were UV crosslinked upon extrusion, and further thermally treated at 280 °C for 30 min. With this procedure the final MOF content was ≈74 wt%. Although, heat treated catalyst presented a lower activity in catalytic hydrolysis of methyl paraoxon attributed to a partial degradation of surface active-sites, they have an easier reusability compared to non-structured UiO-66. Also, Salazar et al.[21] prepared cuboidal and cylindrical monoliths with 90° rotated layers of iron-based MOF/SiC which exhibited good performance in the hydroxylation of phenol with H_2O_2. The paste used in the DIW process was obtained with a pre-prepared MOF:SiC powder mixture (2.5:97.5 and 1.0 wt% Fe) combined with high and low molecular weight polyethylenimine, hydroxypropyl methylcellulose, ammonium polyacrylate, and water. After printing, a heat treatment in air 250 °C for 1 h was realized to rise their thermal stability. The MOF/SiC monoliths showed slight electrical conductivity (7 S m^{-1}). Although, the monolith got less conversion of phenol with relation to the powder form due to a low H_2O_2 decomposition rate, this led to a reduced over-oxidation of phenol, therefore, a good selectivity (80%) and yield (20%) to dihydroxybenzene.

Carbon monoliths have also been synthesized through DIW, either by carbonization of templates and precursors, or by introducing carbonous materials within the printing pastes. As an example of the former case, Zhou et al.[139] prepared porous carbon catalysts with adjustable pore sizes by means of DIW structure templates of carbon sources and SiO_2 spheres. A carbonization process at 1100 °C for 2 h in N_2 atmosphere was held to get the carbon replicas. Additionally, washing with NaOH was needed to complete remotion of the SiO_2 templates (process shown in **Figure 20**). SEM images of carbon catalysts showed precise replicas of the SiO_2 templates. This results, together with low shrinkages obtained, suggest that the pore size and structure of the printed replica can be controlled by the SiO_2 template. Selective liquid phase oxidation of benzyl alcohol was used to analyze the activity of carbon catalysts, which reached up to 96% conversion. On the contrary, Jianhua et al.[140] made a printing ink with graphene oxide. They printed a monolith, with woodpile layers, from an aqueous solution of large-sized graphene oxide (20 mg mL^{-1}) which can be well disperse in water thus presenting a good viscoelasticity without the need of additives. The resulting monolith maintained the designed shape, had low density (12.8 mg cm^{-3}), and high electrical conductivity (41.1 S m^{-1}). Other graphene monolith was synthesized by Quintanilla et al.[141], however, they required the use of additives to get a printable slurry. The inks were formulated by adding to deionized water, 36.6 wt% graphene nanopowder (GNP008), 8.8 wt% sodium polynaphthalenesulfonate, 2.3 wt% of polyethylene glycol, and 2.8 wt% of polyehtylenimine. It is important to mention that the characteristics obtained with this paste allowed that, once printed, the structure did not collapse due to an immediate increment in viscosity of about two orders of magnitude. After the printing process, a spark plasma sintering (SPS) treatment was made to increase mechanical integrity. The monoliths resulted with a diminution of the surface area of about 62%, but with a good compression strength (0.1 MPa), which allows to operate them in the reaction conditions. Besides, the crystalline structure of the GNP remained after the synthesis process. These monoliths were evaluated in the catalytic wet peroxide oxidation (CWPO) of phenol, achieving high phenol conversion (85%) but low TOC conversion (around 20%) due to the presence of condensation species. Similarly, Middelkoop et al.[122] printed an advanced catalyst for CO_2 conversion into cyclic carbonates from CeZrLa/graphene mixed oxide nanocomposites. The authors mixed an aqueous solution of methylcellulose (54 wt%), CeZrLa or CeZrLa/GO nanopowders (42 wt%) and a lubrication additive (4 wt%) to obtain an ink for 3D printing. They printed woodpile layered monoliths which were cautiously dried for several days, and heat treated in inert atmosphere at 500 °C to remove binder and keep mechanical and thermal stability. The printed catalysts presented higher conversion and selectivity compared to their powder counterpart, which was attributed to the higher surface area with an improved distribution of the nanoparticles. According to XRD and XPS, it was confirmed that the phases of Ce, Zr, La oxides and CeZrLa were not modified by the deposition method, printing procedure nor by the thermal treatment. Moreover, the catalyst supported on GO showed greater amount of weak and medium acid sites that can be attributed to the GO. Those weak acid sites contributed to a better performance regarding the unsupported catalyst.

As a clear example of the versatility of DIW, the study realized by Long et al.[142] can be mentioned. The authors immobilized composites of e-E. coli/Au (engineered recombinant Escherichia coli/Au nanoparticles) into a biopolymer matrix through DIW. Sodium alignate and gelatin were added with e-E. coli/Au (5.6 – 13.8 wt% Au) to obtain a homogenous and smooth ink slurry for printing monoliths with squared straight channels. Once printed, the monolithic catalysts were introduced into a $CaCl_2$ solution to complete crosslink reaction, and the drying process was realized by freeze-drying at −80 °C. SEM images (**Figure 21**) showed homogeneous distribution of e-E. coli/Au on the surface

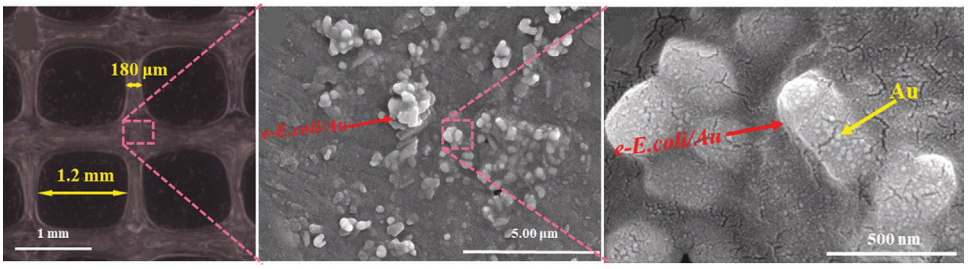

Figure 21. SEM images of 3D printed structure showing the uniform distribution of e-E. coli/Au into the biopolymer matrix. Reproduced with permission.[142]

and confocal laser scanning microscope images (CLSM) exhibited live-cells in the catalyst. Nevertheless, during the application no live-cells were found because of lack of nutrients. This procedure led to a material with a compressive stress of 2 MPa, which was further used in liquid-phase batch reduction of 4-nitrophenol with excellent activity and stability, being useful up to 7 cycles.

Despite the capability of using a vast list of materials and compositions, as mentioned before, the inks rheological properties play a crucial role, not only during the printing process but in the successful conformation of 3D structures (**Figure** 22a). If the formulated slurry does not present the needed characteristics, after its deposition some object deformation can occur (Figure 22b), as noted by Mendez et al.[23] who fabricated TiO_2 square-lattice double-diagonal structures by means of robocasting with a paste made of TiO_2 P25 and deionized water. Although the consistency of the paste allows the proper extrusion to form the catalyst, after the deposition a pronounced smash between layers may be observed because of the material self-weight (Figure 22c). Additionally, the porosity highly decreased due to compaction. These materials were evaluated in the photocatalytic degradation of acesulfame under UV–vis irradiation. Although photocatalysts worked for the degradation of acesulfame, they presented a lower reactivity regarding powder form due to a decrement in the active sites that are illuminated since the smashing of the layers. Therefore, the particle size and solid content are taken into consideration, as well as some binders, plasticizers, and other additives are commonly used to adjust the slurry characteristics.

The binders employed for the preparation of inks affect not only the rheology of the paste, but the drying and calcination processes requirements, and the properties of the final structure. This was corroborated by Lefevere et al.[125] who analyzed the effect of the binder system in the 3D printed structure properties using ZSM-5 as raw material. They studied the bentonite, colloidal silica, and aluminophosphate binders, within a mixture of binder with water (35 wt% single or binary binder system 50/50) and zeolite (65 wt%). Bentonite resulted to give better shear-thinning behavior regarding aluminophosphate and silica (low viscosity at high shear rates and vis versa). In general, the porosity of the zeolite was reduced after its conformation in the monolithic structure due to pore blocking with the binders. Moreover, the results obtained suggest that pore size distribution is related to the particle size of the binder used and the smaller the particle size, the smaller the pores. The mechanical strength and acidity are also dependent of the binder, achieving superior properties with the aluminophosphate. Lefevere et al.[143] used the methanol to olefins reaction to study the importance of binder and 3D printing architecture on catalytic properties without changing the basic zeolite starting material. Even though all the 3D printed catalysts showed lower activity regarding the pure zeolite, bentonite and silica single binder systems achieved good conversion of

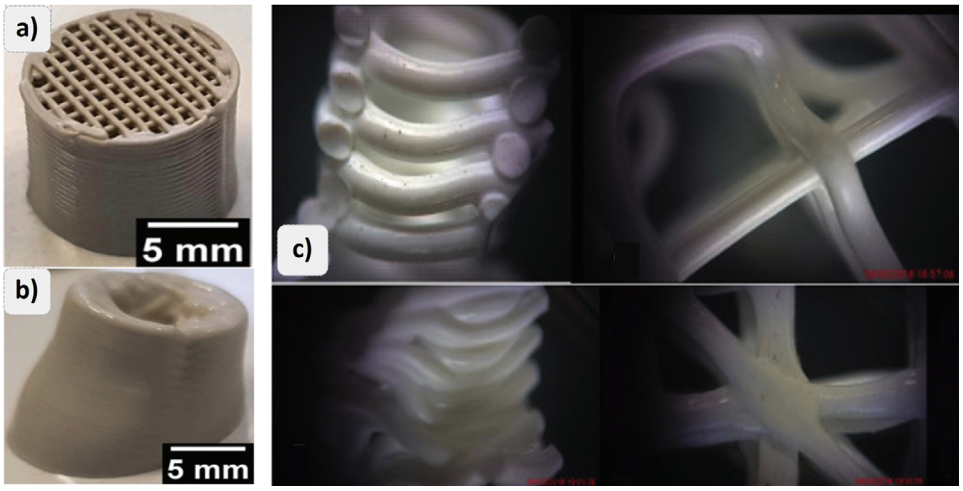

Figure 22. Comparison of the printing result from: a) an adequate ceramic printing ink, and b) an ink with non-adequate rheological properties; c) smashing during the layer deposition because of the self-weight of the catalyst (TiO_2 monolith). Adapted with permission.[23,127]

≈90%. This decrease in activity is related to a diminution of area, diffusivity to the active sites due to porosity, and acid strength. The selectivity of the reaction was influenced by the active surface and acidity whereas the stability and activity were affected by composition as well as porosity, fiber thickness, and stacking of the layers. For this reason, the fewer strong acid sites and lower micro/mesoporosity acquired with the aluminophosphate binder led to a better selectivity toward the desired products. In relation to the binary binder system, all sample exhibited almost full conversion at high temperatures, but they present differences in selectivity and stability.

Within this context, the mainly used binders are bentonite, alumina, and polymeric binders—such as polyester acrylates—(as presented in Table S4, Supporting Information). However, the former turns out to be the most employed owing to its ability to provide mechanical strength and thermal stability. On the other hand, methylcellulose is the most widely used plasticizer due to its ability to improve viscosity and impart pseudoplasticity to the inks. Nevertheless, viscosity has been also adjusted by adding hydroxypropyl methylcellulose, polyethylenimine, or polyethylene glycol. Even when binders are necessary/useful to form the monolithic structures, their incorporation leads to a reduction of the surface area compared to powder raw material.[131–135,137,144] Furthermore, agglomeration of particles, blockage, and diminution of accessibility to active sites has been also associated to the binders.[130] Conversely, some mesopore formation has been ascribed to the methylcellulose decomposition during thermal treatments.[20,124]

In addition to the incorporation of binders, the inks rheological characteristics may be also adjusted by applying different external stimulus including temperature, pH, and light. This alternative was implemented by Elkoro et al.[145] who corrected the slurry characteristics by changing the pH and the printing temperature. To obtain a nanotitania monolith for photocatalytic degradation of acetaldehyde, printable slurries were prepared by adding titanium (IV) oxide powder to water (different solid/liquid ratios) and adjusting the solution pH between 0 and 7. Maximum titania content was achieved when pH was ≈0.3. This decreasing pH tendency is ascribed to a rise of the number of protons adhered to nanotitania surface. Materials prepared at pH ≤1 and T ≥150 °C did not present appreciable degeneration, whereas for pH >2 or T <150 °C some cracking, and disaggregation were observed. The use of thermal treatment increases the rutile content and particle size being greater for acid pastes. Ultraviolet-visible absorbance spectra showed a shift to higher wavelengths that, along with a decrease in band gap, suggested the acid treatment improves the visible light absorption of materials. This method was selected since the absence of binder avoids the decrease in surface area and leads to a better interaction of light with the catalyst, which is fundamental for photocatalysis. Likewise, Lawson et al.[132–135,137] employed temperature increase to formulate their inks. They mixed zeolite (ZSM-5 or H-ZSM-5 ≤ 85 wt%), with aqueous solutions of various proportions of metal oxides (from 3.8 to 30 wt%), methylcellulose, and bentonite clay. The mixtures were shaken, then rolled at 20 rpm for 48 h at 25 °C to homogenize, and later densified at 400 rpm at 60 °C for ≈3 h to achieve a printable rheology. In some cases, this external stimulus needs to be applied together with additives. For example, Zhou et al.[139] prepared a DIW slurry by ultrasonic dispersion and magnetic stirring at 90 °C of a mixture of carbon sources, monodispersed SiO_2 spheres, starch, gelatin, and distilled water. Once the mixture was completely gelatinized, it was cooled down to 70 °C for the printing process. The SiO_2 spheres were employed since they acted as a hard template, but also increased the viscosity of the slurry, and augmented the strength and reduced the shrinkage of materials (≈16%). In this regard, the printing conditions must be also controlled to maintain the desired characteristics and ensure the final product stability. In the previously mentioned example, Zhou et al.[139] held the extrusion process at 70 °C to keep the desired rheological characteristics of the slurry, obtaining structure templates for carbon monoliths.

Light has been applied during printing for curing pastes containing photoinitiators. As an example, monoliths produced from a mixture of UiO-66 particles, polymer binders, and photoinitiator, were crosslinked with a 365 nm UV light source upon extrusion.[123] This treatment provided structure retention for their immersion in different solvents. To further improve their stability and porosity, monoliths went through a thermal treatment at 280 °C during 30 min that degraded the polymeric binder and photoinitiator. Therefore, N_2 physisorption analysis showed the expected microporosity of UiO-66. Similarly, De Hazan et al.[146] synthesized 3D ceramic structures for photocatalytic decomposition of formaldehyde. The ink pastes were made by milling α-Al_2O_3 or hydroxyapatite powders with monomers used to achieve high solid loading and adjust viscosity (4-hydroxybutyl acrylate, polyethylene glycol diacrylate, bisphenol A diacrylate, and/or polyethylene glycol methacrylate), together with surfactant 2-[2-(2-Methoxyethoxy) ethoxy] acetic acid (TODS) to enhance particles dispersion, and photoinitiator, until homogeneous mixture was achieved. Those pastes were used to print monolithic catalysts and, for curing the resin, every two layers the deposition was stopped, and the piece was exposed to a 100 W UV lamp for two minutes. To evaluate the effect of the curing atmosphere, some materials were cured under air and some other under argon, being the latter in which structures presented less cracks and smoother surfaces after sintering. Monoliths underwent subsequent thermal treatments to remove additives and densify the structure. Later, monoliths were dip-coated with a TiO_2-surfactant solution and heated to 500 °C to remove the surfactant. Authors observed that, besides of the ink characteristics, the printing velocity and fiber to fiber spacing influence the fiber deformation during/after deposition, thus the higher velocity and the lower spacing lead to fewer deformation. The structures were shaped after printing by rolling the flexible Al_2O_3/polymer lattices. The printed materials showed similar photocatalytic activity to that of the TiO_2 powder in formaldehyde decomposition, therefore, the conformation in 3D structure did not affect its properties.

Besides, DIW is generally utilized for directly producing catalysts, often including the active phase into the slurry for printing the structure without the need of additional steps.[4,123,147] Therefore, DIW technique allows to rise the loading of active material per volume regarding coated monoliths (65 vs 33.5 wt%) as pointed out by Lefevere et al.[125] In this case, Ni/Al_2O_3-based monoliths for CO_2 methanation were developed by Middelkoop et al.[18] To get the active phase within the structure, Ni/Al_2O_3 catalyst was mixed with bentonite and alumina-based binders to produce the ink pastes. Those pastes were extruded to form

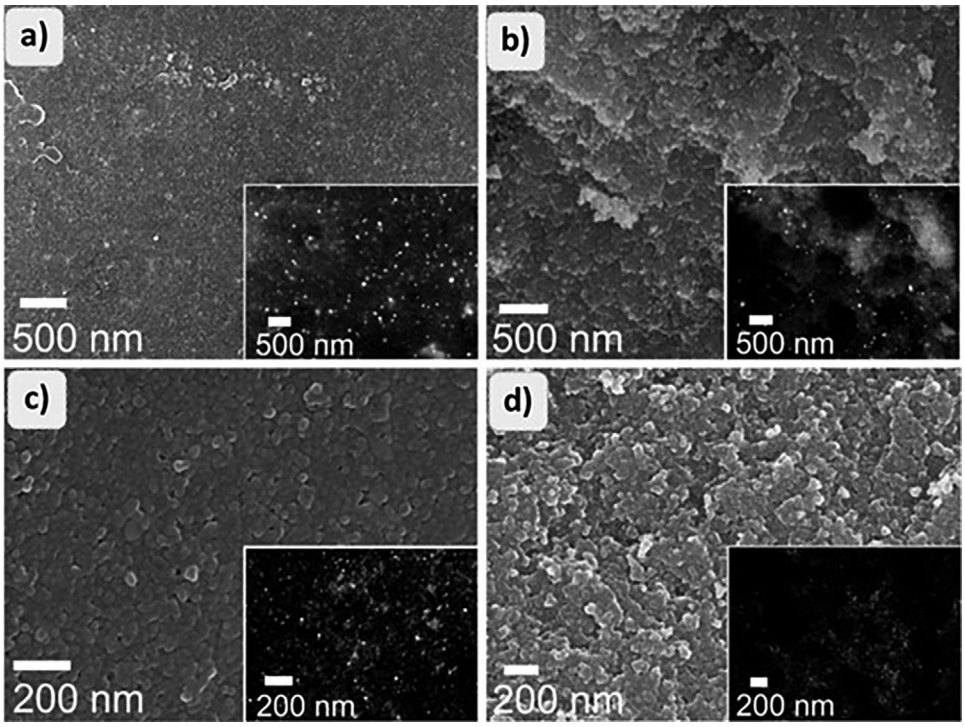

Figure 23. SEM images of the surfaces and cross sections of the Au/TiO_2 monoliths. a) surface of a pre-impregnated Au/TiO_2 monolith (Au 1 wt%); b) cross section of the pre-impregnated Au/TiO_2 monolith (with Au 1 wt%); c) surface of a post-impregnated Au/TiO_2 monolith (Au 0.1 wt%); d) cross section of a post-impregnated Au/TiO_2 monolith (with Au 0.1 wt%). Insets correspond to the same sample areas obtained using a backscattered electrons detector, revealing Au NPs as bright dots. Reproduced with permission.[17]

tetragonal monoliths with mesh pattern which, after a 500 °C treatment, presented an increase of ≈30% in specific surface area. The peaks corresponding to γ-Al_2O_3 phase were not clearly observed within the XRD diffractograms as they overlapped with the nickel aluminate $NiAl_2O_4$ phase present because of the nickel oxide-support interaction. Compared to Ni-alumina pellets and beads, structured catalyst in monolithic shape resulted in a greater CO_2 conversion (≈80%, ≈20% more than beads, and similar to pellets), and methane selectivity (≈86%, ≈5 and 11% more than beads and pellets, correspondingly) showing that the catalyst configuration is of high importance in their performance. Nonetheless, upon long exposure to high temperatures (450 °C) catalysts exhibited some shrinkage affecting their surface area. In like manner, metal-doped ZSM-5 monoliths for methanol to olefins conversion were prepared by including 10 wt% of metal precursors into zeolite, methylcellulose, and bentonite clay mixtures.[20,124] The incorporation of metal precursors—that were the nitrate form of Ce, Cr, Cu, Ga, La, Mg, Y, or Zn—in the printing inks eliminates the additional step of ion-exchange or impregnation commonly used for doping zeolite.

Moreover, Elkoro et al.[17] produced Au/TiO_2 monoliths by means of the DIW technique following two different strategies, impregnating the TiO_2 with Au nanoparticles (Au NPs) before or after the printing process. For the post-printing strategy, an extrudable paste was prepared by mixing P90 TiO_2 with HCl. After printing, the structure was dried, calcined, and impregnated with an Au NPs toluene suspension for a later thermal treatment. On the other hand, for the pre-printing method, the P90 TiO_2 was impregnated with the Au NPs toluene suspension, followed by the same thermal treatment and procedure for obtaining the printing paste and monolithic structure. As observed by SEM (**Figure 23**), the TiO_2 dimensions were similar for both materials. Nevertheless, the materials impregnated pre-printing presented a homogeneous distribution of the Au NPs both in the surface and cross section (Figure 23a,b), while in the post-printing monolith a decrease of the Au NPs concentration along the cross section was observed (Figure 23c,d). This diminution is attributed to the pore size between TiO_2 nanoparticles that reduced the Au NPs suspension diffusion during impregnation, hence the Au NPs remained concentrated in the surface. Also, according to XPS analysis, to attain a similar Au/Ti surface ratio the Au content needs to be more than one order of magnitude higher in the pre-printing method. Considering that the photocatalytic reaction occurs mainly at the surface, the impregnation post-printing route turns out to be the best for a good performance and to save materials.

Aslam et al.[148] also compared both methodologies for obtaining zeolite-based catalysts for syngas to alcohols conversion. In the first case, ZSM-5 zeolite powder was impregnated with ammonium molybdate tetrahydrate, cobalt (II) nitrate, and potassium nitrate prior to the preparation of the ink with silica and bentonite binders. Nevertheless, the monolith had low surface area and collapsed before achieving the reaction conditions. In the second case, zeolite was mixed with the binders and the viscosity of the slurry was adjusted with starch. Once printed, the monolith was dried, calcined, and immersed in a solution of metal precursors with glucose for hydrothermal synthesis, which was further dried and calcined. In this approach, the inorganic binders allow to uniformly structure a zeolite monolith that

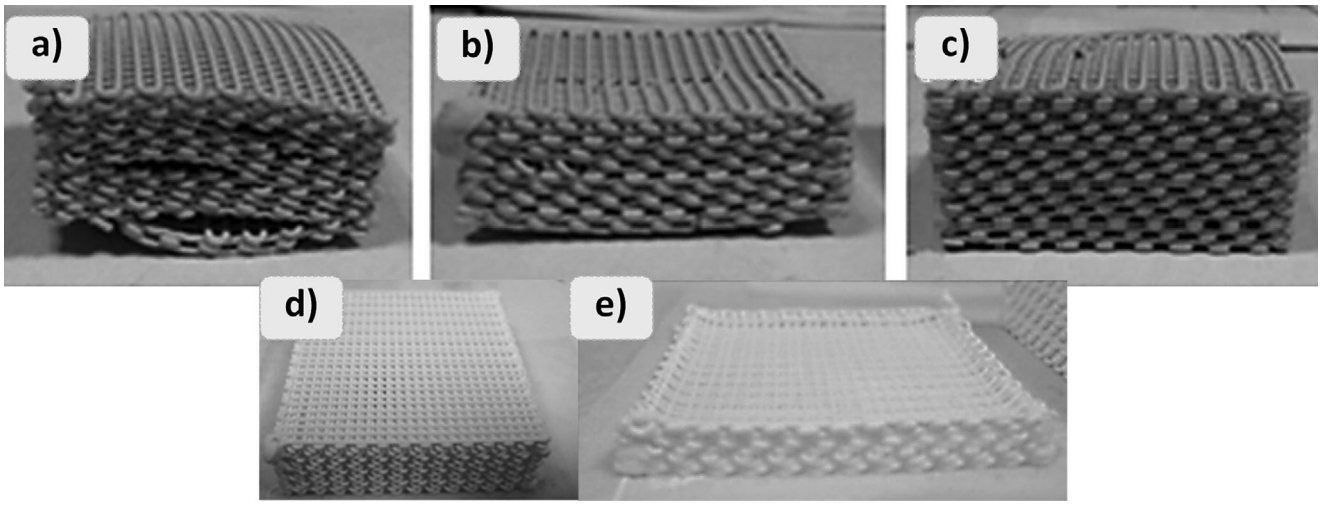

Figure 24. Effect of the drying process on the deformation of porous ZSM-5 materials: structures containing bentonite binder after a) fast drying with heating lamp, b) freeze drying, and c) slow drying in controlled atmosphere (80% relative humidity, RH, and 20 °C); structures containing single silica binder after d) fast drying with heating lamp, and e) slow drying within a regulated environment (80% RH and 20 °C). Reproduced with permission.[125]

remained intact after the hydrothermal treatment. The metal precursors growth homogeneously and a synergism between molybdenum and cobalt active sites was corroborated. Also, the diffusional limitations were reduced over monoliths regarding powder, since they provide better access to catalytic active sites, leading to higher CO conversion.

Once printed, 3D structures must go through a drying process before being subjected to further post treatments. Special attention should be paid to this step due to its relevance in avoiding cracks, imperfections, or breaks in the materials, as exhibited in **Figure 24**. Nevertheless, the drying procedure varies according to the raw material and composition of the inks. In this regard, Lefevere et al.[125] noted that the drying method depends on the characteristics of the binder system used, as they observed in the fabrication of ZSM-5 structures with three different binders (bentonite, aluminophosphate, and silica). In the case of bentonite, since it adsorbs high amounts of water, a fast drying led to ruptures in the structure thus a slow controlled drying at 20 °C helps to avoid defects (Figure 24a–c). On the other hand, aluminophosphate and silica pastes had low viscosity and needed speedy drying to quickly lose water and, therefore, increase their viscosities to retain their geometry without cracks (Figure 24d,e). However, regarding aluminophosphate and silica, bentonite binder leads to a greater shrinkage due to the water lose after drying.

Several drying methods have been used to avert defects in the monoliths. For instance, drying at room temperature usually between 12 and 48 h has been used for materials based on zeolites, ceramics, and some metals.[20,126,132,137,138,148–151] Temperatures over 80 °C have been used to dry monoliths composed of carbonous materials and some metal oxides within few hours.[23,128,145,152] Contrary, longer drying was required for 3D printed structures containing Ni/Al_2O_3 which were placed in a humidity chamber for a week maintained at 85% RH and 25 °C.[18] In some other few cases, such as the e-E. coli/Au and the SiO_2 template for carbon monolith, the authors applied a freeze-drying procedure with temperatures between −80 and −50 °C, to prevent damage within the fragile structures.[139,142] Along with the drying method, choosing adequately the build platform material is also important for conserving the 3D printed objects without defects. Glass,[17,23,152] alumina substrate,[21,125,141,153] aluminum foil,[146] and Teflon[130,134,136,154] are some examples of the build platform materials used for the deposition during DIW, which facilitate the removal of 3D structures, allow a homogeneous drying, thus avoid cracking. Different materials such as silicon and polytetrafluoroethylene (PTFE) films are barely utilized to prevent slippage and ease post-treatment without manipulation of soft pastes, for example those of titania and Au NPs.[120,145]

As result of drying and applying some stabilization treatments, most of the authors have noticed a certain shrinkage percentage which is normally around 10%. However, it depends on the whole fabrication process, therefore shrinkage values from ≈0.4 to almost 40% have been reported.[125,155] In that respect, Román-Manso et al.[156] synthesized silicon carbide monoliths by means of the DIW technique, analyzing the effect of the paste composition in the final structure. They employed three different ceramic powders (submicron-β-SiC: β20 and β7; and nano-β-SiC: N20) together with Al_2O_3 and Y_2O_3 as sintering additives, polyethylenimine aqueous solution as solvent, methylcellulose as viscosifier and ammonium polyacrylate as flocculant. The smaller the particle of the raw material the fewer solid content in the ink. Despite the difference in solids content, the three inks had a highly shear thinning rheology allowing its extrusion in the shear rate region of 30–70 s^{-1} and keeping its shape after deposition due to its great strength. Results also suggested a relation between solid content and shrinkage, the lesser content of solids the bigger shrinkage (28% in N20 regarding 19% of β7 particles). Thus, shrinkage is an important factor to take into consideration when designing the monoliths so, once finished the whole process, the catalyst can be obtained with the desired dimension.

In another aspect, a post treatment is often carried out on monoliths to stabilize them. For example, during the synthesis of graphene monoliths Jianhua et al.[140] realized a reduction process with hydroiodic acid to avoid cracking during thermal treatment caused by rapid liberation of volatile gases (1000 °C in

nitrogen). Moreover, calcination or sintering processes are used either to stabilize the material, enhance its mechanical strength, or foster its catalytic activity. This is the case of the 3D printed Al_2O_3 catalyst prepared by Azuaje et al. to act as Lewis acid in Biginelli and Hantzsch reactions in the absence of solvents.[157] The authors directly produced a woodpile layered monolith by extruding a paste made of Al_2O_3 powder, water, dispersant Darvan 821A, hydroxypropyl methylcellulose, and polyethylenimine. The structure was dried and then sintered at 1500 °C in air to remove solvents and polymers of the ink, improve its mechanical strength, and increase its catalytic activity by increasing its Lewis acid character. The morphology and composition remain the same after 10 use cycles as corroborated by SEM and XRD. The monolithic catalyst displayed a 15–23% yield increment regarding alumina powder and 20–35% comparing to catalyst-free conditions, and this activity remained after ten usage cycles. In addition, monoliths led to a complete consumption of the reactants in short times (20% the time of uncatalyzed system) without side products generation despite a lower porosity. Similarly, Tubío et al.[144] synthesized Al_2O_3 structures with immobilized cooper for different Ullmann reactions. The synthesis consisted of printing by DIW a paste made with Al_2O_3 powder dispersed in an aqueous solution of copper (II) nitrate, polyethylenimine, and viscosity adjusted by adding hydroxypropyl methylcellulose. The woodpile structure was dried and sintered at 1400 °C to obtain a high mechanical strength monolith. The sintering process led to the transformation of $Cu(NO_3)_2$ to CuO and $CuAl_2O_4$ which was visible with the color change and corroborated in XRD patterns. A portion of the metal is lost during the sintering because it diffuses through the structure and remains adsorbed on the supporting plate, hence a final copper load of 2.3 wt% was attained. The SEM images showed a dense group of alumina crystals without open meso or microporosity, and a laminar structure of the copper oxide phases. Despite its low copper loading (regarding 5–10% used in analogous systems) complete conversion was observed in short time (2 h), therefore, the catalyst presented an excellent activity, no leaching, and stability after 10 usage cycles.

In the same manner, Quintanilla et al.[153] studied the immobilization of metals (Fe nanoparticles) within the structure of ceramic (SiC) honeycomb monoliths. They printed on alumina substrate an ink composed of Fe/SiC particles, deionized water, and organics for adjusting pseudoplastic behavior. After the printing process, catalysts were heat treated at 600 °C in air for 2 h to completely burn-out the organics. Later, a spark plasma sintering (SPS under Ar at 1000–1500 °C) was applied in some samples to increase mechanical integrity and induce differences of porosity. The results showed that the SPS was crucial to diminish Fe leaching, nonetheless, as the SPS temperature increased the porosity decreased thus the accessibility of Fe, reducing the catalytic activity. Danaci et al.[151] manufactured copper monoliths by 3D printing a paste made of copper powder (14-25 µm) and hydroxypropyl. After drying and calcining at 550 °C the printed samples, authors followed two methodologies: 1) conventional sintering at 880–1000 °C for 5 hours in N_2 or N_2:H_2 atmospheres; or 2) spark plasma sintering in vacuum of 100 Pa. Later, sintered copper structures were coated with a solution of polyvinyl alcohol (PVA), acetic acid, water, silica and Ni/Al_2O_3 active phase, and finally calcined at 500 °C for 2 h. When using temperatures close to the melting temperature of copper strong bonds were attained together with a reduction in porosity. The reducing atmosphere used during sintering helped to minimize oxide content in the fibers and to obtain denser copper fibers. The copper oxides layer on the surface led to a reduction of coating adhesion. All monolithic samples showed a CO_2 conversion as high as that of the powder catalyst (50%) at 400 °C with a slightly higher selectivity (≈98%), and higher stability for 80 h time-on-stream.

Apart from calcination and sintering processes, some materials needed different treatments in preparation for the subsequent catalyst loading. As an example, prior to the growth of MOFs through hydrothermal reaction, ceramic monoliths fabricated by Liu et al.[154] underwent an alkaline etching to withdraw SiO_2 nanoparticles from the surface and, thereby, creating additional pores. Then, monoliths were coated with polydopamine via self-polymerization of dopamine and treated through hydrothermal process for in situ MOFs growing.

When the catalytic compound was not included in the ink, it was mostly deposited on the structure by dip-coating. In some cases, usually for metals with smoother surface, within the coating solution different additives (particularly polyvinyl alcohol, silica, and methylcellulose) were included to increase adherence of active phase.[129,150,151] To give an example, the ZSM-5 coating of a stainless-steel monolith was attained by adding 1 wt% methylcellulose and 1 wt% colloidal silica to an aqueous coating slurry containing 30 wt% ZSM-5.[129] The sintered structures underwent a washcoating procedure, followed by drying and calcination at 550 °C to remove organic compounds. The addition of silica was necessary to increase viscosity and reduce the weight loss of the coating from 47 to 5 wt%, moreover, the deposition of zeolite augmented 80% due to an increase in contact between particles and support. The particle size of the zeolite also influenced in the loading, the smaller the particle the higher the load.

Notwithstanding, in addition to washcoating different active phase deposition techniques including electrodeposition, hydrothermal reactions, and chemical surface modifications, have been tried. For instance, Lin et al.[152] produced electrocatalyst by 3D printing polyethyleneimine cross-linked oxygenated carbon nanotubes (O-CNT) with further nickel electrodeposition. The ink slurry containing the O-CNT, PEI, and acetic acid was deposited at room temperature onto glass wafers. After printing, samples were dried at 100 °C and calcined under nitrogen atmosphere (450–650 °C) for 1 h, then the nickel was electrodeposited, and samples were again dried but at 70 °C in vacuum. Element mapping confirmed uniform distribution of C, O, and Ni in the outer surface (**Figure 25a**). FTIR showed CNT were cross-linked with PEI in the monolith, whereas XPS, XRD, and Raman results showed that this loading methodology acquired nickel deposited in form of Ni and $Ni(OH)_2$. Moreover, D and G bands were observed in the Raman spectra, and I_D/I_G ratios confirmed more defective carbon generation with higher temperature annealing. The monolithic catalyst thermal treated at 650 °C presented more carbon defects which acted as active sites for alkaline hydrogen evolution reaction.

Fumed SiO_2-based thixotropic inks were used in direct ink writing by Liu et al.[154] to further in situ growth of MOFs for catalytic degradation. Once printed materials were left to dry at ambient temperature for 12 h, then further dried and heated at 900 °C to form hierarchical porous ceramics (HPC). Before the MOFs growth, monoliths went through a basic etching

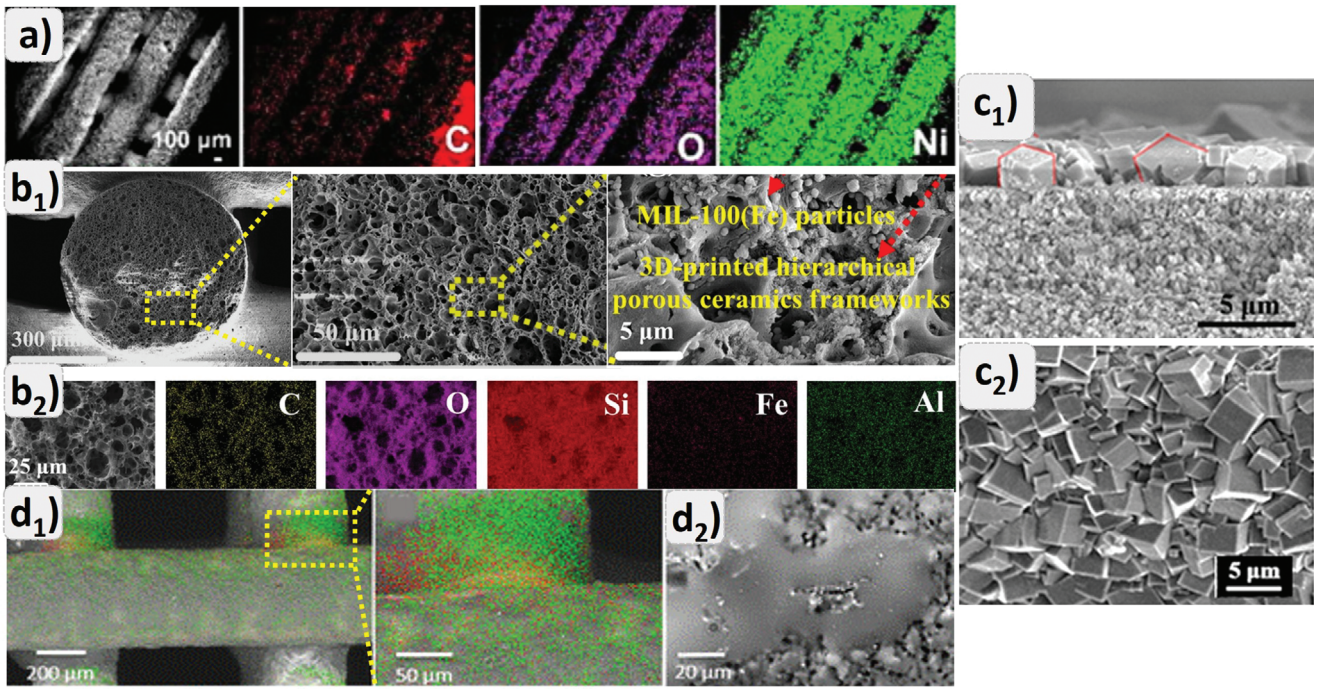

Figure 25. Images of active phases incorporated in 3D printed supports following different strategies: a) Elemental mapping of carbon monolithic catalyst loaded with nickel by electrodeposition (named as 3DPC-650@Ni/Ni(OH)$_2$; b$_1$) SEM, and b$_2$) EDS images of hierarchical porous ceramic structure hydrothermally treated to in situ MOFs growth; c$_1$) lateral and c$_2$) top view images of the load of SAPO-34 grown through hydrothermal treatment—SAPO-34 cubic crystals on 3D-HZSM5 monolith surfaces, marked with red frames—; d$_1$) EDS and d$_2$) SEM images of PI-Pd composite deposited on silica monolith surface by chemical modification. Adapted with permission[130,152,154,155]. Additionally, Sanchez et al.[27] also realized a similar procedure to generate monoliths with immobilized cooper and palladium. In this case, the functionalization consisted of a surface activation with H_2O_2, followed by a silanization with (3-aminopropyl)trimethoxysilane (APTS) or [3-(2-aminoethylamino)propyl] trimethoxysilane (AAPTS) to modify the material surface preparing it for the final metalation to immobilize Cu or Pd, respectively. It was also corroborated that the Cu and Pd loaded (0.6 mg and 1.6 mg, respectively) were present only on the surface of the monoliths with a homogeneous distribution. The leaching of Cu and Pd was negligible, representing less than 0.07%.

to remove some SiO_2 nanoparticles of the surface and form more pores and coated (by dopamine self-polymerization) with polydopamine (PDA). Finally, a modified hydrothermal reaction using a MIL-100 (Fe) precursor solution was carried out to form the 3D printed HPC-MOFs. The successful growth of MOFs on HPC was confirmed by XRD analysis. SEM images confirmed that the structural integrity was maintained after sintering and hydrothermal treatment, whereas C, O, Si, Fe, and Al elements were evenly distributed into the architectures, according to EDS results (Figure 25b$_{1\text{-}2}$). The HPC-MOFs displayed excellent catalytic degradation efficiency (≈97%) and reaction rate constants (0.16 – 0.29 min^{-1}) for different organic dyes. In same manner, Li et al.[130,131] investigated the integration of SAPO-34 in the surface of 3D printed monoliths of HZSM-5 using the secondary growth technique. This methodology consisted of dipping the HZSM-5 supports in an aqueous SAPO-34 suspension and then apply a hydrothermal treatment. A homogeneous and dense growth of SAPO-34 crystals over the HZSM-5 surface was confirmed by SEM (Figure 25c$_{1\text{-}2}$).

In another way, a chemical surface modification was used to obtain monolithic catalysts with immobilized palladium to test in the Suzuki reaction. Sanchez et al.[155] employed the DIW technique to print a silica monolith whose surface was further chemically modified. The silica monolith was generated from a paste of SiO_2, poly(vinyl butyral-co-vinyl alcohol-co-vinyl acetate) (PVB-PVA-PVAc, 80 wt% vinyl butyral), polyethylene glycol and 2-propanol. Posterior to printing, the monoliths were dried, deagglomerated (400 °C) to remove solvent and polymers, and sintered (1500 °C) to attain mechanical and chemical stability. Later, the monolith underwent a chemical surface modification via submersion in a solution containing polymide resin, $Pd(AcO)_2$, and anhydrous N,N-dimethylformamide (DMF). The authors selected this strategy to deposit the catalytic species only in the surface of the monolith since metal introduction inside the mass of the support (without porosity, 0.3 m^2 g^{-1}) would not be accessible to the reagents, thus representing an unnecessary expense. As confirmed by SEM, PI-Pd composite was deposited on the monolithic silica surface and carbon from the resin and Pd (1.6 mg Pd) were present exclusively on the monolith surface (presented in Figure 25d$_{1\text{-}2}$). The catalyst was stable with almost no changes in its activity after 10 cycles of use, moreover, negligible leaching of Pd was detected.

The DIW technique has demonstrated its advantages compared to traditional methods for directly producing monolithic catalysts. Among these advantages, its compositional versatility expands its capability to generate a large range of materials not achievable through usual extrusion, pressing, or corrugating foil techniques. In this regard, the technique allows for the

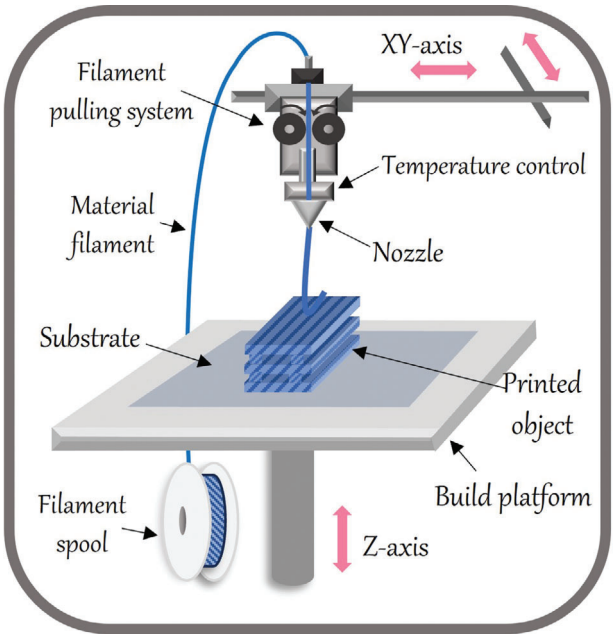

Figure 26. Schematic illustration of the fused deposition modeling (FDM) technique.

incorporation of additives, thus altering the characteristics of the catalysts produced (e.g., porosity, chemical or mechanical strength, etc.). The incorporation of active phases within the ink paste is another alternative presented in this method and may be considered depending on the porosity and availability they will have for the reagents during its application. Additionally, the generation of complex structures, a general benefit of AM technology, is also proved.

5.2. Fused Deposition Modeling

Fused deposition modeling (FDM), also named as fused filament fabrication (FFF), is one of the most employed AM techniques.[158] In FDM the raw material filament is unwound from a reel and then supplied to an extrusion nozzle. The filament reaches its melting point as it passes through the nozzle, which accurately extrudes and deposits it on the print bed. The extruder moves in the X-Y direction over the build platform according to the required geometry while extruding the plastic to form each layer (**Figure 26** presents a schema of FDM system).

It should be mentioned that the printing speed and printing chamber temperature have been proven to significantly impact in the 3D printed object features.[159] Too high speeds lead to structures malformation and nozzle clogging, therefore moderated speeds are preferred to acquire consistent and quality structures. Moreover, keeping the printing chamber temperature aids to avoid the structure to bend from the platform during printing. When deposition has finished, the fused material cools and solidifies on the heat bed which is maintained at a lower temperature to ease this process.[160] Nevertheless, the temperature difference between the extruder end and the print platform is reduced to avoid imperfections in the printed structure, such as breaks or warping due to the change in temperature.[161] The extruder temperature is fixed depending on the properties of the filament but is usually set around 220 °C; instead, the build platform temperature depends also on its material—including glass, adhesive foils, and Teflon—, values ranging from 70 and 120 °C have been reported.[162–165]

On the other hand, for FDM technique thermoplastic filaments of polylactic acid (PLA), acrylonitrile butadiene styrene (ABS), polyester, and polyurethane are commonly used. Nonetheless, these thermoplastic polymers have low glass transition temperature and low surface area, and their properties may be affected by heat, which reduces its catalytic applications.[31,164] Consequently, the use of commercial filaments for producing monolithic catalyst has been poorly studied (see Table S5, Supporting Information). In particular, FDM was applied by Hock et al.[163] to fabricate advanced polymeric monoliths which were further functionalized to act as acid catalysts in sucrose hydrolysis. The authors employed a commercial high impact polystyrene (HIPS) filament to print monoliths with orthogonal orientation of woodpile pattern layers. For printing, the nozzle was heated to 220 °C to extrude the filament, while the build platform was kept at 90 °C for assuring adhesion. Once printed, the HIPS monoliths were immersed in a 96 wt% H_2SO_4 solution at 22 °C for times varying between 1 h to 7 days to introduce sulfonic acid groups. After this time, they were washed with water until reaching a neutral pH. This functionalization method was chosen due to its reproducibility and the larger mechanical strength achieved regarding other treatments at higher temperatures. No structural changes were observed in the monoliths even after 7 days of sulfonation, from which a sulfonation degree above 0.7 mmol g^{-1} was attained. Optimal treatment was set for three days in which the sulfonation degree was 0.48 mmol g^{-1}. Functionalized monoliths showed better catalytic performance in the hydrolysis of sucrose regarding a commercial reference catalyst sulfonic acid-functionalized by ion exchange even though commercial catalyst has ≈7–10 times more sulfonic acid groups. This improvement has been ascribed not only to the better mass transfer which boosts the reaction kinetics, but to a greater availability to the sulfonic acid groups. Authors corroborated the increased mixing when using complex channel structures compared to straight channeled monoliths, this based on the Reynolds number.

To extend the chemical functioning of commercial thermoplastics for catalytic reactions, some researchers have opted for modifying them to prepare their own filaments. For example, Hock et al.[162] synthesized nanoporous hyper-crosslinked polymers which were further mixed with different thermoplastics (PLA, PVA, PS, or a mixture) to extrude a filament of 3 mm of diameter. The filament extrusion was realized at ≈200 °C, however, the higher content of hyper-crosslinked polymers the higher the temperature required. The fused deposition was realized at around 220 °C, over an adhesive foil at 120 °C to assure the adhesion of deposited material during printing. With this procedure, a 40 wt% loading of nanoporous solid materials, together with specific surface area of ≈171 m^2 $g^{-1}$was attained. Besides, the channel geometry proved to be significant for reaction purposes due to hydrodynamic properties, pressure drop, and residence time distribution. In a similar manner, an alumina-based filament was extruded by Li et al.[165] The filaments were prepared by mixing thermoplastic elastomer (TPE), grafted polyolefin, and alumina. The authors used these filaments to print monoliths with

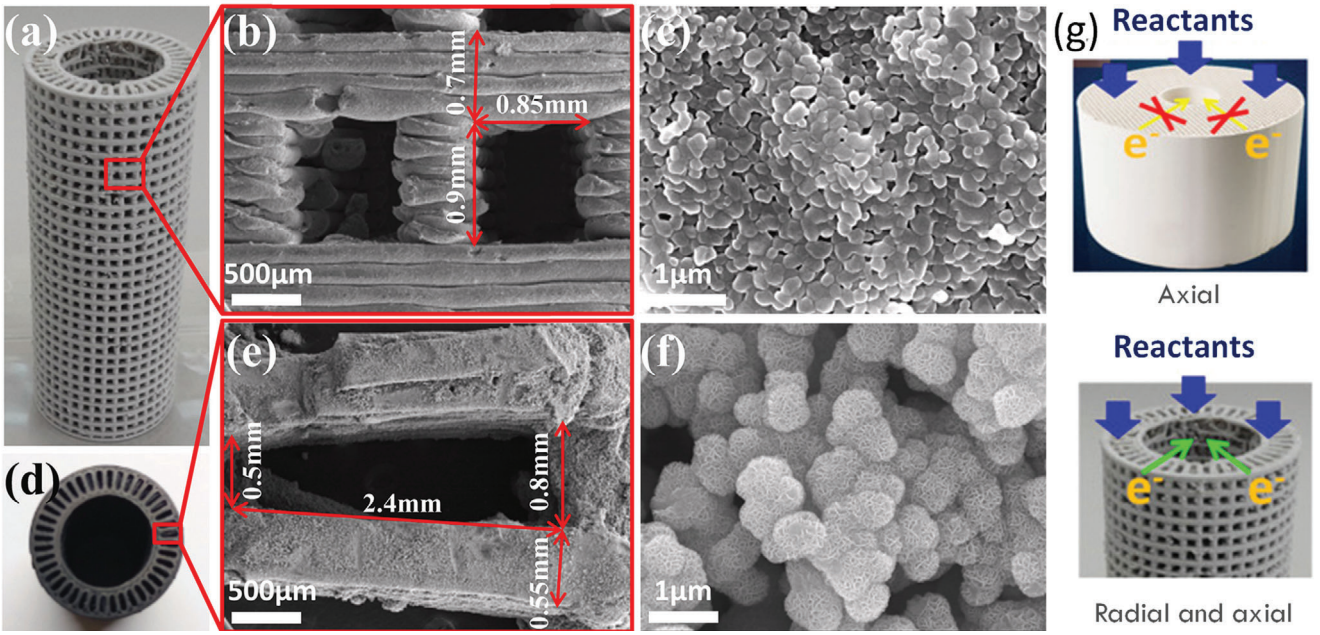

Figure 27. Mn-Co nanospheres coated Al_2O_3 monolith with axial and radial channels for plasma-catalytic oxidation of toluene. a–c) Photograph and SEM micrographs of the 3D printed Al_2O_3 monolith (radial channels); d–f) Photograph and SEM micrographs of the Mn-Co nanospheres coated structure; and g) Effect of radial channels in high-energy electrons transport. Adapted with permission.[165]

conventional straight channels and biaxial channels (**Figure 27a**), which were evaluated in the plasma-catalytic oxidation of toluene. Once the monoliths were printed, they were submerged into cyclohexane to remove binders, later subjected to a sintering treatment and an immersion reaction to load Mn-Co nanospheres. Some defects were observed within the structures because of clogging of the nozzle and an irregular extrusion since a variability in the filament dimensions.

Layers from the FDM printing are clearly observable in the SEM images of the radial channels (Figure 27b) as well as the porosity among sintered alumina nanoparticles (Figure 27c). A bigger amount of Mn-Co loaded in the advanced design (0.234 vs 0.102 wt%) was attributed to a higher specific surface area and better mass transfer during the immersion reaction. SEM images of axial channels of a coated monolith are presented in Figure 27d–f showing Mn-Co nanospheres of ≈680 nm covering the Al_2O_3 surface. The conventional design reduced up to 95% the by-products obtained by the powder counterpart, whereas the radial channels increased the energy efficiency with a negligible raise in by-products. Radial channels were more relevant at lower input power because they provide a conduit for high-energy electrons, thus increasing the catalytic oxidation of toluene (Figure 27g).

Contrasting, some studies have been realized with the incorporation of active compounds into the filaments, thus obviating a second step to deposit them after printing. Among those studies, the one carried out by Evans et al.,[166] in which they synthesized catalyst of Zeolitic-based MOFs with chemically active porous surface, can be pointed out. Zeolitic-based MOFs were evenly integrated into poly lactic acid (PLA) and thermoplastic polyurethane (TPU) matrices with high loadings close to 50 wt%. Those composites were extruded at 185 °C into filaments (1.6 mm diameter) and used in the FDM process. After printing, the structures underwent a solvent exchange either in CH_3OH or acetone, followed by an activation step at 75 °C, which did not generate any morphological changes. Besides, this activation led to an increase in thermal stability in accordance with the reduction in mass loss from 100 to 200 °C observed in TGA measurements. Thus, these materials are also limited to work under this temperature. XRD results confirmed the retention of the ZIF-8 crystallinity after the fabrication procedure, while N_2 isotherms show the high surface areas achieved, 531–706 $m^2\ g^{-1}$. Although some MOFs particles remained embedded in the plastic matrices, they conserved their characteristic ability to perform chemical interactions. Filaments of TiO_2 nanoparticles incorporated in ABS thermoplastic were developed by Skorsi et al.[159] to be used in photodegradation. ABS polymer was chosen since it has higher stability and less propensity to decompose during extrusion in comparison to other commercial polymers. The filaments were created by dispersing mixtures of ABS and TiO_2 nanoparticles (0–10 wt% TiO_2, larger contents led to printing difficulties) in acetone during several hours at 35 °C and sonication. Later, the solution was placed in a Teflon substrate at 80 °C to evaporate the solvent, so it could be fed to an extruder for getting the 1.75 mm-wide filaments. These filaments were used to 3D print photocatalyst for the degradation of rhodamine 6G, in which the presence of TiO_2 was confirmed by XRD. Although, FTIR results exhibited that TiO_2 interacts with polymer and increases its degradation during processing, the larger TiO_2 contents presented increased mechanical strength. Additionally, TiO_2 within the printed matrix was able to quench the intrinsic fluorescence of the rhodamine 6G up to 22% after 4 h of sunlight exposure. Martín de Vidales et al.[19] also made their own TiO_2 doped filaments to 3D print floating photocatalysts for

degradation of methylene blue (MB). To prepare the filament they mixed granulated low-density polyethylene (LDPE) and TiO_2 with a dispersing agent. Then the mixture was extruded, and the filaments were used in the FDM printer to obtain square meshed structures. The 3D printed structure resulted with an increased in degradation since a higher active surface is available to oxidize the MB and, compared to TiO_2 powder, the structure has the additional benefit of not requiring a separation step. Carbon materials have also been integrated into filaments for FDM. This is the case of the study reported by Gnanasekaran et al.[164] who prepared their own filaments of polymer and nanocomposites of carbon nanotubes (CNT) and graphene. To formulate their filaments, they dispersed CNT or graphene in isopropanol by sonication. Then, a certain amount of thermoplastic polybutylene terephthalate (PBT) was added, and later the isopropanol was let to evaporate at 90 °C. After drying, the melt mixed composite was fed to an extruder to get filaments of 3 mm diameter. Those filaments were used in a FDM printer in which the nozzle was heated between 200 and 260 °C for the deposition and, to prevent the material warping, double-sided tape was set as printing substrate over the platform at 70 °C. TEM images showed that the graphene platelets were perfectly dispersed without agglomeration when printing at low temperatures. Contrary, for higher temperatures some voids are generated driving to surface roughness. In relation to their functioning, CNT-based materials presented better conductive and mechanical characteristics and performance regarding the graphene-based structure. The preparation of these conductive polymers is very interesting for electrochemical applications where conductivity of the 3D printed electrodes is mandatory for the final application. Thus, the preparation of good conductive filaments in which the polymeric matrix does not affect the conductive properties of the conductive materials used is a hot topic theme of study. C.Y. Foo et al.[167] studied the preparation of printable graphene-based conductive filament to create a range of 3D printed electrodes (3DEs) for its use as supercapacitors and photochemical sensors. This 3D printed electrode showed a promising capacitive performance (98.4 F g^{-1}) and stable cycling stability (up to 100 charge/discharge cycles) as well as a good sensing behavior with a photocurrent response that exceeded expectations (≈724.1 µA) and a lower detection limit (0.05 µM) than a conventional ITO/FTO glass electrode. In turn, Z. Rymansaib et al.[168] prepared new conductive blends suitable for 3D printing by adding CNFs and graphite flake microparticles to thermoplastic polystyrene. For that, the polystyrene was first dissolved in the appropriate solvent and the conductive additives added. Once the solvent has completely evaporated, the solid thermoplastic composite is extruded into composite conductive filament using a heated aluminum barrel at 220 °C equipped with a 2 mm orifice. A compromise of good electrical conductivity and excellent electrode surface properties with good mechanical and printing characteristics was achieved with 80 wt% polystyrene, 10 wt% carbon nanofibers, 10 wt% graphite flakes. The electrode obtained with this formulation was used in the detection of trace metals obtaining a good performance comparable to results achieved with other types of conventional electrodes.

Despite the possibility of this methodology to be applied to diverse active compounds, the combination with thermoplastics maintains the limitation of the operational temperature Moreover, results suggest that a big part of the particles remains embedded in the plastic matrix together with the porosity blockage, also reducing its activity and cost-effectiveness. In addition to this methodology, there are other alternatives to structure novel catalytic materials: printing with more than one material—when using a FDM printer with double head—to produce a composite product;[84] and use the FDM to create templates of the desired structure for filling them with appropriate materials, and then eliminate the template through thermal treatment. The latter option has already been studied for the synthesis of carbonous and ceramic catalyst. In this regard, Chaparro et al.[16,169,170] proposed a strategy that combines the FDM and sol-gel polymerization processes, which has enabled the obtention of integral carbon monoliths with complex channel architecture and tailorable porosity. The influence of the channel geometry and carbon porosity on CuO/CeO_2 catalytic performance was identified with the CO-PrOx reaction. The synthesis methodology consisted of printing polymeric templates from FDM of Co-polyester (CPE+, selected owing to its high chemical stability) which served as negative of complex interconnected channels. Later, those printed templates were put into glass tubes and filled with a solution of resorcinol, formaldehyde, and water in different ratios (R/W). The controlled polymerization process was held at room temperature 1 day, at 50 °C for 1 day, and at 80 °C for the subsequent 5 days. Once this process had finished, the organic gel was unmolded and dried for its further slow carbonization (in N_2 atmosphere at 900 °C for 2 h). The selected active phase, Cu/CeO_2, was loaded via dip-coating in an ethanolic solution, achieving a deposition of ≈110 mg. Drying and a thermal treatment at 250 °C in air were also realized. According to TGA analysis, thermal stability was affected by active phase distribution, however, all supported catalysts exhibited stability up to 500 °C in oxidizing conditions, thus being useful in a wide range of reactions and overcoming the limitations imposed by previous methodology. The pore size distribution and macropore volume are related to the size and interconnection of primary particles, which can be controlled by varying the water content for polymerization. The higher the water content, the greater the particle size and lower their interconnection leaving larger pore size and macropore volume. As the pore size and macroporosity increase, the active phase distribution along the carbon improves thus the catalytic activity as well. Nevertheless, too high-water content generates heterogeneous pore size distribution and leads to preferential flow pathways. High and stable CO conversion (≈98%) and CO selectivity (≈99%) were achieved at 104 °C. Authors followed same procedure to produce carbon monoliths but employed them as support for Ni/CeO_2 catalyst for CO_2 methanation.[170] The textural and chemical properties of carbon can be tuned to improve the dispersion and attaching of active phases. They noted that their novel design forced turbulent flow regime within the channels, thus enhancing the CO_2 methanation rate ≈25% at 300 °C. This approach allowed the fabrication of pure and integral carbon monoliths with specific and complex designed channels not attainable by conventional methods, as well as a controlled porosity. Similarly, Li et al.[171] combined template printing by FDM and polymerization process to generate carbon monoliths. In this case, the authors employed a PLA filament to print templates made of cylinder, tetrahedron, and tetrakaidecahedron periodic units. Those templates were filled with a phenol-formaldehyde paste to later follow polymerization, calcination,

and wash-coating processes. High structural integrity, precise replica of the templates, but a high shrinkage of about 67% were obtained in the fabricated monoliths. The tortuous channels in the monoliths synthesized with tetrahedron units led to a CO conversion increase of ≈32% regarding straight channels, which is related to the reactant and products transport enhancement between the catalyst surface and fluid, as well as the heat release.

In relation to the use of ceramic fillers, equivalent methodology was followed by Alimi et al.[8] to obtain alumina monoliths with immobilized palladium for its use in the epoxidation of styrene. Polylactic acid (PLA) filament was fused to print the conventional monolithic template that was further filled with γ-Al_2O_3 and sodium silicate, dried, and calcined, for the final immobilization of palladium nanoparticles by deposition-precipitation method. The XRD analysis confirmed the obtention of ordered silica since the characteristic peaks of Al_2O_3 were observed, though, those peaks were reduced after the addition of palladium nanoparticles. In terms of porosity, an increment in the surface area from the powder to the monolith was observed probably due to the incorporation of SiO_2, however, this area was later reduced because of pore blockage with Pd. The authors observed that the lower the flow rate the greater the conversion, and that a low residence time prevents the formation of side products. As expected for its endothermic nature, the styrene conversion raised (58%) with the increment in temperature (>85 °C) with a good selectivity (70%) to styrene oxide. Also, the high surface area to volume ratio between the substrate and the catalyst helped to improve the conversion. It is important to highlight the effectiveness of the deposition method since the samples presented only 0.3% of the Pd leached after 7 cycles.

This methodology has been proven to enable the synthesis of monoliths of different geometries with an excellent replica of the templates. The use of filler materials such as carbon precursors and ceramics have improved the catalysts chemical properties and stability, Additionally, compared to other synthesis methods which required the use of binders and plasticizers, the absence of additives in the fillers allows to keep unchanged the desired characteristics of the precursors (e.g., surface area and active sites). Also, the need of some additional steps like polymerization, carbonization, or sintering, is compensated by the increase in their possible catalytic applications. Notwithstanding, authors have reported the existence of shrinkage in the final structure (varying from 10 to 67% depending on the materials and process conditions) which must be taken into consideration while designing the monoliths.

6. Binder Jetting

The binder jetting (BJT) technology consists of the injection layer-by-layer of a liquid binder agent on a powder bed to build the object (**Figure 28**). The process begins with the deposition of a powder coat of a certain thickness on a build platform. Then, by means of a print head, the binder is injected to selectively join or fuse the material according to the CAD pattern. Later, the build platform is moved, and a new powder coat is disposed to continue with the printing process.[84] Due to the residual powder and the binder, no support structure is needed.[172] Once the printing is finished and the binder is completely set, the so-called "green object" is removed from the printing bed and excess powder is withdrawn by compressed air. In order to grant mechanical properties, the curing of the binder, and sintering are done.[173]

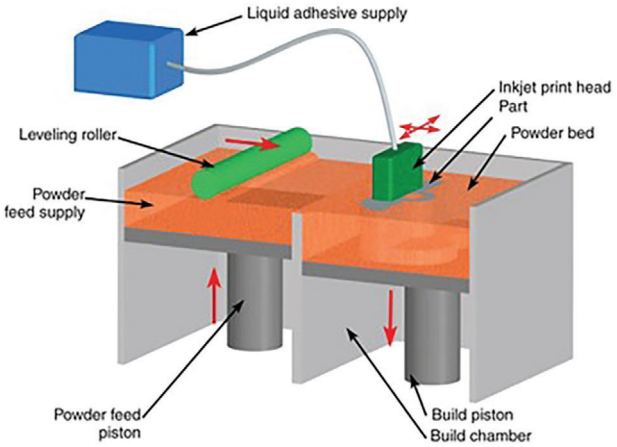

Figure 28. Schematic of the binder jetting (BJT) printing process. Reproduced with permission.[174]

Compared to powder bed processes such as LM and LS, a wider range of materials can be used since there is no restriction of melting point.[84,172,173] Nevertheless, several factors such as materials used (the relationship of the properties of powders and binders), layer thickness, and delay time of spreading a new layer must be taken into account to prevent defects in the printed object.[175] Because of those drawbacks, the binder jetting methodology has practically not been used in the production of 3D structures for supporting catalysts.

In this regard, Bui et al.[176,177] have reported the use of the BJ technique to produce catalysts, initially in pellet configuration, but later in monolithic shape. In their first approach, the authors applied the binder jetting technique to print spherical and cylindrical pellets of Ni-Al catalyst for CO_2 methanation. Later, the authors also leveraged this procedure to obtain monolithic shaped catalyst and compared it to the DIW process.[178] In this case, alumina monolithic supports were fabricated by both DIW and BJ and later loaded with Pt by dip-coating to test them in the dehydrogenation of perhydro-dibenzyltoluene. For the BJ process, authors prepared the bed material mixing boehmite and bayerite powdered binders with polyvinylpyrrolidone (PVP) to bind the powder upon contact with the printing liquid. On the other hand, the printing liquid formulation consisted of boehmite, isopropyl alcohol, and butanediol. After printing, the sample is depowdered, dried, and calcined (600 °C for 2–4 h) to remove PVP binder. Then, a further infiltration with an aqueous solution of boehmite to introduce additional particles into the porous particle framework and increase stability, was realized. In comparison, the DIW ink was formulated just with boehmite and acetic acid. A calcination step was carried out in the same way for both techniques (1100 °C for 3 h), followed by the dip-coating with $H_3Pt(SO_3)_2(OH)$. While DIW creates smoother surfaces, the BJ process produced more porous and rougher surfaces. In this respect, porosity of BJ catalyst seems to be affected by the addition of binders, therefore, with the debinding treatment the surface area increased, whereas from the calcination step a reduction is observed probably due to some Ni sintering. Also, the BJ printed structure exceeded the designed dimensions which is caused by

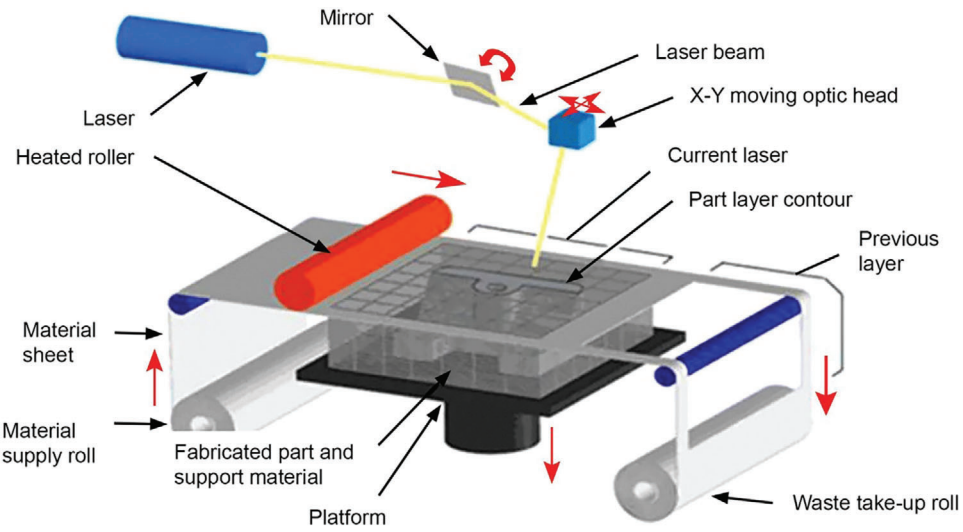

Figure 29. Schematic of the sheet lamination (SHL) printing process. Reproduced with permission.[181]

hardware related printing inaccuracies or bleeding (which is a macroscopic flow of binder caused by high ink saturation level). Besides, shrinkage is 3 times higher than that of the DIW support for low calcination temperatures and are almost the same for 1000–1200 °C calcined structures (≈12%). At calcination temperatures above 1000 °C compressive strength of DIW increases almost four times regarding BJ, though, for both materials this treatment led to a drastic surface area reduction. The Pt loading resulted higher for the BJ monolith since it contained more meso and macropores, however, both catalysts showed equal dehydrogenation rates of ≈2.7 $gH_2\ g_{Pt}^{-1}min^{-1}$.

Taking this case, the achievement of the desired design and dimensions is apparently harder with the binder jetting technique since the deposition of the binder ink is not as precise as other AM technologies above presented. Moreover, the use of binders, as usually observed with other techniques, implies a porosity blockage and thus a post treatment to eliminate them from the structures is needed. Nevertheless, the liquid ink properties are not as challenging as those required for preparing inks for DIW or resins for vat photopolymerization processes. Therefore, when controlling the printing hardware and ink level, binder jetting may be an attractive option for producing monolithic catalysts with rough surface. This characteristic can be used as an asset by avoiding the necessity of pre-treatments that are often required to facilitate the deposition of active compounds on other materials.

7. Sheet Lamination

The sheet lamination (SHL) technique, also named as laminated object manufacturing (LOM), consists of laminating a sheet of printing material with the help of rollers, then bonding and cutting (or vice versa depending on the configuration of the equipment) consecutive layers of the material until the construction of the piece is completed (**Figure 29**). To bond layers different thermal and mechanical sources of energy are used, involving bonding mechanisms such as adhesive bonding, thermal bonding, sheet metal clamping, and ultrasonic welding.[179] The cutting is made with a laser (usually CO_2) or a blade (mechanical cutting), with a depth of the thickness of a layer following a pattern generated by a computer program.[84]

This is a hybrid additive manufacturing process, which allows the construction of larger parts at higher production speeds, also avoiding defects caused by solidification process, however, in some cases a final processing is required to improve the surface quality. Moreover, traditional SHL is not able to produce multimaterial structures and the capability for obtaining complex geometries is not comparable with other AM techniques since it is not adapted to finely detailed structures and depends on the shape and thickness of the sheets.[179,180] In consequence, the limitations of laminated object manufacturing have inhibited its application in catalysts synthesis.

Scarcely, the work realized by Lei et al.[182] can be pointed out, who have proposed the combination of LM and laminated object manufacturing to obtain a novel catalyst for hydrogen production via methanol steam reforming. 316 L stainless steel sheets were produced by laser melting, subsequently cleaned and coated with an aqueous solution of $Cu(NO_3)_2$, $Zn(NO_3)_2$, $Al(NO_3)_3$, $Zr(NO_3)_4$, and Al_2O_3 to strength the adhesion. Later, multiple hexahedral mesh sheets were bonded through sheet lamination to conform a structure with periodic units. This material had large specific surface area and connectivity, and some surface roughness that favored the active phase adhesion was also observed. Additionally, catalyst displayed a good performance in methanol steam reforming (reaching up to 90% methanol conversion), which also resulted superior compared to a commercial stainless-steel fiber sintered felt (≈10% higher). Whereas the structure of commonly used metal foams for this catalytic process cannot be entirely controlled or reproduced,[183–185] the procedure proposed by Lei et al. allows to obtain reproducible materials with a high exposed surface area for depositing the active phase.

8. Structure Geometry Effect

Thus far, the research of additive manufacturing applied as an innovative tool in monolithic catalysts synthesis has been focused on the modification or generation of new materials—either

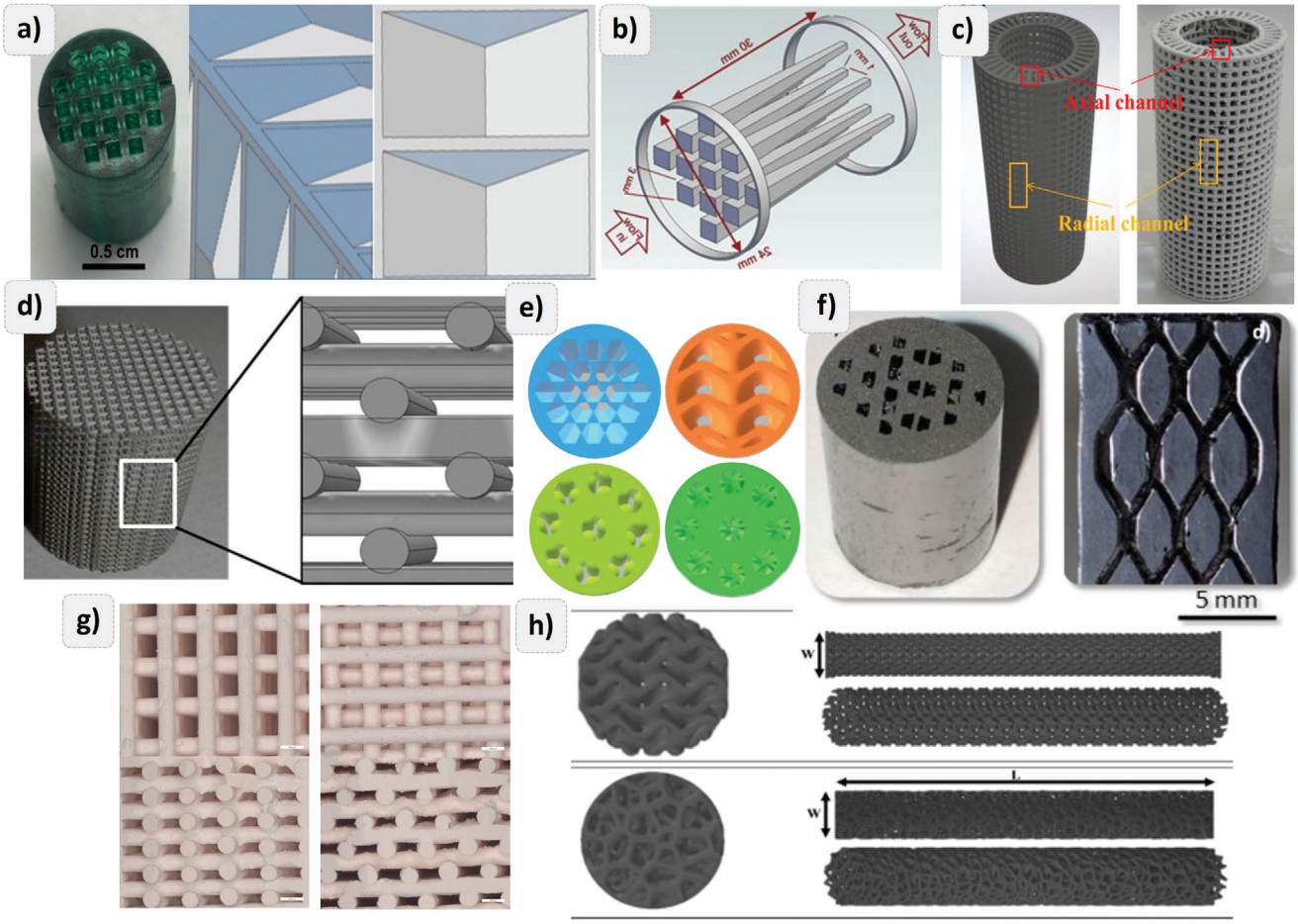

Figure 30. Examples of novel and non-straight channels designs: a) prismatic cavities along the channels[45]; b) asymmetrical channels[54]; c) incorporation of axial and radial channels[165]; d) stacked zigzag channels[150]; e) periodic lattices of different shapes[99]; f) interconnected crisscrossed channels[16]; g) stacked woodpile-like layers[143]; and h) Gyroid and Voroni periodic units.[2] Adapted with permission.[16,45,54,143,150,165]

resins, inks, or filaments—, adjustment of printing techniques, and/or implementation of post printing treatments to modify the structure or load it with other compounds. Notwithstanding, most works report the use of additive manufacturing to prepare monoliths of conventional configuration of straight and parallel channels, and few studies have been realized to analyze the effect of channel geometries on catalytic performance. Though, it is important to point out that additionally to the properties provided by the diverse available materials and additive manufacturing techniques, 3D printing offers the possibility of designing the channel geometry, therefore, exceeding the limit of straight configuration imposed by conventional synthesis methods. This may result in a huge advantage in reactions where diffusion, mixing, and/or heat transfer limit the performance, regardless of the base material (either polymer, ceramic, carbon, metal, etc.).

In regard to the scarce non-traditional monolithic structures developed so far the following modifications can be mentioned: i) addition of circular or square grooves lengthwise the channels (**Figure 30a**), ii) asymmetrical channels with reduction of the cross section (Figure 30b), iii) combination of axial and radial channels (Figure 30c), iv) zigzag shaped channels (Figure 30d), v) pseudo-random and periodic lattices (Figure 30e), and vi) interconnected channels—either by crisscrossed channels (Figure 30f), stacking woodpile like layers with different offset angles (Figure 30g), or use of periodic units or fluid guiding elements (Figure 30h)—. One of the benefits of using complex designs is the amelioration of the deposition of active phases, as corroborated by Chaparro et al.[45] The authors used SLA technique to print two non-conventionally shaped monoliths with hollows through the structure (Figure 30a). They explored and compared the effect on the active phase anchoring of those grooves and the doping of the liquid resin with inorganic materials. The results demonstrated that the use of the advanced design leads to load similar quantities of active phase in relation to doped monoliths while necessitating a reduced number of steps.

Furthermore, some authors have reported the advantages of their novel and sophisticated monoliths designs in comparison to conventional honeycomb like structure. The principal effect of non-straight channels has been proven to be the generation of turbulence within them due to tortuous paths, contrary to conventional straight channels which force laminar flow creating radial diffusion limitations.[54,163] This, in turn, boosts the interaction between reagents and catalyst, increases the fluid diffusion and mass transfer, as well as improves the heat transfer.[143] In

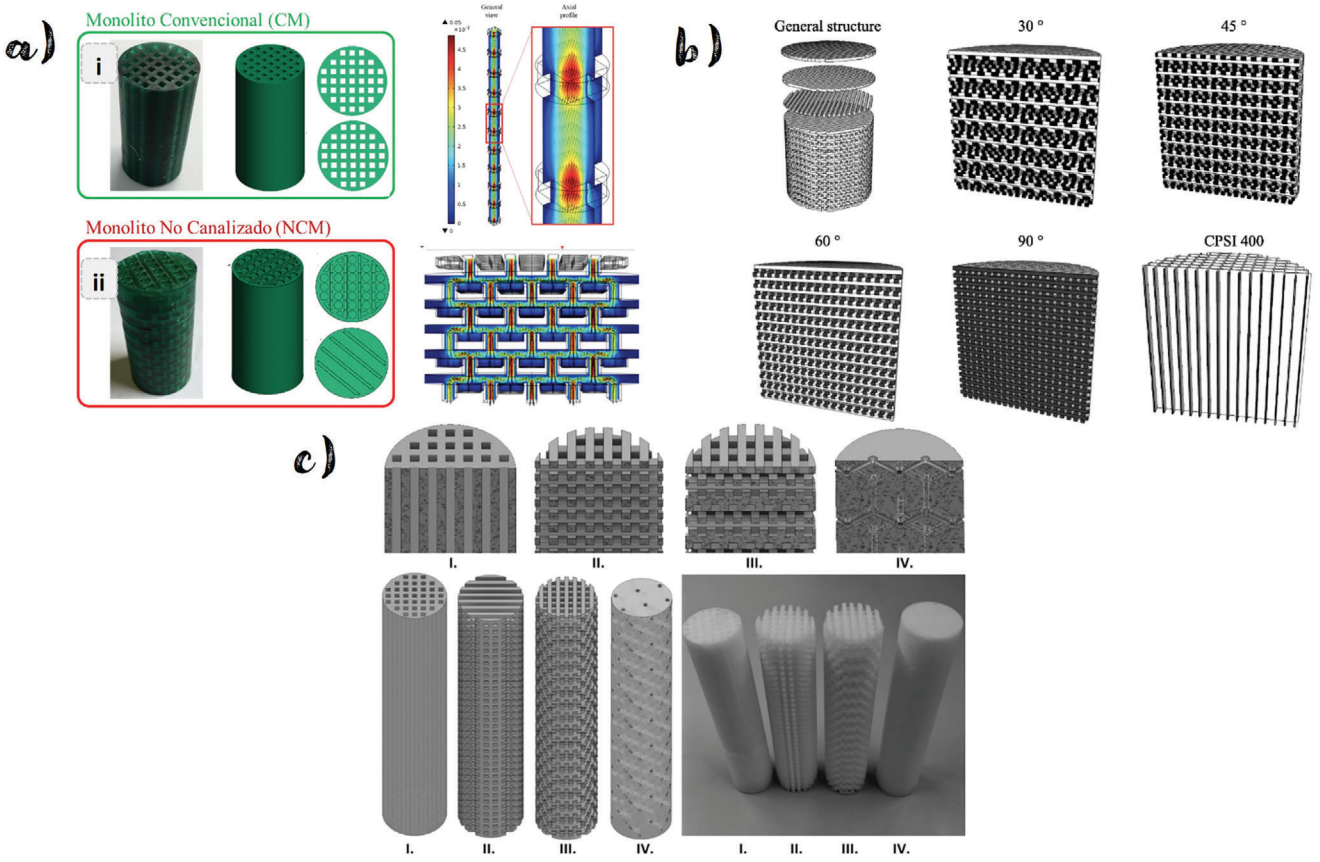

Figure 31. a) Geometry of conventional honeycomb monolith (CM) with straight channels (i) and advanced non-channeled (NCM) design composed by several transversal discs containing deposits for the active phase loading and slits through which the gas circulates (ii), and velocity profiles inside of NCM, adapted from[46]; b) General structure and cross sectional view of 3D printed ceramic substrates utilizing different offset angles between meshed layers from[126]; and c) Four geometry designs used for FDM of polymeric monoliths: straight channels (I), orthogonal mesh layers (II), shifted orthogonal mesh layers (III), and diamond structure in which each channel connects to three other channels in a tetrahedral node (IV) from.[162]. Adapted with permission.[46,126,162]

relation to catalytic activity, the transfer improvement is associated to a better and faster transportation of reactants and products between the catalyst surface and the fluid, consequently resulting in an augment of reaction rates and conversions.[2,16,99]

In that respect, Chaparro et al.[169] compared a carbon monolith of interconnected crisscrossed channels (that split and join successively along the structure as shown in Figure 30f) with a carbon monolith of conventional straight channels to analyze the influence of the channel geometry on their catalytic performance. The carbon monoliths were used as supports of Cu/CeO_2 active phase in the preferential oxidation of CO in the presence of H_2. Due to their porosity, the active phase was loaded both in the surface and carbon matrix. Results showed that the gas diffusion through the channels and carbon matrix is influenced by the design. The tortuous path in the advanced design favors the turbulent flow regime, despite the flow rate employed. This implies an improvement of the gas diffusion through the carbon network which, in turn, increases the active phase accessibility and its interaction with the reactants. Together with the activity and availability of the Cu/CeO_2, the catalytic efficiency enhanced with the non-straight channels as observed in the T_{50} (Temperature to achieve the 50% of CO conversion) that decreased around 13 °C (using 240 mL min^{-1}) regarding the conventional straight-channeled monolith.

Utilizing the flexibility offered by 3D printing, C. Chaparro-Garnica et al.[46] reimagined the conventional concept of channeled monoliths for catalysis, creating advanced non-channeled monolithic (NCM) supports (Figure 31a-$_{ii}$). These supports are constructed from multiple transversal discs featuring active phase deposits, with strategically placed slits allowing gas circulation. The advantages of this new NCM were evaluated in the CO-PrOx reaction. Remarkably, this material exhibited superior catalytic activity compared to traditional channeled monoliths (Figure 31a-$_{i}$), showcasing the potential of this innovative approach for enhanced catalytic processes. Turbulence manifests within the fluid pathway in the NCM, facilitating the transfer of reagents and products to and from the active sites within the fluid bulk, thereby promoting the rate of chemical reactions. Additionally, the non-channeled monolith enhances heat dispersion through its convoluted pathways, thereby reducing local temperatures at the active sites. Consequently, the transportation of reactants and products within the monoliths plays a pivotal role, with the inner geometry of the monoliths exerting a significant influence on this process.

Hajimirzaee et al.[126] prepared cordierite non-linear channel catalysts washcoated with a Pd:Pt/Al_2O_3 active phase for the oxidation of methane. Cordierite was obtained by a solid-state reaction at 1200 °C after 3D printing a paste made with cordierite precursors, water, and ethylene glycol. The structure was printed using diverse offset angles between meshed layers (Figure 31b), nevertheless, the walls obtained were 70% thicker than a commercial monolith due to limitations for extruding the paste. Therefore, less open area is achieved, especially for lower offset angles, leading to a higher backpressure compared to commercial straight channels cordierite monoliths. On the positive side, turbulence is induced causing irregular fluctuations and mixing so a better catalytic activity is reached. At moderate and high inlet temperatures, in which the reaction rate is controlled by mass transfer, the turbulence produced within the non-straight channels also increases reaction rates, despite the fact it had a minor cell density and lower amount of precious metal in relation to conventional diesel oxidation catalyst, making it more cost-effective. Besides, the same methodology was followed by the authors using a commercial porcelain paste fixing the offset angle between layers in 90°.[149] The nozzle blockage with the highly viscous ink difficulted the use of a nozzle smaller than 0.7 mm in diameter, thus limiting the cell density that resulted fourfolds lower than a conventional diesel oxidation catalyst (DOC) employed as reference. The catalyst was also evaluated in the methane oxidation but in a dual fuel system. Similar conclusions were attained since the 3D structure induces internal turbulence, thus improving internal and external mass transfer which increases the reaction rate.

The effect of the channel geometry in the hydrodynamic properties, pressure drop, and residence time distribution was analyzed by Hock et al.[162] They obtained cylindrical monoliths with varying geometries of transport channels by a fused deposition modeling (FDM) 3D printer from thermoplastic polymers (Figure 31c). The hydrodynamic properties, pressure drop, and residence time distribution are affected by the monolith design. Monoliths with less complex structures (I and II) present minor pressure drop whereas monoliths with significantly higher tortuosity of the pore channels results in higher pressure drops (III and IV). However, the effect of the channel geometry in the catalytic performance was not analyzed.

Moreover, the heat transfer also helps in exothermic reactions to the heat release, thus avoiding the generation of hot spots within the material. In that context, Gonzalez et al.[102] prepared advanced-designed monolithic catalysts for CO_2 methanation using stainless steel powder in LM printing. The channels configuration was based on different sized flow guiding elements used to bifurcate the stream and switch its position throughout the catalyst. The obtained results evidenced the highest sized channels performed better regarding the others. This was attributed to a favored radial heat transfer, mixing, and turbulence established, which enhanced the catalytic activity and obtained almost 75% conversion at 400 °C. Moreover, there was not possible to establish a linear relation between the channels size and their catalytic activity, however, all of them presented better performance and selectivity regarding parallel straight channels used as reference. Lefevere et al.[129] used DIW to obtain ZSM-5-coated stainless steel (316L) monoliths with woodpile-like layers of straight or zigzag channels. Monolithic catalyst achieved higher conversions of methanol compared to its powder counterpart (≈20%), while maintaining the selectivity over 99%. These results were attributed to better diffusional transport and, since the dehydration of methanol to dimethyl ether is an exothermic reaction, the structures could help to remove the heat of the reaction. Additionally, the monolith with "zigzag" tortuous channels favors turbulence, thus raising the yield of light olefins. Similar procedure but with a different coat (Ni/alumina) was realized to test the catalytic activity in CO_2 methanation.[150] In which the improvement of CO_2 conversion (≈30%) over the "zigzag" channeled monoliths due to a higher contact reagent-catalyst was also confirmed.

Likewise, other benefits of advanced designs have been observed: enlargement of the temperature region in which chemical control is maintained since transport limitations imposed in straight channels are overcome[46]; possibility of adjusting the catalytic product distribution due to material selectivity[99]; smaller pressure drop compared to powder counterpart[66,171]; even with fewer amount of active phase, the dispersion together with the promoted turbulence allow greater conversions regarding conventional catalyst, thus resulting more cost-effective; and the higher cell density, the higher catalytic activity due to distribution and accessibility of active sites.[66]

9. Perspectives and Future Directions

Recently, the inclusion of additive manufacturing in the production of novel catalysts has proven to be an excellent approach. AM technology has overcome limitations in monolithic manufacturing by allowing the development of a wide range of compositions, geometries, and configurations with exceptional dimensional precision. Numerous materials, including polymers, metals, ceramics, carbon, zeolites, composites, and biopolymers, according to their characteristics, have been processed through different AM techniques (mainly SLA, FDM, and DIW), to successfully produce valuable monolithic catalysts for distinct reactions.

Nevertheless, some constraints have been encountered in the application of these technologies or the catalysts obtained. For instance, the use in catalysis of certain polymer monoliths obtained by VPP of resins is restricted to low maximum operational temperatures due to their thermal stability. Therefore, research on resin modification/preparation to enhance resultant stability, and/or improve active phase loading, would be of great interest. Similarly, the use of some raw materials in extrusion techniques has presented difficulties. Exploration of inks/filaments preparation, as well as the use of external stimuli for improving the conformation of these materials during 3D printing without affecting the final properties may be helpful to wider their application. In this sense, the incorporation of the active phase could also be improved to attain homogeneous distribution and high accessibility, hence avoiding further processing steps. Additionally, the use of metals in PBF which can be activated after printing to be used directly in catalytic reactions is another feasible fabrication improvement worthy of further study to avoid active phase loading steps.

Although it is known that traditional synthesis methods restrict monolithic structure geometry to parallel straight channels, which, in turn, impose laminar flow and present heat and mass transfer limitations, the potential for surpassing these issues through AM has not yet been extensively explored. The feasibility

offered by AM in achieving diverse unconventional, sophisticated, and complex monolithic designs, may be an opportunity to create tortuous paths for avoiding or diminishing the laminar flow regime. Thus, investigating and assessing the impact of novel non-straight designs on fluid dynamics, catalyst-reagent interaction, and ultimately catalytic performance represents a path toward the breakthrough in monolithic catalyst development. Moreover, enhancing fluid-catalyst interaction through intricate pathways may not only boost reaction rates and increase flow rate processed, but also optimize the utilization of active phases, typically costly, thereby offering cost benefits.

Overall, the accessibility, high-speed production, reduction of material wastage, and consequent cost-effective products achieved through AM are continuously expanding its applications, study, and significance in the catalytic field.

10. Conclusions

Due to the diversity of printing methods and materials, 3D printing has become a powerful tool for advanced manufacturing of monolithic catalyst. This review includes the AM technologies applied so far in this field. Nonetheless, it is important to mention that some other AM techniques have not been explored yet in the synthesis of monolithic catalyst—Material Jetting (MJT) and Directed Energy Deposition (DED)—. Those technologies present several drawbacks, such as limitation of materials due to operating temperatures, expensive and detrimental powders (DED process), expensive equipment, poor accuracy, thick layers, null recyclability of materials, and slow building time.[186,187] Despite that, owing to their mechanism these 3D printing technologies are suitable for coating on complex surfaces, hence having potential for their use in the preparation of catalyst. The implementation of MJT and DED, not to conform monolithic supports but to cover them and deposit catalytically active compounds, results interesting for attaining highly developed catalysts.

Regarding the most used methods, each one has its advantages and drawbacks in terms of resolution, applicable materials, printing speed, or operational conditions. Therefore, the selection of the additive manufacturing technique depends on the properties that are sought to be obtained in the 3D printed catalyst as well as the printing requirements. However, regardless of the chosen method, there is an opportunity to explore different materials and novel configurations/shapes non attainable with traditional methods. The latter remarkably distinguishes the benefit of this alternative technology since complex designs have proven to promote turbulence within the catalysts. Contrary to traditional straight channels that force laminar flow of the fluid with radial diffusion limitations, the turbulence generated in advanced designs further leads to better mass and heat transfer, enhanced reactant-active sites interaction, thus increasing reaction rate, conversion, and selectivity.

Likewise, the active phase charging procedure must be adequately selected. It could be carried out either before, during, or after the printing process, and is also associated to the material nature, printing method, and accessibility of active sites after deposition. On the other hand, an important aspect to consider during the design, mainly when requiring thermal post treatments, is the possible shrinking of the structure. Taken the shrinkage into account, we can assure the obtainment of the catalyst with the desired dimensions at the end of the manufacturing process. Once all these aspects are covered, specifically designed monolithic catalyst with outstanding characteristics that exceed the performance of conventional catalyst in terms of activity, stability, reusability, and ease of manipulation may be attained. Based on all the above, it can be stated that 3D printing versatility is an alternative that enables outperform conventional catalysis.

Supporting Information

Supporting Information is available from the Wiley Online Library or from the author.

Acknowledgements

This research has been supported by the Spanish project PID2021-127803OB-I00 funded by MCIN/AEI/ 10.13039/501100011033/ and by "ERDF A way of making Europe". Authors also thanks the "Unidad de Excelencia Química Aplicada a Biomedicina y Medioambiente" of the University of Granada (UEQ – UGR) for its technical assistance. A. Parra-Marfil appreciates the financial support provided by CONACYT through the PhD grant 818974, and E. Bailón-García is grateful to MICINN for her postdoctoral fellowship (RYC2020-029301-I). Funding for open access charge: Universidad de Granada/CBUA.

Conflict of Interest

The authors declare no conflict of interest.

Keywords

3D printing, additive manufacturing, innovative catalyst, monolithic structure

Received: January 15, 2024
Revised: February 21, 2024
Published online:

[1] O. H. Laguna, P. F. Lietor, F. J. I. Godino, F. A. Corpas-Iglesias, *Mater. Des* **2021**, *208*, 109927.
[2] A. Zhakeyev, M. C. Jones, C. G. Thomson, J. M. Tobin, H. Wang, F. Vilela, J. Xuan, *Addit. Manuf.* **2021**, *38*, 101828.
[3] J. C. Védrine, *Chin. J. Catal.* **2019**, *40*, 1627.
[4] J. Zhu, P. Wu, Y. Chao, J. Yu, W. Zhu, Z. Liu, C. Xu, *Chem. Eng. J.* **2022**, *433*, 134341.
[5] M. Kundra, B. Bin Mohamad Sultan, D. Ng, Y. Wang, D. L. J. Alexander, X. Nguyen, Z. Xie, C. H. Hornung, *Chem. Eng. Process.* **2020**, *154*, 108018.
[6] M. Kundra, Y. Zhu, X. Nguyen, D. Fraser, C. H. Hornung, J. Tsanaktsidis, *React. Chem. Eng.* **2022**, *7*, 284.
[7] X. Hu, J. Karnetzke, M. Fassbender, S. Drücker, S. Bettermann, B. Schroeter, W. Pauer, H. Moritz, B. Fiedler, G. Luinstra, I. Smirnova, *Chem. Eng. J.* **2020**, *387*, 123413.
[8] O. A. Alimi, T. B. Ncongwane, R. Meijboom, *Chem. Eng. Res. Design.* **2020**, *159*, 395.
[9] F. D. Troncoso, G. M. Tonetto, *Chem. Eng. Process.: Process Intensif.* **2022**, *170*, 108669.
[10] M. Roustapisheh, D. Karami, N. Mahinpey, *Catal. Today.* **2022**, *397–399*, 497.

[11] E. Hajili, Z. Suo, A. Sugawara, T. Asoh, H. Uyama, *Carbohydr. Polym.* **2022**, *275*, 118680.
[12] A. Aranzabal, D. Iturbe, M. Romero-Sáez, M. P. González-Marcos, J. R. González-Velasco, J. A. González-Marcos, *Chem. Eng. J* **2010**, *162*, 415.
[13] T. Chafik, *Mater. Today: Proc* **2021**, *37*, 3834.
[14] D. F. M. Santos, O. S. G. P. Soares, J. L. Figueiredo, O. Sanz, M. Montes, M. F. R. Pereira, *Chem. Eng. J.* **2020**, *382*, 122923.
[15] Z. Yang, D. Li, Y. Zhao, Y. miao, J. Rao, D. Cai, X. Duan, P. He, D. Jia, Y. Zhou, *J. Alloys Compd.* **2019**, *811*, 151687.
[16] C. Y. Chaparro-Garnica, E. Bailón-García, A. Davó-Quiñonero, D. Lozano-Castelló, A. Bueno-López, *Chem. Eng. J.* **2022**, *432*, 134218.
[17] A. Elkoro, L. Soler, J. Llorca, I. Casanova, *Appl. Mater. Today.* **2019**, *16*, 265.
[18] V. Middelkoop, A. Vamvakeros, D. de Wit, S. D. M. Jacques, S. Danaci, C. Jacquot, Y. de Vos, D. Matras, S. W. T. Price, A. M. Beale, *J. CO2 Util.* **2019**, *33*, 478.
[19] M. J. Martín de Vidales, A. Nieto-Márquez, D. Morcuende, E. Atanes, F. Blaya, E. Soriano, F. Fernández-Martínez, *Catal. Today* **2019**, *328*, 157.
[20] F. Magzoub, X. Li, J. Al-Darwish, F. Rezaei, A. A. Rownaghi, *Appl. Catal. B.* **2019**, *245*, 486.
[21] A. D. Salazar-Aguilar, A. Quintanilla, S. M. Vega-Díaz, J. A. Casas, P. Miranzo, M. I. Osendi, M. Belmonte, *Open Ceram* **2021**, *5*, 100047.
[22] Y. Xie, Y. Yu, H. Xie, F. Huang, T. C. Hughes, *J. Hazard. Mater.* **2022**, *436*, 129170.
[23] F. Mendez-Arriaga, E. d. l. Calleja, L. Ruiz-Huerta, A. Caballero-Ruiz, R. Almanza, *Mater. Sci. Semicond. Process.* **2019**, *100*, 35.
[24] X. Zhou, C. Liu, *Adv. Funct. Mater.* **2017**, *27*, 1701134.
[25] H. Shen, R. Zou, Y. Zhou, X. Guo, Y. Guan, D. Na, J. Zhang, X. Fan, Y. Jiao, *Chin. J. Chem. Eng.* **2022**, *42*, 82.
[26] J. Tang, X. Guo, H. Chang, K. Hu, Z. Shen, W. Wang, M. Liu, Y. Wei, Z. Huang, Y. Yang, *J. Eur. Ceram. Soc.* **2021**, *41*, 7516.
[27] A. S. Díaz-Marta, C. R. Tubío, C. Carbajales, C. Fernández, L. Escalante, E. Sotelo, F. Guitián, V. L. Barrio, A. Gil, A. Coelho, *ACS Catal.* **2018**, *8*, 392.
[28] A. Bhatia, A. K. Sehgal, *Mater. Today: Proc* **2023**, *81*, 1060.
[29] P. Blyweert, V. Nicolas, V. Fierro, A. Celzard, *Carbon* **2021**, *183*, 449.
[30] I. Gibson, D. Rosen, B. Stucker, in *Additive Manufacturing Technologies: 3D Printing, Rapid Prototyping, and Direct Digital Manufacturing*, (Eds: I. Gibson, D. Rosen, B. Stucker), Springer, New York, NY, USA, **2015**, Ch. 2.
[31] N. Li, K. Tong, L. Yang, X. Du, *Mater. Today Energy.* **2022**, *29*, 101100.
[32] A. Andreu, P. Su, J. Kim, C. S. Ng, S. Kim, I. Kim, J. Lee, J. Noh, A. S. Subramanian, Y. Yoon, *Addit. Manuf.* **2021**, *44*, 102024.
[33] R. V. Pazhamannil, P. Govindan, *Mater. Today: Proc* **2021**, *43*, 130.
[34] A. Al Rashid, W. Ahmed, M. Y. Khalid, M. Koç, *Addit. Manuf.* **2021**, *47*, 102279.
[35] X. Bai, G. Ding, K. Zhang, W. Wang, N. Zhou, D. Fang, R. He, *Open Ceram* **2021**, *5*, 100046.
[36] B. J. Lee, K. Hsiao, G. Lipkowitz, T. Samuelsen, L. Tate, J. M. DeSimone, *Addit. Manuf.* **2022**, *55*, 102800.
[37] D. Loterie, P. Delrot, C. Moser, *Nat. Commun.* **2020**, *11*, 852.
[38] A. Amini, R. M. Guijt, T. Themelis, J. De Vos, S. Eeltink, *J. Chromatogr. A.* **2023**, *1692*, 463842.
[39] Y. Wang, Y. Chen, C. Wen, K. Huang, Z. Chen, B. Han, Q. Zhang, *Mater. Des.* **2023**, *227*, 111732.
[40] S. Lamnini, H. Elsayed, Y. Lakhdar, F. Baino, F. Smeacetto, E. Bernardo, *Heliyon.* **2022**, *8*, e10651.
[41] S. Mora, N. M. Pugno, D. Misseroni, *Mater. Today.* **2022**, *59*, 107.
[42] H. Miyanaji, N. Momenzadeh, L. Yang, *Addit. Manuf.* **2018**, *20*, 1.
[43] Q. Porter, M. Moghadasi, Z. Pei, C. Ma, *Ceram. Int.* **2023**, *49*, 17363.
[44] F. I. Azam, A. M. A. Rani, M. A. A. Razak, S. Ali, A. A. Aliyu, in *Progress in Engineering Technology III*, (Eds: M. H. A. Bakar, M. N. Zahelem, A. Öchsner) Springer, New York, **2021**, pp. 93.
[45] C. Y. Chaparro-Garnica, A. Davó-Quiñonero, E. Bailón-García, D. Lozano-Castelló, A. Bueno-López, *ACS Appl. Mater. Interfaces.* **2019**, *11*, 36763.
[46] C. Y. Chaparro-Garnica, P. Jordá-Faus, E. Bailón-García, R. Ocampo-Pérez, C. G. Aguilar-Madera, A. Davó-Quiñonero, D. Lozano-Castelló, A. Bueno-López, *ACS Appl. Mater. Interfaces.* **2020**, *12*, 54573.
[47] F. S. Franchi, M. Ambrosetti, R. Balzarotti, M. Bracconi, G. Groppi, E. Tronconi, *Catal. Today.* **2022**, *383*, 123.
[48] R. Chava, D. Purbia, B. Roy, V. M. Janardhanan, A. Bahurudeen, S. Appari, *Int. J. Hydrogen Energy.* **2021**, *46*, 6341.
[49] M. Zang, C. Zhao, Y. Wang, S. Chen, X. Liu, Y. Zhang, *Mater. Lett.* **2019**, *253*, 196.
[50] P. Patil, U. T. Nakate, K. Harish, S. P. Pavan, N. P. Rakesh, D. Selvakumar, N. S. Kumar, *Mater. Chem. Phys.* **2020**, *240*, 122269.
[51] L. Tan, B. Tan, *Chem. Eng. J.* **2020**, *390*, 124485.
[52] P. S. Barbato, A. Di Benedetto, G. Landi, L. Lisi, *Chem. Eng. J.* **2015**, *279*, 983.
[53] B. Cifuentes, A. Cifuentes, F. Bustamante, L. Soler, J. Llorca, M. Cobo, *Int. J. Hydrogen Energy.* **2021**, *46*, 2166.
[54] A. Davó-Quiñonero, D. Sorolla-Rosario, E. Bailón-García, D. Lozano-Castelló, A. Bueno-López, *J. Hazard. Mater.* **2019**, *368*, 638.
[55] İ. Aktitiz, R. Varol, N. Akkurt, M. F. Saraç, *Polym. Test.* **2020**, *90*, 106724.
[56] Y. Gao, J. Ding, *Procedia Manuf* **2020**, *48*, 749.
[57] Z. Weng, Y. Zhou, W. Lin, T. Senthil, L. Wu, *Compos. – A: Appl. Sci. Manuf.* **2016**, *88*, 234.
[58] R. M. Hensleigh, H. Cui, J. S. Oakdale, J. C. Ye, P. G. Campbell, E. B. Duoss, C. M. Spadaccini, X. Zheng, M. A. Worsley, *Mater. Horiz.* **2018**, *5*, 1035.
[59] Y. Chang, Q. Cao, B. J. Venton, *Curr. Opin. Electrochem.* **2023**, *38*, 101228.
[60] C. Yang, Q. Cao, P. Puthongkham, S. T. Lee, M. Ganesana, N. V. Lavrik, B. J. Venton, *Angew. Chem., Int. Ed.* **2018**, *57*, 14255.
[61] A. Jaiswal, C. K. Rastogi, S. Rani, G. P. Singh, S. Saxena, S. Shukla, *iScience* **2023**, *26*, 106374.
[62] Z. Han, G. Wang, J. Zhang, Z. Tang, *Nano Energy* **2022**, *102*, 107615.
[63] J. Zhao, Q. Li, F. Jin, N. He, *Addit. Manuf.* **2021**, *41*, 101962.
[64] Y. Zhang, S. Li, Y. Zhao, W. Duan, B. Liu, T. Wang, G. Wang, *Addit. Manuf.* **2021**, *39*, 101897.
[65] K. Gyak, N. K. Vishwakarma, Y. Hwang, J. Kim, H. Yun, D. Kim, *React. Chem. Eng.* **2019**, *4*, 1393.
[66] E. Bogdan, B. Michorczyk, A. Rokicińska, M. Basta, M. Myradova, P. Kuśtrowski, P. Michorczyk, *Appl. Surf. Sci.* **2021**, *553*, 149554.
[67] P. Michorczyk, E. Hędrzak, A. Węgrzyniak, *J. Mater. Chem. A.* **2016**, *4*, 18753.
[68] E. Hędrzak, A. Węgrzynowicz, R. Rachwalik, B. Sulikowski, P. Michorczyk, *Appl. Catal. A.* **2019**, *579*, 75.
[69] A. Rokicińska, M. Drozdek, E. Bogdan, A. Węgrzynowicz, P. Michorczyk, P. Kuśtrowski, *Catal. Today.* **2021**, *375*, 369.
[70] S. Yoneda, W. Han, U. Hasegawa, H. Uyama, *Polymer* **2014**, *55*, 3212.
[71] J. A. Chae, Y. Oh, H. J. Kim, G. B. Choi, K. M. Lee, D. Jung, Y. A. Kim, H. Kim, *Polym. Chem.* **2019**, *10*, 5142.
[72] Y. Shen, L. Qi, L. Mao, *Polymer* **2012**, *53*, 4128.
[73] Y. Xin, T. Fujimoto, H. Uyama, *Polymer* **2012**, *53*, 2847.
[74] X. Sun, G. Sun, X. Wang, *Polymer* **2017**, *108*, 432.
[75] J. Ye, C. Qian, Y. Dong, Y. Zhu, Y. Fu, *Eur. Polym. J.* **2023**, *183*, 111730.
[76] J. Han, K. Xie, Z. Du, W. Zou, C. Zhang, *Carbohydr. Polym.* **2015**, *120*, 85.
[77] J. Liu, J. M. Tobin, Z. Xu, F. Vilela, *Polym. Chem.* **2015**, *6*, 7251.

[78] D. Kuzmicz, P. Coupillaud, Y. Men, J. Vignolle, G. Vendraminetto, M. Ambrogi, D. Taton, J. Yuan, *Polymer* **2014**, *55*, 3423.
[79] Y. Xin, J. Sakamoto, A. J. van der Vlies, U. Hasegawa, H. Uyama, *Polymer* **2015**, *66*, 52.
[80] S. Kuppusamy, D. Jagadeesan, A. M. Mohan, A. Pavoor Veedu, A. E. Jiji, A. M. John, P. Deivasigamani, *J. Environ. Chem. Eng.* **2023**, *11*, 110355.
[81] J. A. Chae, S. Jeong, H. J. Kim, T. Tojo, Y. Oh, W. S. Chi, H. Yoon, H. Kim, *Polym. Chem.* **2021**, *12*, 2464.
[82] J. D. Roehling, S. A. Khairallah, Y. Shen, A. Bayramian, C. D. Boley, A. M. Rubenchik, J. DeMuth, N. Duanmu, M. J. Matthews, *Addit. Manuf.* **2021**, *46*, 102186.
[83] R. Goodridge, S. Ziegelmeier, in *Laser Additive Manufacturing*, (Eds: M. Brandt), Woodhead Publishing, Cambridge, UK, **2017**, 181.
[84] C. Y. Chaparro-Garnica, Doctoral Thesis, University of Alicante, Spain, February **2021**.
[85] B. Soundararajan, D. Sofia, D. Barletta, M. Poletto, *Addit. Manuf.* **2021**, *47*, 102336.
[86] J. Zhang, W. Zheng, J. Wu, K. Yu, C. Ye, Y. Shi, *Ceram. Int.* **2021**, *48*, 1173.
[87] S. I. A. Qadri, *Mater. Today: Proc* **2021**, *49*, 1980.
[88] M. Schwentenwein, J. Homa, *Int. J. Appl. Ceram. Technol.* **2015**, *12*, 1.
[89] K. Cheng, W. Xiong, Y. Li, D. Tang, H. Geng, M. Sun, L. Hao, H. S. Wang, H. Zhang, *Mater. Lett.* **2021**, *299*, 130050.
[90] F. Agueniou, H. Vidal, J. de Dios López, J. C. Hernández-Garrido, M. A. Cauqui, F. J. Botana, J. J. Calvino, V. V. Galvita, J. M. Gatica, *Catal. Commun.* **2021**, *148*, 106181.
[91] K. Cheng, W. Xiong, Y. Li, L. Hao, C. Yan, Z. Li, Z. Liu, Y. Wang, K. Essa, L. Lee, X. Gong, T. Peijs, *Compos. -A: Appl. Sci. Manuf.* **2020**, *135*, 105904.
[92] A. Lind, Ø. Vistad, M. F. Sunding, K. A. Andreassen, J. H. Cavka, C. A. Grande, *Mater. Des.* **2020**, *187*, 108377.
[93] L. Fratalocchi, G. Groppi, C. G. Visconti, L. Lietti, E. Tronconi, *Chem. Eng. J.* **2020**, *386*, 123988.
[94] C. S. D. Rodrigues, V. Guimarães, M. F. R. Pereira, O. S. G. P. Soares, L. M. Madeira, *J. Environ. Manage.* **2022**, *322*, 116084.
[95] E. F. S. Sampaio, O. S. G. P. Soares, M. F. R. Pereira, C. S. D. Rodrigues, L. M. Madeira, *Catal. Today.* **2023**, *418*, 114143.
[96] Z. Li, W. Cai, L. Song, Y. Hu, W. Xing, Z. Gui, *Appl. Surf. Sci.* **2023**, *639*, 158253.
[97] S. Saud, D. B. Nguyen, R. M. Bhattarai, N. Matyakubov, V. T. Nguyen, S. Ryu, H. Jeon, S. B. Kim, Y. S. Mok, *J. Hazard. Mater.* **2022**, *426*, 127843.
[98] S. Katheria, G. Deo, D. Kunzru, *Appl. Catal. A.* **2019**, *570*, 308.
[99] Q. Wei, H. Li, G. Liu, Y. He, Y. Wang, Y. E. Tan, D. Wang, X. Peng, G. Yang, N. Tsubaki, *Nat. Commun.* **2020**, *11*, 4098.
[100] M. Komendová, S. Nawada, R. Metelka, P. J. Schoenmakers, J. Urban, *J. Chromatogr. A.* **2020**, *1610*, 460537.
[101] J. L. Lapp, M. Lange, R. Rieping, L. de Oliveira, M. Roeb, C. Sattler, *Appl. Therm. Eng.* **2017**, *127*, 46.
[102] M. González-Castaño, F. Baena-Moreno, J. C. Navarro de Miguel, K. U. M. Miah, F. Arroyo-Torralvo, R. Ossenbrink, J. A. Odriozola, W. Benzinger, A. Hensel, A. Wenka, H. Arellano-García, *Energy Convers. Manage.* **2022**, *258*, 115464.
[103] S. Kumar, in *Comprehensive Materials Processing*, (Eds: S. Hashmi, G. F. Batalha, C. J. Van Tyne, B. Yilbas), Elsevier, Oxford, **2014**, 93.
[104] S. Rahmati, in *Comprehensive Materials Processing*, (Eds: S. Hashmi, G. F. Batalha, C. J. Van Tyne, B. Yilbas), Elsevier, Oxford, **2014**, 303.
[105] W. Peters, M. Eypasch, T. Frank, J. Schwerdtfeger, C. Körner, A. Bösmann, P. Wasserscheid, *Energy Environ. Sci.* **2015**, *8*, 641.
[106] X. Nguyen, A. Carafa, C. H. Hornung, *Chem. Eng. Process.: Process Intensif.* **2018**, *124*, 215.
[107] C. H. Hornung, X. Nguyen, A. Carafa, J. Gardiner, A. Urban, D. Fraser, M. D. Horne, D. R. Gunasegaram, J. Tsanaktsidis, *Org. Process Res. Dev.* **2017**, *21*, 1311.
[108] T. Knorr, P. Heinl, J. Schwerdtfeger, C. Körner, R. F. Singer, B. J. M. Etzold, *Chem. Eng. J.* **2012**, *181–182*, 725.
[109] K. Y. Koo, H. J. Eom, S. C. Kwon, U. H. Jung, W. L. Yoon, *Catal. Today.* **2017**, *293–294*, 129.
[110] Z. Le, W. Zhang, W. Li, J. Tan, R. Li, X. Wang, Y. V. Kaneti, X. Jiang, J. Chu, Y. Yamauchi, M. Hu, *Matter* **2020**, *3*, 879.
[111] F. Gao, Y. Tang, J. Liu, K. Pan, M. Zhou, G. Qian, M. Liu, F. Yu, J. Dan, B. Dai, *Chem. Eng. J.* **2023**, *474*, 145713.
[112] J. Wang, J. Yang, H. Zhu, B. Li, S. Zhu, *Chem. Eng. J.* **2023**, *456*, 141026.
[113] M. U. D. Sheikh, G. A. Naikoo, M. Thomas, M. Bano, F. Khan, *J. Sol Gel Sci. Technol.* **2015**, *76*, 572.
[114] M. Sharma, A. Mishra, A. Mehta, D. Choudhury, S. Basu, *J. Sol Gel Sci. Technol.* **2017**, *81*, 704.
[115] M. Sharma, S. Hazra, S. Basu, *Adv. Powder Technol.* **2017**, *28*, 3085.
[116] P. Jeyachandran, S. Bontha, S. Bodhak, V. K. Balla, M. Doddamani, *Composites Sci. Technol.* **2021**, *213*, 108966.
[117] M. Casini, in *Construction 4.0*, (Eds: M. Casini), Woodhead Publishing, Cambridge, UK, **2022**, 405.
[118] M. T. Mollah, R. Comminal, M. P. Serdeczny, D. B. Pedersen, J. Spangenberg, *Addit. Manuf.* **2021**, *46*, 102193.
[119] Y. Rao, N. Wei, S. Yao, K. Wang, Y. Peng, *Addit. Manuf.* **2021**, *39*, 101857.
[120] C. Zhu, Z. Qi, V. A. Beck, M. Luneau, J. Lattimer, W. Chen, M. A. Worsley, J. Ye, E. B. Duoss, C. M. Spadaccini, C. M. Friend, J. Biener, *Sci. Adv.* **2018**, *4*, eaas9459.
[121] S. Ma, S. Fu, S. Zhao, P. He, G. Ma, M. Wang, D. Jia, Y. Zhou, *Addit. Manuf.* **2021**, *46*, 102202.
[122] V. Middelkoop, T. Slater, M. Florea, F. Neaţu, S. Danaci, V. Onyenkeadi, K. Boonen, B. Saha, I. Baragau, S. Kellici, *J. Clean. Prod.* **2019**, *214*, 606.
[123] A. J. Young, R. Guillet-Nicolas, E. S. Marshall, F. Kleitz, A. J. Goodhand, L. B. L. Glanville, M. R. Reithofer, J. M. Chin, *Chem. Commun.* **2019**, *55*, 2190.
[124] X. Li, F. Rezaei, A. A. Rownaghi, *Microporous Mesoporous Mater.* **2019**, *276*, 1.
[125] J. Lefevere, L. Protasova, S. Mullens, V. Meynen, *Mater. Des.* **2017**, *134*, 331.
[126] S. Hajimirzaee, A. M. Doyle, *Fuel* **2020**, *274*, 117848.
[127] A. Shahzad, I. Lazoglu, *Compos. B Eng.* **2021**, *225*, 109249.
[128] S. S. Hossain, H. Son, B. Gao, S. Park, C. Bae, *Mater. Today Commun.* **2023**, *34*, 105246.
[129] J. Lefevere, M. Gysen, S. Mullens, V. Meynen, J. Van Noyen, *Catal. Today.* **2013**, *216*, 18.
[130] F. Magzoub, X. Li, S. Lawson, F. Rezaei, A. A. Rownaghi, *Fuel* **2020**, *280*, 118628.
[131] X. Li, W. Li, F. Rezaei, A. Rownaghi, *Chem. Eng. J.* **2018**, *333*, 545.
[132] S. Lawson, K. A. Newport, A. Axtell, C. Boucher, B. Grant, M. Haas, M. Lee, F. Rezaei, A. A. Rownaghi, *ACS Sustainable Chem. Eng.* **2021**, *9*, 5716.
[133] F. Magzoub, S. Lawson, F. Rezaei, A. A. Rownaghi, *Energy Fuels* **2021**, *35*, 2619.
[134] S. Lawson, A. Farsad, F. Rezaei, D. Ludlow, A. A. Rownaghi, *ACS Appl. Mater. Interfaces.* **2021**, *13*, 781.
[135] S. Lawson, A. Farsad, B. Adebayo, K. Newport, K. Schueddig, E. Lowrey, F. Polo-Garzon, F. Rezaei, A. A. Rownaghi, *Adv. Sustainable Syst.* **2021**, *5*, 2000257.
[136] S. Lawson, K. Baamran, K. Newport, F. Rezaei, A. A. Rownaghi, *Chem. Eng. J.* **2022**, *431*, 133224.
[137] A. Farsad, S. Lawson, F. Rezaei, A. A. Rownaghi, *Catal. Today.* **2021**, *374*, 173.

[138] C. R. Tubio, C. Malatini, V. L. Barrio, C. F. Masaguer, M. Amorín, W. Nabgan, P. Taboada, F. Guitián, A. Gil, A. Coelho, *Mater. Today Chem.* **2023**, *27*, 101355.
[139] X. Zhou, C. Liu, *Catal. Today.* **2020**, *347*, 2.
[140] J. Ma, P. Wang, L. Dong, Y. Ruan, H. Lu, *J. Colloid Interface Sci.* **2019**, *534*, 12.
[141] A. Quintanilla, J. Carbajo, J. A. Casas, P. Miranzo, M. I. Osendi, M. Belmonte, *Catal. Today.* **2020**, *356*, 197.
[142] L. Long, R. Pei, Y. Liu, X. Rao, Y. Wang, S. Zhou, G. Zhan, *J. Hazard. Mater.* **2022**, *423*, 126983.
[143] J. Lefevere, S. Mullens, V. Meynen, *Chem. Eng. J.* **2018**, *349*, 260.
[144] C. R. Tubío, J. Azuaje, L. Escalante, A. Coelho, F. Guitián, E. Sotelo, A. Gil, *J. Catal.* **2016**, *334*, 110.
[145] A. E Ugarteburu, I. Casanova, *3D Print. Addit. Manuf.* **2018**, *5*, 220.
[146] Y. de Hazan, M. Thänert, M. Trunec, J. Misak, *J. Eur. Ceram. Soc.* **2012**, *32*, 1187.
[147] Y. Ge, T. Zhang, B. Zhou, H. Wang, Z. Zhang, J. Shen, A. Du, *J. Mater. Res.* **2018**, *33*, 2052.
[148] W. Aslam, M. H. Ahmed, T. Qui, M. Konarova, *Chem. Eng. J. Adv.* **2020**, *3*, 100024.
[149] S. Hajimirzaee, D. Shaw, P. Howard, A. M. Doyle, *Chem. Eng. Sci.* **2021**, *231*, 116287.
[150] S. Danaci, L. Protasova, J. Lefevere, L. Bedel, R. Guilet, P. Marty, *Catal. Today.* **2016**, *273*, 234.
[151] S. Danaci, L. Protasova, F. Snijkers, W. Bouwen, A. Bengaouer, P. Marty, *Chem. Eng. Process.: Process Intensif.* **2018**, *127*, 168.
[152] Y. Lin, W. Zhu, Y. Li, *J. Energy Chem.* **2022**, *73*, 41.
[153] A. Quintanilla, J. A. Casas, P. Miranzo, M. I. Osendi, M. Belmonte, *Appl. Catal. B.* **2018**, *235*, 246.
[154] D. Liu, P. Jiang, X. Li, J. Liu, L. Zhou, X. Wang, F. Zhou, *Chem. Eng. J.* **2020**, *397*, 125392.
[155] A. Sanchez Díaz-Marta, S. Yáñez, C. R. Tubío, V. L. Barrio, Y. Piñeiro, R. Pedrido, J. Rivas, M. Amorín, F. Guitián, A. Coelho, *ACS Appl. Mater. Interfaces.* **2019**, *11*, 25283.
[156] B. Román-Manso, Á. De Pablos, M. Belmonte, M. I. Osendi, P. Miranzo, *Bol. Soc. Esp. Ceram. Vidrio.* **2014**, *53*, 93.
[157] J. Azuaje, C. R. Tubío, L. Escalante, M. Gómez, F. Guitián, A. Coelho, O. Caamaño, A. Gil, E. Sotelo, *Appl. Catal. A.* **2017**, *530*, 203.
[158] P. Jain, A. M. Kuthe, *Procedia Eng* **2013**, *63*, 4.
[159] M. R. Skorski, J. M. Esenther, Z. Ahmed, A. E. Miller, M. R. Hartings, *Sci. Technol. Adv. Mater.* **2016**, *17*, 89.
[160] S. Paul, *Measurement* **2021**, *178*, 109320.
[161] A. Cano-Vicent, M. M. Tambuwala, S. S. Hassan, D. Barh, A. A. A. Aljabali, M. Birkett, A. Arjunan, Á. Serrano-Aroca, *Addit. Manuf.* **2021**, *47*, 102378.
[162] S. Hock, M. Rose, *Chem. Ing. Tech.* **2020**, *92*, 525.
[163] S. Hock, C. Rein, M. Rose, *Chem. Cat. Chem.* **2022**, *14*, e202101947.
[164] K. Gnanasekaran, T. Heijmans, S. van Bennekom, H. Woldhuis, S. Wijnia, G. de With, H. Friedrich, *Appl. Mater. Today.* **2017**, *9*, 21.
[165] T. Li, J. Gonzalez-Gutierrez, I. Raguž, C. Holzer, M. Li, P. Cheng, M. Kitzmantel, L. Shi, L. Huang, *Addit. Manuf.* **2021**, *37*, 101700.
[166] K. A. Evans, Z. C. Kennedy, B. W. Arey, J. F. Christ, H. T. Schaef, S. K. Nune, R. L. Erikson, *ACS Appl. Mater. Interfaces.* **2018**, *10*, 15112.
[167] C. Y. Foo, H. N. Lim, M. A. Mahdi, M. H. Wahid, N. M. Huang, *Sci. Rep.* **2018**, *8*, 7399.
[168] Z. Rymansaib, P. Iravani, E. Emslie, M. Medvidović-Kosanović, M. Sak-Bosnar, R. Verdejo, F. Marken, *Electroanalysis* **2016**, *28*, 1517.
[169] C. Chaparro-Garnica, E. Bailón-García, D. Lozano-Castelló, A. Bueno-López, *Catal. Sci. Technol.* **2021**, *11*, 6490.
[170] C. Chaparro-Garnica, E. Bailón-García, A. Davó-Quiñonero, P. Da Costa, D. Lozano-Castelló, A. Bueno-López, *Materials* **2021**, *14*, 5017.
[171] Y. Li, S. Chen, X. Cai, J. Hong, X. E. Wu, Y. xu, J. Zou, B. H. Chen, *J. Mater. Chem. A.* **2018**, *6*, 5695.
[172] T. Tancogne-Dejean, C. C. Roth, D. Mohr, *Int. J. Mech. Sci.* **2021**, *207*, 106647.
[173] N. Lecis, M. Mariani, R. Beltrami, L. Emanuelli, R. Casati, M. Vedani, A. Molinari, *Mater. Sci. Eng. A.* **2021**, *828*, 142108.
[174] T. Moritz, S. Maleksaeedi, in *Additive Manufacturing*, (Eds: J. Zhang, Y. Jung), Butterworth-Heinemann, Oxford, UK, **2018**, 105.
[175] R. Hamano, Y. Nakagawa, V. Irawan, T. Ikoma, *Appl. Mater. Today.* **2021**, *25*, 101160.
[176] H. M. Bui, P. F. Großmann, T. Gros, M. Blum, A. Berger, R. Fischer, N. Szesni, M. Tonigold, O. Hinrichsen, *Appl. Catal. A.* **2022**, *643*, 118760.
[177] H. M. Bui, R. Fischer, N. Szesni, M. Tonigold, K. Achterhold, F. Pfeiffer, O. Hinrichsen, *Addit. Manuf.* **2022**, *50*, 102498.
[178] H. M. Bui, P. F. Großmann, A. Berger, A. Seidel, M. Tonigold, N. Szesni, R. Fischer, B. Rieger, O. Hinrichsen, *Chem. Eng. J.* **2023**, *458*, 141361.
[179] H. A. Derazkola, F. Khodabakhshi, A. Simchi, *Polym. Test.* **2020**, *90*, 106690.
[180] P. M. Bhatt, A. M. Kabir, M. Peralta, H. A. Bruck, S. K. Gupta, *Addit. Manuf* **2019**, *27*, 278.
[181] F. Mercado, A. R Arciniegas, *Int. J. Adv. Manuf. Technol.* **2020**, *109*, 17.
[182] H. Lei, J. Li, Q. Wang, Z. Xu, W. Zhou, C. Yu, T. Zheng, *Int. J. Hydrogen Energy.* **2019**, *44*, 24782.
[183] C. Ha, Z. Wang, C. Wang, J. Qin, Z. Zhou, S. Wang, Z. Liu, B. Li, *Int. J. Hydrogen Energy.* **2024**, *52*, 1163.
[184] Q. Wu, Y. Wang, D. Mei, S. Si, *Int. J. Hydrogen Energy.* **2022**, *47*, 6282.
[185] H. Yu, H. Chen, M. Pan, Y. Tang, K. Zeng, F. Peng, H. Wang, *Appl. Catal. A.* **2007**, *327*, 106.
[186] K. J. A. Brookes, *Met. Powder Rep.* **2015**, *70*, 68.
[187] A. Kulkarni, G. D. Sorarù, J. M. Pearce, *Addit. Manuf.* **2020**, *32*, 100988.

Adriana Parra-Marfil is a Ph.D. student in Chemistry at the University of Granada (UGR), Spain, and at the Autonomous University of San Luis Potosí (UASLP), Mexico. She obtained her bachelor's and master's degrees in Chemical Engineering from UASLP. Currently, she is conducting research on the development of advanced monolithic catalysts for CO_2 methanation using additive manufacturing techniques. Her research interests span materials science, adsorption processes, photodegradation, chemical kinetics, and reactor engineering, with a particular emphasis on environmental applications.

Agustín F. Pérez-Cadenas holds a degree in Chemical Sciences from the University of Jaén (1997). Doctorate in Chemical Sciences from the University of Granada (2002). Professor of Inorganic Chemistry at the University of Granada (2018). Member of the UGR-Carbon research group (Polyfunctional Carbon-based Materials), his research has focused on the design of carbon-based materials and the study of their industrial, energy, and environmental applications. He is currently the coordinator of the Doctoral Programme in Chemistry at the UGR and President of the Spanish Carbon Group (GEC).

Francisco Carrasco-Marín is the Chair of the UGR-Carbon research group (Polyfunctional Carbon-based Materials), Full Professor in Inorganic Chemistry at the University of Granada since 2009. His research is focused on the synthesis, characterization and applications of different forms of carbon materials, activated carbons, carbon xerogels and aerogels, carbon micro and nanospheres, doped carbons and metal-containing nanoparticles. He has made the most relevant contributions in the synthesis of high surface area porous carbons and in the modification of the surface chemistry in order to optimize their applications in the areas of catalysis, environmental protection, and energy storage.

Raúl Ocampo-Pérez is a full professor in the Center of Investigation and Postgraduate Studies, Faculty of Chemical Science, Autonomous University of San Luis Potosí, Mexico. His main research is primarily focused on the preparation of materials for adsorption and advanced oxidation process with application for the treatment of contaminated water. Additionally, collaborates in mathematically modeling mass transfer phenomena in reactive systems.

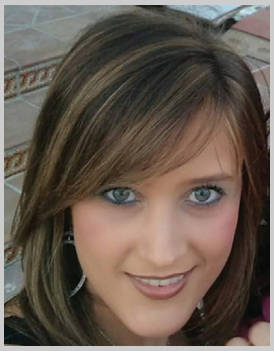

Esther Bailón García is Ramon y Cajal Fellow at the University of Granada. She holds a degree in Chemical Engineering (2010) and doctorate in Chemistry from the University of Granada (2015). Currently, she is the leader of the research line "Toward digitally controlled advanced catalysts through 3D printing" in the UGR-Carbon research group (Polyfunctional Carbon-based Materials). Her present research focuses on the design and synthesis of advanced catalysts for environmental and energy applications such as advanced oxidation processes, water splitting, O_2 reduction reaction, and CO_2 electroreduction.